Alexandria Engineering Journal (2023) 74, 195–229

HOSTED BY

Alexandria University

Alexandria Engineering Journal

www.elsevier.com/locate/aej
www.sciencedirect.com

REVIEW

Compactness and performance enhancement techniques of ultra-wideband tapered slot antenna: A comprehensive review

Sahar Saleh [a,b,c], Mohd Haizal Jamaluddin [c,*], Faroq Razzaz [d,e], Saud M. Saeed [d], Nick Timmons [a], Jim Morrison [a]

[a] WiSAR Lab, Atlantic Technological University (ATU), Letterkenny, Co. Donegal F92 FC93, Ireland
[b] Department of Electronics and Communications Engineering, Faculty of Engineering, Aden University, Aden 5243, Yemen
[c] Wireless Communication Centre, Universiti Teknologi Malaysia (UTM), Johor Bahru, Johor 81310, Malaysia
[d] Electrical Engineering Department, College of Engineering, Prince Sattam Bin Abdulaziz University, Al-Kharj 16278, Saudi Arabia
[e] Faculty of Engineering and Information Technology, Taiz University, Taiz 6803, Yemen

Received 30 August 2022; revised 13 April 2023; accepted 4 May 2023
Available online 18 May 2023

KEYWORDS

Vivaldi tapered slot antenna (VTSA);
5G;
Ultrawide band (UWB);
Microstrip to slot (M/S) transition;
Broadband;
Corrugations;
Parasites;
Metamaterials;
Dielectric loads;
Lenses;
Stable radiation patterns;
And high gain

Abstract Higher performance, lower cost, and compact size antennas are important in today's wireless communication system where everything is connected. Many approaches are developed over the past twenty years to sustain suitable compact broadband antennas with efficient performance in many applications for easy integration and connection of devices, especially in the internet of things (IoT) technology and cognitive radio networks (CRNs). Broadband planar antennas, such as the Vivaldi tapered slot antenna (VTSA), are suitable for these applications due to their wide bandwidth, high gain, simple planner structure, low profile, lightweight, low fabrication cost, and easy integration with circuits. Although many approaches proposed for TSAs' compactness and performance enhancement, this work for the first time presents a comprehensive review of different types of ultrawide band (UWB) TSA designs focusing on the compactness and performance enhancement strategies pointing out to pros, cons, and practical applications for the last twenty years which are also addressed using extensive comparison tables. This comparison seeks to help both researchers and RF designers grasp the fundamentals of establishing effective steps for Vivaldi antenna design with high resilience by combining multiple strategies and exploiting their benefits while avoiding or mitigating their drawbacks.

* Corresponding author.
E-mail addresses: saharalmatri@gmail.com (S. Saleh), haizal@utm.my (M.H. Jamaluddin), f.kasim@psau.edu.sa (F. Razzaz), s.saeed@psau.edu.sa (S.M. Saeed), nick.timmons@atu.ie (N. Timmons), jim.morrison@atu.ie (J. Morrison).

Peer review under responsibility of Faculty of Engineering, Alexandria University.

https://doi.org/10.1016/j.aej.2023.05.020
1110-0168

Contents

1. Introduction

Modern wireless communication systems require efficient and compact RF/microwave components. These devices should be compatible with the recent application requirements and simple to integrate into the system to meet commercial demand and reduce the power budget needed for mass production [1]. To meet these requirements, size miniaturization and performance enhancement are of the more concern issues.

Antennas are key components in most wireless communication systems that represent their operational characteristics. They are used to transfer radio electromagnetic waves between a guided device and a free space [2]. Due to rapid development in the internet of things (IoT) technology where all devices are connected, small antennas are required for such connection. Besides, the easy integration of devices within a wireless communication system, compact antennas help in decreasing the system power budget that makes them more desirable, especially in sensor wireless networks [3].

Ultrawide band (UWB) wireless communication is a revolutionary technology that opens excellent opportunities in the modern wireless communication system due to its special characteristics such as low cost, high data rate, small physical size, and less power consumption [4]. In 2002, Federal Communications Commission (FCC) released the first report and order to authorize the unlicensed use of UWB in 3.1–10.6 GHz with a restriction in transmit power level to −41.3 dBm/MHz avoiding interference with the coexisting narrow band frequency technologies such as wireless fidelity (WiFi). Each radio channel in UWB technology has >500 MHz or 20% bandwidth depending on its center frequency [5].

The special characteristics of UWB technology make it more beneficial in many applications. These characteristics include simple and low-cost architecture, fine resolution and long-range low-radiated power, high data rate transmission, resistance to jamming, reduced signal diminishing, high multi-path resolution, and low interference with the existing signals [6]. Many wireless application areas are enhanced by UWB technology such as military, security, civilian commerce, and medicine. In military and security, high resolution, and penetration of UWB signals are used for target locations such as in synthetic aperture radar (SAR) technology. However, in civilian and commercial applications due to its available large bandwidth, it enhances the accuracy of positioning measurements (in sub-centimeters and sub-millimeters) for precision locating and tracking of abnormal conditions of civil structures such as pavements, bridges, buildings, buried and underground pipes. Also, it is used for peer-to-peer fine-ranging applications such as the monitoring of personal properties. Furthermore, it helps in avoiding collisions and obstacles for automobiles and aviation. In medical applications, it helps in replacing cables, allowing easy patient examination, and monitoring, detection, and imaging of tumors. It also can be used as a relay to work along with longer-range multimedia technology such as Wi-Fi, worldwide interoperability for microwave access (WiMAX), and cellular wide-area communication [6,7]. Also, the radar system exploits the large bandwidth of UWB technology to offer a precise radar resolution that helps to differentiate between two closely spaced targets [8].

Recent technologies including software-defined radio, reconfigurable wireless communication, and UWB systems are becoming increasingly attractive to broadband planar antennas. This is due to the ease of broadening their bandwidth (BW) to $>70\%$ and the ability to cover multiple operating bands. Moreover, the design of broadband antennas is usually simpler than the multiband narrowband antennas which will help in reducing the design and fabrication tolerances [9,10].

UWB technology requires an antenna with large BW, high gain, and stable end-fire radiation. To satisfy these requirements, exponential or Vivaldi taper slot antenna (ETSA or VTSA) with symmetrical radiation pattern (end fire), wide BW, simple planner structure, low profile, lightweight, low fabrication cost, and easy integration with circuits are preferably used in many applications such as UWB see through wall (STW) [11], mm-wave imaging or focal- plane arrays [12], microwave imaging (MWI) [13-18], ground penetrating radar (GPR) [19-27], ground and space communication [28], vehicular wireless communication [29], stealth aircraft [30], vehicular to anything (V2X) communication [31], near field imaging [32], radio astronomy or telecommunication [12,33], wind profile radar (WPR) [34], satellite microwave power transmission [35], 2D indoor wireless positioning [36], through-wall radar (TWR) [37,38], water communication [39], long-distance electromagnetic detection [40] and microwave moisture detection (MMD) [41].

TSA is a UWB antenna and it was first proposed in [42] to be used in mobile telecommunications and radars due to its low cost and small size. Three slot profiles with different radiation characteristics can be obtained in the TSA: (1) linearly tapered slot antenna (LTSA), (2) constant width slot antenna (CWSA), and (3) ETSA or VTSA [43]. The three different profiles are illustrated in Fig. 1.

The VTSA shown in Figs. 1 (c) and 2 was proposed by Gibson in 1979 for broadband application. It is called a traveling-wave antenna because when the wave is coupled from the microstrip line to the slot line, its energy is tightly bound to the opening width (W_{min}) at the beginning of the tapered slot where the separation between the two conductors is very small. As the wave leaks away from the microstrip to slot (M/S) transition moving toward the aperture width (W_{max}) in which the separation is increased gradually, its energy becomes weaker and the wave is radiated to the free space [44]. The current of this antenna will have the same amplitude but different phases [45].

As it is shown from the configuration of VTSA in Fig. 2, a quarter wavelength slot (L_{qw}) is connected to the exponentially tapered slot which is according to [2] defined by.

$$y(x) = \pm Ae^{r} * ^{x} \tag{1}$$

where A is half W_{min}, r is the taper rate which plays a significant role in its bandwidth and gain. $\times$ is the position along the tapered slot length (L_T). As the antenna length (L_{ant}) is increased by increasing L_T, the directivity and beamwidth will also improve. W_m, L_m, re in Fig. 2, are the microstrip feed line width, microstrip feed line length, and offset of the slot from the ground, respectively.

Theoretically, the BW provided by the exponentially tapered slot (flare) should be unlimited but it is practically limited by other parameters in the antenna such as the whole antenna size and the matching parameters in the M/S transition [46].

The best design equations for VTSA performance are described in [2]. The microstrip feed line is preferably located

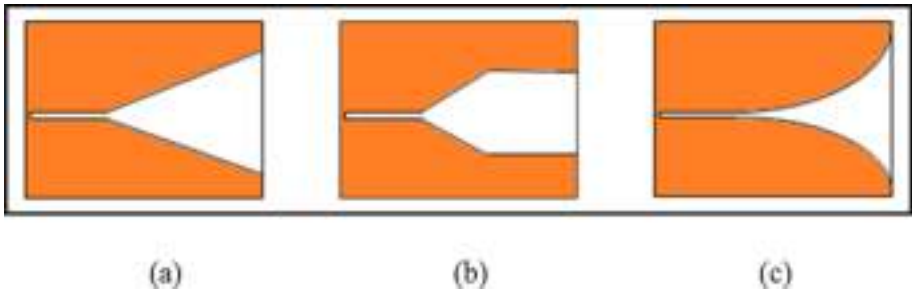

Fig. 1 TSA types: (a) LTSA, (b) CWSA, and (c) ETSA or VTSA.

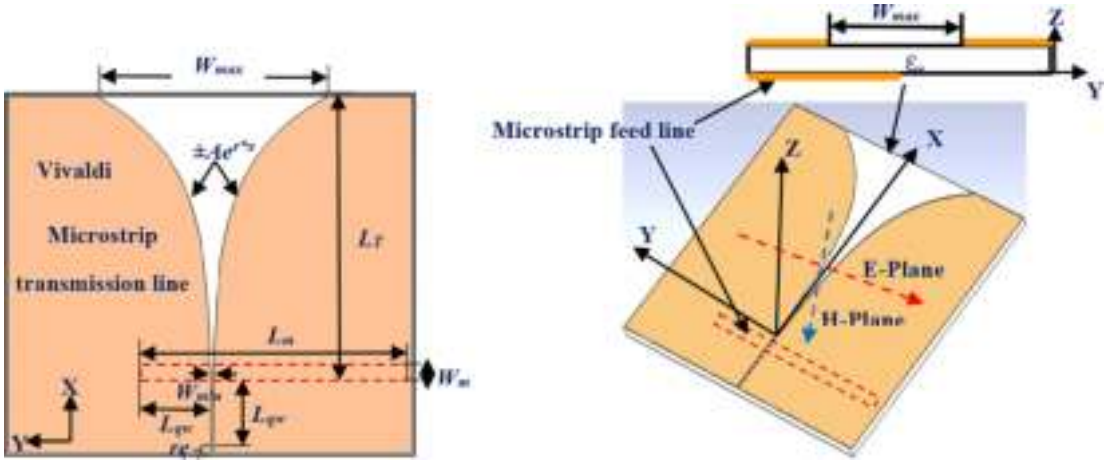

Fig. 2 (a) 2D and (b) 3D configuration of VTSA [47].

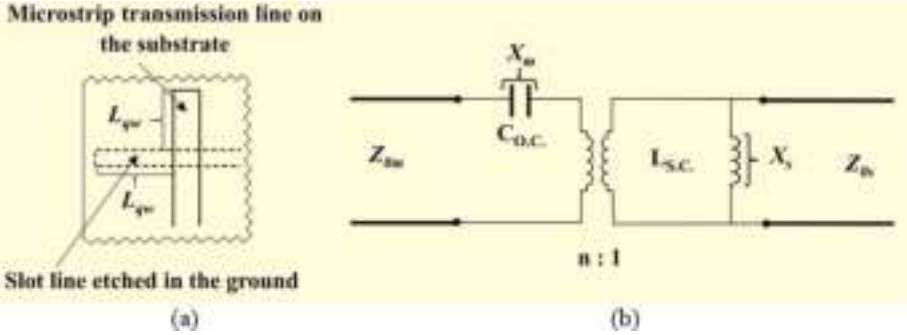

Fig. 3 The VTSA (a) M/S transition (b) equivalent circuit [50].

along the X-axis to eliminate any unwanted radiation from it and to be easily attached to the SMA connector as shown in Fig. 2 [48]. Fig. 3(b) depicts the equivalent circuit for the uniform (rectangular/rectangular) M/S feeding transition, which is utilized to improve matching by coupling the electromagnetic waves from the microstrip stub and slot line in the transition via a n:1 transformer [49]. The series X_m and shunt X_s reactances are used to represent the capacitive and inductive effects of the open-ended microstrip line and short-ended slot line, respectively. Z_{0m}, Z_{0s} are the microstrip and slot line characteristics impedances, respectively [50].

There are many other M/S transitions shapes used in the literature to improve the matching and enhance the BW and gain such as (Rectangular/Circular) [51–53], (Radial/Circular) [11,15,16,24,25,27,35,36,40,43,45,54–73], (Circular/Circular) (Chareonsiri et al., 2017a; K. Ma et al., 2014; Y.-W. Wang et al., 2013 2014; J. Wu et al., 2012), (Radial/Quasi-circular) [79] (Radial/Rectangular) [80], (Radial/Rhombus) [81], (Radial/Radial) [82–84], collinear [85] and (Y/Y) in [14]. In addition to M/S transition, other types of transitions and techniques are used to feed the TSAs such as strip to microstrip line (S/M) transition [86], via to open slotline [87], grounded coplanar waveguide (GCPW) to substrate integrated waveguide (SIW) [88], microstrip-to-coplanar parallel strips (M/CPS) transition [89], stripline-to-slotline (S/S) transition [30,39,90], coplanar waveguide (CPW)[17], CPW to slot line (CPW/S) transition [17,20,91–100], CPW to coupled stripline (CPW/CPS) transition [22], microstrip to coplanar stripline (M/CPS) [101] and balun [13,31,33,98,102–105].

Besides LTSA, CWSA, and ETSA many TSA profiles are designed to enhance the antenna performance such as doubled exponentially tapered slot antenna (DETSA) or bunny ear [22,106–110], dual-parabola tapered-slot antenna (DPTSA) [64] and [55], logarithmically tapered slot profile antenna (logTSA) [111], asymmetric TSA (Asym TSA) [51,52], asymmetrical LTSA (ALTSA) [100], Chebyshev transformer profile TSA [57,112], Fourier series profile TSA [113], square cosine profile TSA [114], binomial impedance transformer profile TSA [78], spidron fractal TSA (SFTSA) [115] and double slot TSA [75,76,116–122]. These types are summarized in Fig. 4.

In general, an antenna should be designed to perform well within the operating frequencies of a certain wireless communication application [9]. Because of the unique characteristics of VTSA in the UWB applications, researchers have worked for years to compact its size while maintaining good performance to satisfy the consumer demand for compatibility and low cost. A hot topic in microstrip antenna design is the challenge of designing a compact antenna with a large BW [10]. So, to avoid the drawbacks of reducing the TSA's size, the focus in this comprehensive review is also on improving the antenna performance in terms of enhancing gain, broadening the BW, and reducing the cross-polarization and side lobe levels (SLLs). In addition to this section, Section 2 talks about the different applications of TSA, while Section 3 discusses the miniaturization and performance enhancement techniques applied in the literature to TSA. Finally, Section 4 concludes the work.

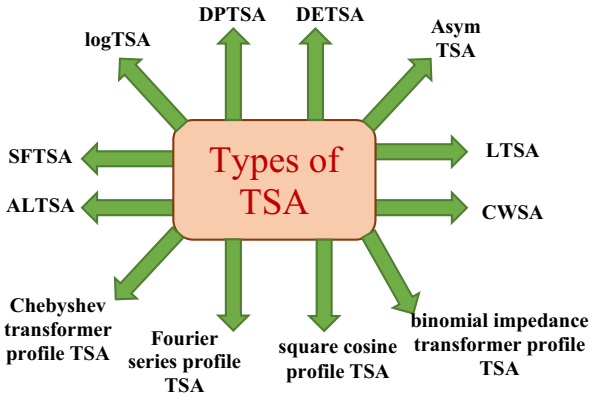

Fig. 4 Different types of TSA.

2. Applications of different TSAs

Various TSA configurations with enhanced performance are designed for suitable applications. To meet the performance of target identification and imaging in an airborne long-range surveillance radar, DETSA was first designed in [106]. A complete study of the main VTSA features and properties used for MWI detection is addressed in [13], where NEC2 code simulations are used to prove the exponential taper scaling invariance and the current distribution. Furthermore, a feeding Y-balun between a coplanar waveguide and a slotline with the use of some air bridges linking the Y-balun slots are used for the first time. However, in [104] they derived a scaling principle for the VTSA and used a double Y-balun feeder. Asym TSA is designed in [51] to meet the requirement for vertical pattern synthesis in the base station of a mobile communication system such as filling nulls and suppressing SLLs in the lower and upper part of the vertical pattern to avoid blind spot

and mitigate the multipath fading, respectively. For UWB applications such as radar and positioning, impulse distortion is minimized in [87] by replacing M/S (radial/circular) transition with via to open slotline transition. A Compact 8 × 1 (2–4 GHz) VTSA array based on a Wilkinson power divider (WPD) feeding network is designed in [11] with a gain higher than 12 dBi suitable for STW applications. Authors Vu et al designed compact UWB (1–5 GHz) VTSA suitable for impulse-based electromagnetic beamforming [123]. Authors in [15] and [14] designed VTSAs with improved performance and low cross-polarization, respectively suitable for UWB MWI applications.

DPTSA phased array (45° wide scan: 1.6–9 GHz) is used in [55] for telecommunication and radar applications. A compact VTSA with a novel small size wide band collinear M/S transition, a metallic reflector, and a fork-shaped metallic carrier is proposed in [85] to be used for wireless personal area network (WPAN). For the application of detection systems with high resolution such as the detection of human body-worn concealed weapons, UWB (0.25–4 GHz) VTSA with high directive properties is proposed in [124]. A novel wideband (2.2–6 GHz) DETSA is proposed in [22] and tested for GPR application for detecting a buried target in soil.

UWB (3–8 GHz), and (2.28–5.68 GHz) VTSAs are proposed in [81] and [80], respectively for microwave breast imaging. However, the UWB (5.81–9.83 GHz) VTSA in [125] is designed for brain tumor detection. A novel compact TSA similar to VTSA with larger BW (0.64–6 GHz) suitable for GPR application is proposed in [20]. Compact UWB ALTSA with essential time-domain fidelity suitable for portable RF imaging systems, or a possible sensor element in a UWB radar array application is proposed in [100]. UWB VTSA (5–10 GHz) is used in [45] for microwave breast-based cancer detection. Authors in [115] designed SFTSA with reduced size for S and X bands radar applications. To reduce the number of telescope receivers for a square kilometer array (SKA) radio telescope feeding system, authors in [126] used a combination of CPW/S and M/S feeding to design a compact UWB VTSA with two exponential taper profiles. Experimental time-domain validation of near field to near filed (NFNF) and near field to far filed (NFFF) transformations is presented in [21] using UWB (0.5–3 GHz) VTSA for GPR applications. A compact wide-band dual-polarized VTSA suitable for passive electronic reconnaissance, passive radar, and wideband communication and detection is designed in [98]. Dual and single polarized VTSAs with λ/4 bulan and Y-Y transition are proposed in [31,29] for V2X communication measurements and vehicular IEEE 802.11a WLAN applications, respectively. In [127], the Vivaldi monopole antenna with omnidirectional radiation pattern is proposed to cover a wide range of LTE mobile communication (LTE700, GSM850, GSM900, DCS1800, PCS1900, WCDMA2100, Bluetooth, WiMAX2350, WLAN2400, and LTE2600 standards). For radio astronomy and telecommunication application, mm-Wave TSA with optimized profile, three variable corrugation zones, and enhanced radiation properties such as low cross-polarization and reduced SLLs is proposed in [12]. In [25], a compact UWB (1.17–4.75 GHz) with corrugations is proposed to get a narrow beam and high gain suitable for GPR and STW applications. A compact double slot structure (0.7–2.7 GHz) VTSA with in-phase and 180° out-of-phase differential feeding cases, is proposed in [121] with a rotated angle of 29° between them for base station diversity applications in cellular and LTE bands. The small size, wide BW, and stable gain of (0.5–2.5 GHz) VTSA is used in [38] to build UWB MIMO radar system for through-wall radar (TWR) imaging. In [84], a compact wideband LTSA is proposed for radar sensor application. Without the use of a plano-convex aspherical lens and a parabolic mirror, a compact Vivaldi antenna is proposed in [128] to work efficiently for terahertz (THz) photomixing devices. In [129], a 3D Vivaldi antenna is used to build a compact system-on-antenna (SoA) front-end module that outperforms a ridged horn antenna-based design in terms of power reception. A high gain 2 × 4 TSA array is proposed in [39] for water communication. Recently, in [130], [131,132] and [41] lenses are loaded with Vivaldi antennas (VAs) for high gain applications imaging, wireless Communications and through-the-wall imaging, and microwave moisture MMD, respectively. A compact UWB (2.5–8.5 GHz) VA is designed in [40] for long-distance electromagnetic detection., Fig. 5 summarizes the applications of TSA in the period 2004–2022.

3. The miniaturization and performance enhancement techniques

This section includes two main subsections: Section 3.1, discusses various techniques used in the literature to reduce the size of TSA; however, Section 3.2 focuses on the techniques used to enhance the performance of TSA in terms of matching,

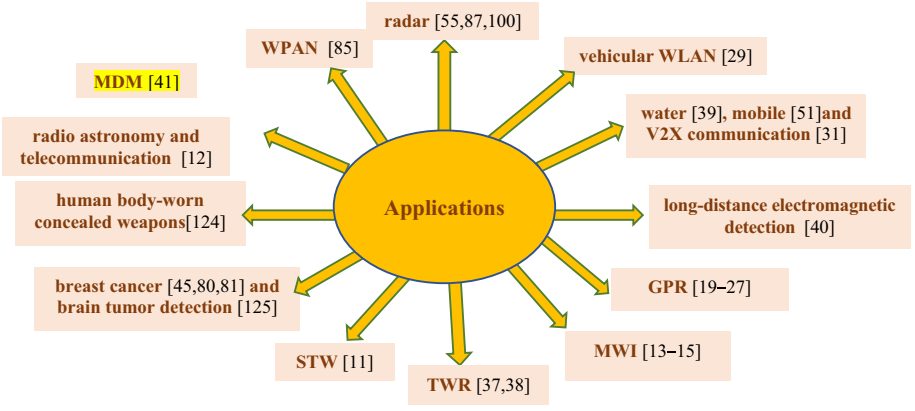

Fig. 5 Use of TSA in different applications.

BW, gain (directivity), diversity, radar cross section (RCS), SLLs and cross-polarization.

3.1. Miniaturization techniques

The main goal of reducing the antenna size is to be compatible with the recent industrial requirements and easily integrated with other circuits, resulting in a cost-effective wireless communication system with lower power consumption [1]. The followings are the techniques used in the literature for the last 18 years to reduce the size of the TSA or more specifically the VTSA.

3.1.1. Removing parts from the radiator's edge

In order to reduce the size of the ETSA (flared notch antenna), the conducting edges of its radiating patch (or ground plane edge) are removed so the surface current is mainly distributed in the narrow area of the slotline sides which in turn increases the electrical length. This idea was first established in designing DETSA in [106] by exponentially tapering the outer edge of the slot line conductor and using a coaxial cable to feed the antenna as shown in Fig. 6. In addition to the compactness purpose, DETSA was proposed to overcome the limitation of ETSA in terms of asymmetric surface current distribution on the radiating element that hinders the propagation of low-frequency components [106].

Following the same concept of [106] and to get more compactness, a CPW/CPS transition is used to design low band UWB DETSA in [99,22] as shown in Fig. 7(a) and (b), respectively. Also, a compact flexible UWB DETSA based on liquid crystal polymer (LCP), suitable for conformal packing and integration with other components is designed in [107] as depicted in Fig. 7(c). The author in [108] exploited the high dielectric constant of FR4 substrate to design a compact UWB DETSA with good impedance matching (VSWR < 1.9) and stable radiation patterns. Other compact wideband (6–9 GHz) and UWB (6–18 GHz) DETSAs are proposed in [109,110], respectively. A 7.7 % size reduction is obtained when the VTSA in [55] is modified so its inner and outer edges are parabola tapered getting DPTSA as shown in Fig. 7(d).

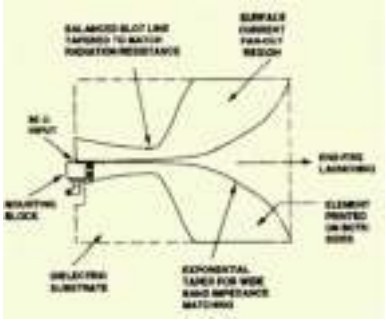

Fig. 6 Configuration of the first DETSA [106].

The same concept in etching the radiator's edges is applied in [115,101] to reduce the antenna size resulting in spidron fractal tapered slot antenna (SFTSA) and ETSA with Electric-Magnetic type as depicted in Fig. 8(a) and (b), respectively. For more compactness in [101], the substrate is cut at the corner as shown in Fig. 8(b).

Authors inserted a pair of triangular slots, a pair of quarter circular slots, a pair of tapered slots, two pairs of eye-shaped slots, a pair of annular slots, a pair of symmetrically tapered slots, a pair of semi-elliptical slots, a pair of symmetrical exponential slots, a pair of tapered slot edge (TSE) and a pair of symmetrical resonant structure in the radiation patches to reduce the size of the proposed UWB LTSA [94], UWB elliptically TSA [95], UWB VTSA [83,77], X- band VTSA [73], tapered slot edge antenna (TSEA) [67], double-layered structure (2.2–19 GHz) and (2.5–11 GHz) VTSAs [86,90], broadband (2.6–20 GHz) TSA [97], and wideband VTSA used for circular array [133], as illustrated in Fig. 9(a-j), respectively.

3.1.2. Corrugations

Generally, corrugations are added to the antenna by inserting or etching slits or slots in its radiator. They help to concentrate the current [106] which will increase the electrical length and reduce the size of the antenna. In [93], corrugations of horizontally loaded slots are added to the UWB (3–11.4 GHz) broken line TSA for compactness as shown in Fig. 10(a). An additional 21.25 % size reduction is obtained in [94] by modifying the compact LTSA explained in Fig. 9(a) to have one triangular slot only resulting in asymmetrical LTSA (ALTSA) and adding rectangular slots to the non-slotted edge as illustrated in Fig. 10(b). 15.47 % and 50 % size reductions are obtained in the proposed (3.55–12 GHz) and (0.8–15.5 GHz) UWB VTSAs by inserting five pairs of rectangular slits [59] and 37

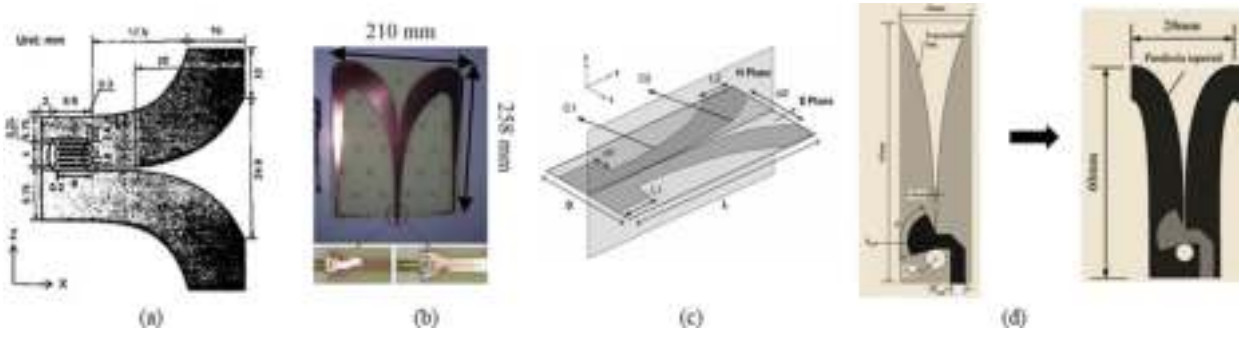

Fig. 7 Layouts of (a) CPW-fed UWB DETSA [99], (b) modified (2.2–6 GHz) DETSA with CPW to CPS transition [22], (c) conformal UWB DETSA with C1 = 0.76 exp(0.16y), 0 < y < 8.53 cm, C2 = 0.012 exp(0.48y), 0 < y < 10.67 cm, d1 = 12 mm, d2 = 42.92 mm, L1 = 24 mm, L2 = 21.4 mm, D = 66.4 mm and L = 130.7 mm [107], and (d) DPTSA as compared to VTSA [55].

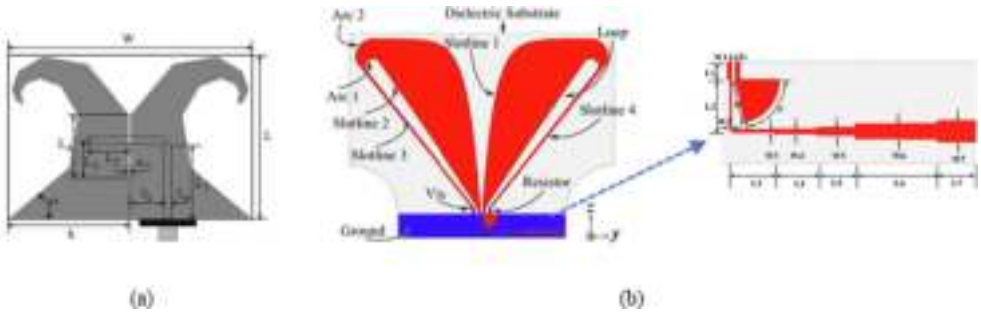

Fig. 8 Layouts of (a) SFTSA with W = 35.8 mm, L = 24 mm, L_1 = 10.74 mm, L_2 = 6.25 mm, L_3 = 5.49 mm, L_4 = 9.28 mm, w_1 = 0.27 mm, f_s = 5 mm, f_w = 1.12 mm, α = 40.2°, h = 17.9 mm and t = 0.51 mm [115] and **(b)** ETSA with Electric-Magnetic type having W1 = 1.3 mm, L1 = 5 mm, W2 = 0.6201 mm, R = 12.6521 mm, L2 = 15.3502 mm, L3 = 12.0250 mm, W3 = 0.9286 mm, L4 = 12.2245 mm, W4 = 1.4509 mm, W4 = 2.4430 mm, W5 = 2.4430 mm, L5 = 11.3123 mm, W6 = 4.4424 mm, L6 = 11.8757 mm, W7 = 4.6130 mm, L7 = 11.7312 mm, W8 = 6.3621 mm, L8 = 11.2550 mm and ɵ = 78.4998° [101].

pairs of rectangular slots [30] into the two edges of the radiator. Fig. 10(c-d) shows the layout of compact TSA and UWB (3–11.4 GHz) proposed in [134] and [38] where rectangular corrugations with multi-section binomial transformer (BTSA) and different-size rectangular slots are used to reduce their size. Specially shaped [131] and gradient elliptical slots (ES) [135]corrugations are etched on the outer edges of the VA arms for compactness as shown in Fig. 10(e) and (f), respectively. Recently, in [40], an 80 % size reduction is achieved by etching a series of optimized symmetric triangular slots in the UWB (2.5–8.5 GHz) VA shown in Fig. 10(g).

3.1.3. Short pins and resistive loading

Short pins and resistors are loaded at the end of the open microstrip stub and slot of the TSA M/S feeding transition to control and lower down the resonant frequency which will increase the electrical length. This control is achieved by mitigating the capacitive and inductive effect of the frequency-dependent components of the open stub and short-circuited slot line which mainly affects the matching and increases the resonant frequency. Using this concept, the short pin and chip resistor are loaded to the microstrip stub and slot line (M/S transition feeding), respectively to miniaturize the size of the proposed (1–20 GHz) and (0.36–4 GHz) VTSAs in [136,137] as illustrated in Fig. 11(a) and 11(b), respectively.

3.1.4. Optimization via parametric studies

Effective parametric studies can be utilized to successfully reduce antenna size while evaluating the influence of compactness on its performance. In [15,82,74,80,65,26] the size of UWB (1.18–4.4 GHz) VTSA, UWB (2.8–10.3 GHz) VTSA, wideband (2.6–10.2 GHz) LTSA, (2.28–5.68 GHz), (0.7–12.7 GHz) and 0.5 GHz VTSAs, respectively was reduced based on the simulator's parametric studies. The proposed antennas with their dimensions are illustrated in Fig. 12(a–f).

3.1.5. Changing the antenna structure

Also, compactness can be achieved by changing the shape of the antenna's tapered slot profile or M/S transition. Compactness is used to sustain a suitable small taper slot profile length while maintaining good performance in terms of BW and gain as in [57,112] where a closed design procedure for the taper slot profile of (0.46–2.98 GHz) TSA is used by applying a stepped quarter wave Chebyshev transformer with simple curve fitting as shown in Fig. 13. In [20], compactness with enhanced BW is achieved by changing the structure of CPW feed (0.64–6 GHz) TSA to have an approximate elliptic metal area and one triangular slot to the left and the other right slot is similar to VA which is considered as the main aperture. At the end of the triangular slot, a resistor is used to mitigate the strong reflections of discontinuous points of the antenna. The layout and VSWR of the proposed antenna are shown in Fig. 14(a) and (b), respectively. However, in [127], 77.61 % size reduction is obtained by modifying the complete VA to half Vivaldi (Monopole) as depicted in Fig. 14(c) and (d) in order to get wideband omnidirectional radiation suitable for LTE mobile communications.

mm, R_3 = 18.048 mm, and R_4 = 19.2 mm, and (b) VSWR of the proposed antenna in [20] and(c) layouts of modifying the VA from complete to half to the modified one with L = 73 mm, W = 69 mm and Sp = 26.4 mm [127].

Recently, in [47], a detailed parametric study is performed on the simply designed UWB VTSA proposed in [138] to analyze the effect of changing the M/S transition shape. Fig. 15(a–d) illustrates the layouts with the final reduction percentages of the analyzed VTSAs with different transition shapes (Model A: (Rectangular/Rectangular), Model B: (Taper/Taper), Model C: (Trapezoidal/Rectangular), and Model D: (Circular/Circular)). As illustrated in Fig. 15(d), a 19.25 % size reduction is obtained in Model D as compared to Model A. The optimized parameters of each model can be found in Ref. [47] (Table 3). Avoiding the difficulties of the previous methods and based on nonuniform transmission line (NTL) theory [139–145], a new theory called exponential or Vivaldi non-uniform slot profile antenna (ENSPA) or (VNSPA) theory is developed in [146] to simply reduce the size of the taper slot length of the compact UWB VTSA (Model D) designed in [47] by 33 % and a final size reduction of 51.94 % by performing parametric studies. This new antenna is called Vivaldi nonuniform slot antenna (VNSA) and its layout is shown in Fig. 16.

A comparison between these techniques is addressed in Table 1. In addition to the compactness (C) discussed in Section 3.1, different strategies are employed on the same antenna to improve BW (B↑), gain (G↑), directivity (D1↑), diversity (D2↑), matching (M↑), radiation efficiency (RE↑) or reduce

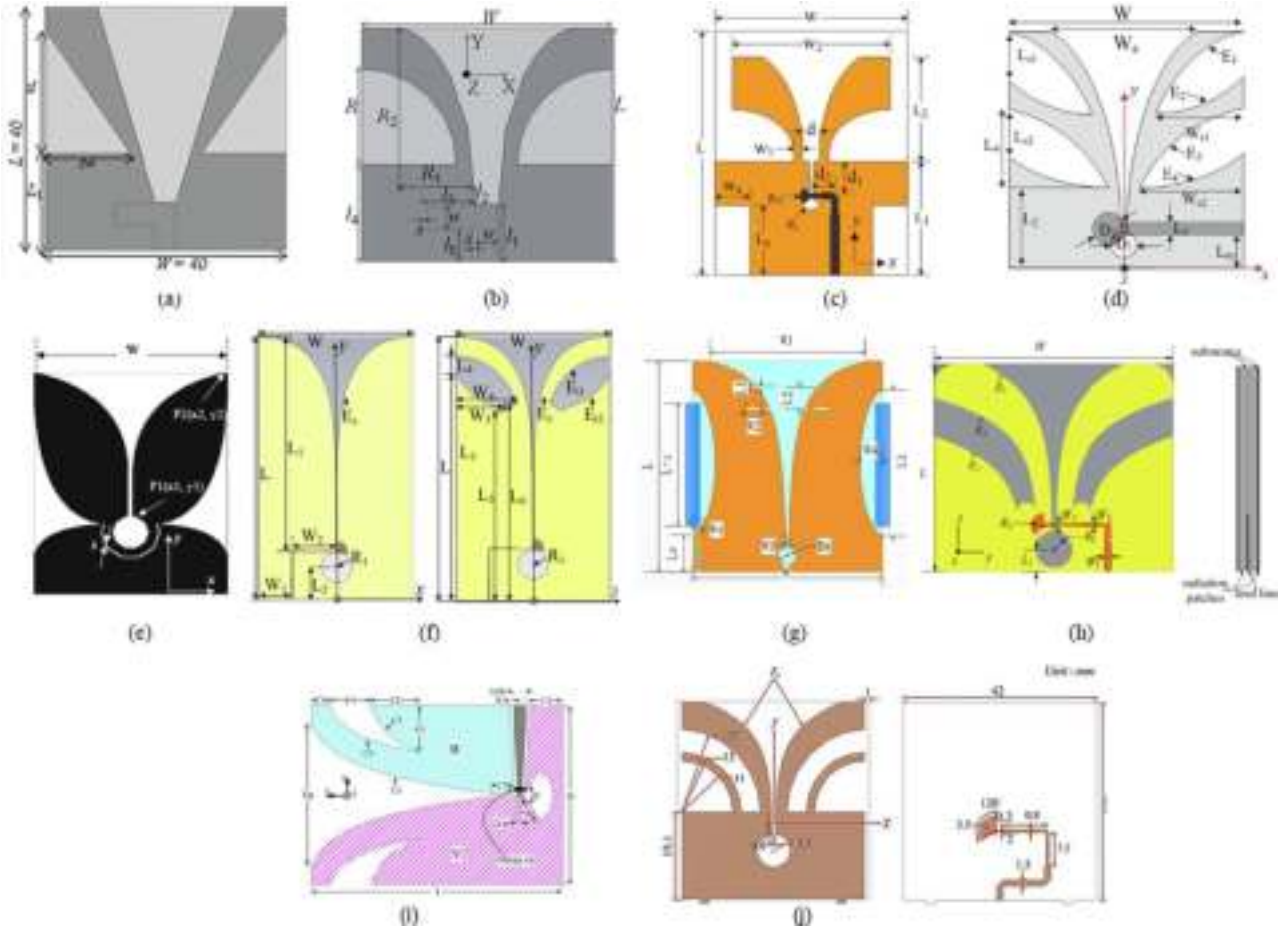

Fig. 9 Layouts of (a) UWB LTSA with a pair of triangular slot having L_1 = 17 mm, tw = 15 mm and tl = 18 mm [94], (b) UWB elliptically TSA with a pair of quarter circular slots having W = 37 mm, L = 34 mm, R = 14 mm, R_1 = 12 mm, R_2 = 24 mm, w = 3.2 mm, s = 0.3 mm, l_1 = 8.3 mm, l_2 = 1.8 mm, l_3 = 7.4 mm, l_4 = 4.4 mm and l_5 = 1.4 mm [95], (c) UWB VTSA with a pair of tapered slots having W1 = 2.5 mm, W2 = 38.2 mm, Wa = 8 mm, L1 = 15.5 mm, L2 = 27.2 mm, La = 7.5 mm, d1 = 5.8 mm, d2 = 5.6 mm, S_1 = 1.5 mm, S_2 = 1.1 mm, S_3 = 0. 75 mm, R_m = 3.1 mm, R_s = 3.8 mm, d = 1.8 mm and g = 0.7 mm [83], (d) UWB VTSA with two pairs of eye-shaped slots having L = 36 mm, L_1 = 21 mm, L_2 = 11.5 mm, L_3 = 14.8 mm, L_4 = 11.6 mm, W = 36 mm, W_a = 20 mm, W_{s1} = 14.5 mm, W_{s2} = 16.5 mm, D_1 = 4 mm, D_2 = 4.8 mm, L_f = 1.46 mm, L_m = 5.02 mm, L_{s1} = 7.7 mm, and L_{s2} = 6.5 mm, (e) X-band VTSA with a pair of annular slots having L = 18 mm, W = 14 mm and s = 0.2 mm [73], (f) TSEA with a pair of symmetrical tapered slots having W = 150 mm, W1 = 31 mm, W_2 = 43.3 mm, W_3 = 47 mm, W_4 = 58.9 mm, L = 258 mm, L1 = 206.2 mm, L_2 = 36 mm, L_3 = 221.8 mm, L_4 = 17.3 mm, L_5 = 185.2 mm, L_6 = 193 mm, and R_1 = 15 mm [67], (g) VTSA with semi elliptical slots having L = 60 mm, W = 50 mm, L-u = 35 mm, Ls = 10.5 mm, Ws = 3 mm, W1 = 44.8 mm, W2 = 4.3 mm, W3 = 0.9 mm, W4 = 6.35 mm, L1 = 1 mm, L2 = 7 mm and L3 = 42.6 mm [86], (h) VTSA with symmetrical exponential slots having W = 36 mm, L = 32 mm, W_1 = 1 mm, W_2 = 0.55 mm, W_3 = 0.35 mm, R_1 = 2.8 mm, R_2 = 2.6 mm, and L_1 = 3.4 mm [90], (i) broadband TSA with a pair of tapered slot edges having L = 70 mm, L1 = 10.8 mm, l2 = 6 mm, L3 = 5 mm, L4 = 11.5 mm, L5 = 13.5 mm, L6 = 15 mm, Rs = 8 mm, W = 50 mm, Wf1 = 2 mm, Wf2 = 0.4 mm, Wp = 40 mm, g = 0.2 mm and ɵ = 2pi/3 (rad) [97] and (j) wideband VTSA with a pair of symmetrical resonant structure [133].

SLL↓, RCS↓, cross-polarization (CP↓) and HPBW↓. Details of enhancement techniques will be addressed in the following section (Section 3.2).

3.2. Performance enhancement techniques

Despite the fact that certain wireless communication applications prefer a compact antenna over one with better performance, others aim for better performance regardless of the size. Additionally, some applications need a compact, highly effective antenna. This section discusses the most common methods in the literature used to improve the TSA performance such as corrugations, adding directive elements, modifying the structure of antenna and feeding, optimization techniques, and arrays.

3.2.1. Corrugations

In addition to reducing the size of an antenna, corrugations are used to improve the BW and gain by adding additional resonances [80] and extending the electrical length due to current distributed in the narrow area of the slots or slits [106], respectively. To enhance the gain, BW, and radiation at the lower

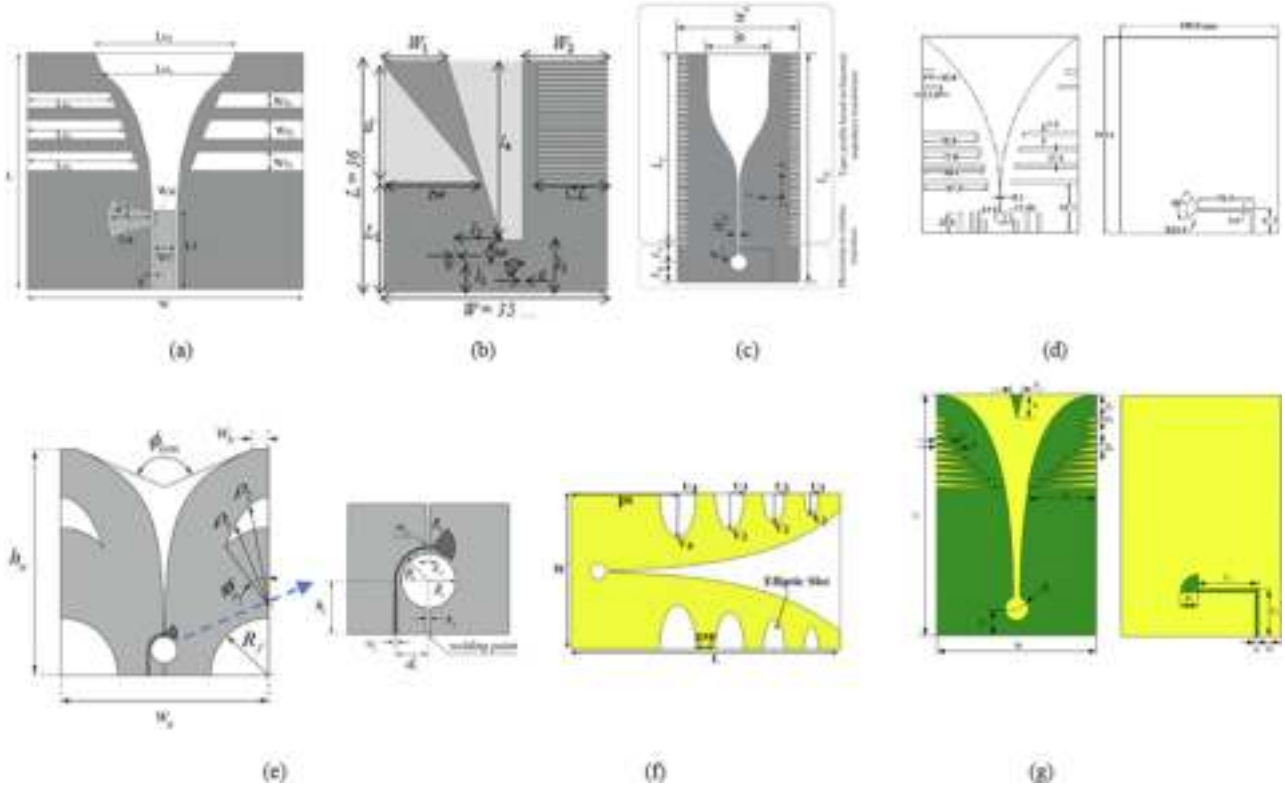

Fig. 10 Layouts of UWB TSA with (a) three pairs o of horizontally loaded slots having W = 35 mm, L = 30 mm, Ws_1 = 2 mm, Ws_2 = 2.5 mm, Ws_3 = 2.5 mm, Ls_1 = 10 mm, Ls_2 = 11.2 mm, Ls_3 = 12.7 mm, Lo_1 = 15.9 mm, Lo_2 = 18 mm, Wst = 1.6 mm, Lst = 6 mm, Wf = 2.6 mm, Lf = 10 mm, g = 0.3 mm, and $\alpha = 12.8^{\circ}$ [93], (b) ALTSA with rectangular slits having L = 36 mm, W = 35 mm, W_1 = 9.7 mm, W_2 = 13.2 mm, L_1 = 17 mm, tw = 15 mm, tl = 18 mm, l_1 = 4.1 mm, l_2 = 7.3 mm, l_3 = 8 mm, l_4 = 27.5 mm, w = 3.2 mm, s = 0.3 mm and CL = 11 mm [94], (c) with rectangular slots having W_a = 50 mm, L_a = 100 mm, L_g = 8 mm, L_s = 8 mm, L_t = 84 mm, W = 26 mm, W_s = 1 mm and W_{sl} = 1 mm [78], (d) different size rectangular slots[38], (e) specially shaped corrugations having wa = 220 mm, wb = 17.13 mm, ha = 238 mm, Rf = 60 mm, Ce = 77.6 mm, $\varphi e = 37.13^{O}$, l1 = 1.7 mm, wl2 = 0.75 mm, Rs = 12 mm, Rl = 17.38^{O}, $\varphi s = 80^{O}$, dl = 18.25 mm, Sc = 1.4 mm, Rc = 14 mm, hc = 26.5 mm and hs = 0.813 mm [131], (f) gradient elliptical slots (ES) having L = 72 mm, W = 41 mm, ps = 29 mm, V_1 = 6 mm,V_2 = 8 mm,V_3 = 10 mm, V_4 = 12 mm, U_1 = 2 mm, U_2 = 3 mm, U_3 = 4 mm, U_4 = 5 mm, gap = 5 mm [135] and (g) series of optimized symmetric triangular slots having W = 55 mm, L = 82 mm, a = 4 mm, b = 8 mm, R = 4 mm, d_1 = 9 mm, d_2 = 7.5 mm, d_3 = 1.5 mm, d_4 = 2.5 mm. d5 = 8 mm, l_1 = 5 mm, l_2 = 8 mm, l_3 = 23 mm, R_1 = 6 mm, w = 1 mm, C_1 = 20.6 mm and C_2 = 16 mm [40].

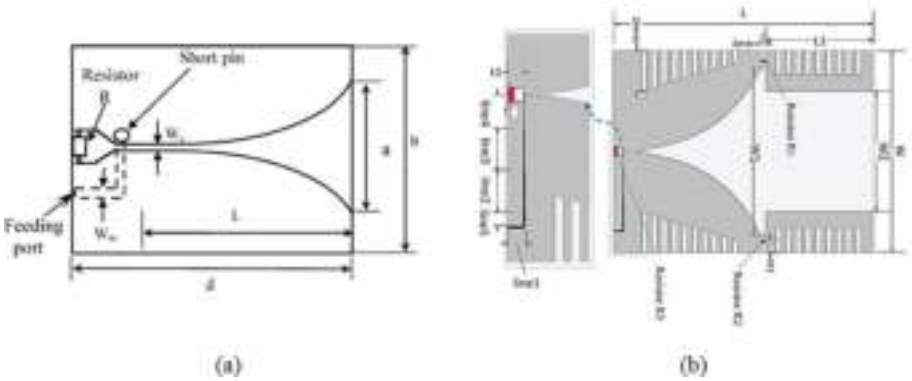

Fig. 11 Layouts of (a) broadband (1–20 GHz) VTSA with short pin and a resistor having L = 46 mm, W_m = 0.5 mm, W_s = 0.4 mm, a = 22 mm, b = 70 mm, and d = 62 mm [136] and (b) wideband (0.4–4 GHz) VTSA with a short pin, three resistors and comb slots having W = 120 mm, L = 155 mm, W1 = 100 mm, W2 = 72 mm, L1 = 64 mm, R1 = 100 Ω, R2 = 100 Ω, R3 = 1000 Ω, t1 = 6 mm, Lr = 5 mm, line1 = 5 mm, line 2 = 15 mm, line3 = 15 mm, line4 = 12 mm and line5 = 5 mm [137].

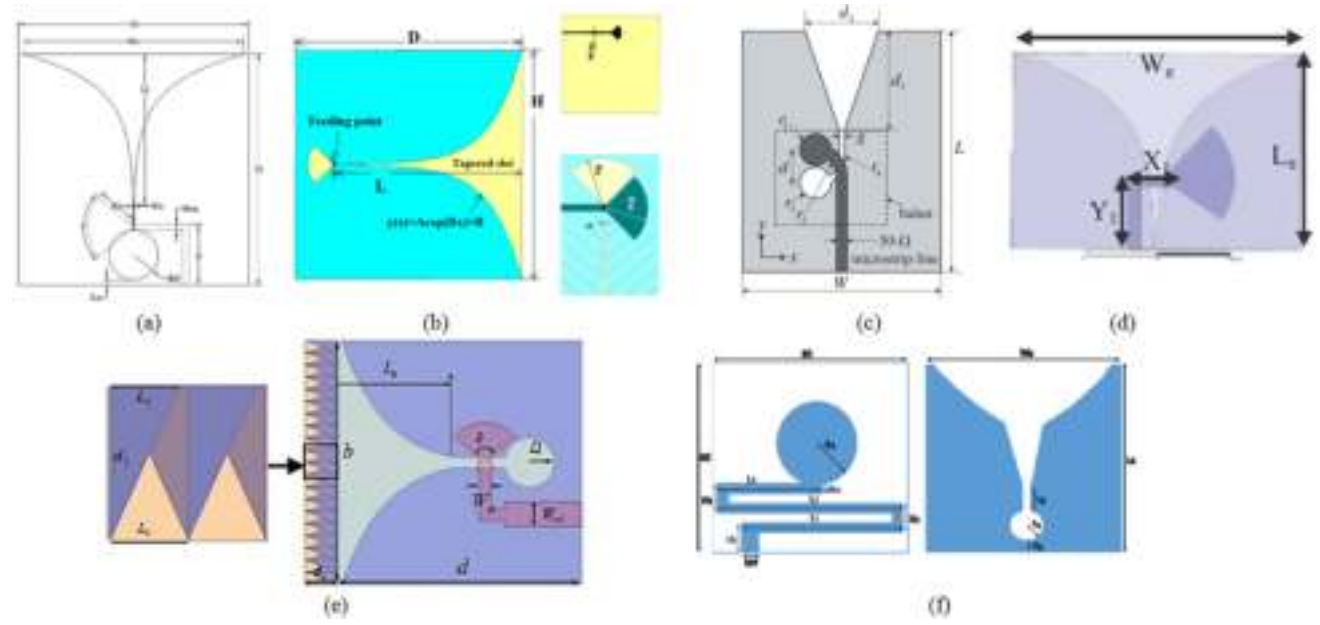

Fig. 12 Layouts of (a) UWB (1.18–4.4 GHz) VTSA with Ws = 0.15 mm, Wm = 1.9 mm, Wt = 71.92 mm, Lt = 53 mm, R0 = 8.015 mm, Lo = 1.7 mm, d = 19.68 mm, R1 = 15 mm, k = 80 mm and R = 0.1 mm [15], (b) UWB (2.8–10.3 GHz) VTSA with L = 30 mm, H = 36 mm, D = 36 mm, Wm = 0.6 mm, S = 0.12 mm, R = 0.21 mm, Rm = 4 mm, and Rs = 4.1 mm, (c) wideband (2.6–10.2 GHz) LTSA with L = 38 mm, W = 32 mm, r_1 = 3.5 mm, r_2 = 1.5 mm, r_3 = 2.5, r_4 = 1.6 mm, g = 0.4 mm, s = 4 mm, d = 3, $d1$ = 12 mm, and d_2 = 8 mm, (d) UWB (2.28–5.68 GHz) VTSA with L_g = 28 mm, W_g = 21 mm, Y_1 = 8.8 mm and X_1 = 8 mm [80], (e) (0.7–12.7 GHz) antipodal structure Vivaldi (ASV) antenna with b = 25 mm, d = 25 mm, L_0 = 13.5 mm, W_{st} = 1.27 mm, W_{st1} = 3.2 mm, α = 110°,D_r = 1.9 mm, d_1 = 3 mm, L_2 = 1.25 mm, and L_1 = 1.125 mm [31], and (f) 0.5 GHz VTSA with pipe like structure feedline having ls = 65 mm, Ws = 60 mm, Wa = 3 mm, Wf = 4.5 mm, L1 = 54.5 mm, l2 = 63 mm, L3 = 33 mm, H1 = 8.5 mm, H2 = 9 mm, H3 = 8 mm, Ra = 12.5 mm, Rg = 5 mm, Lg = 6.5 mm and Hg = 1.75 mm [26].

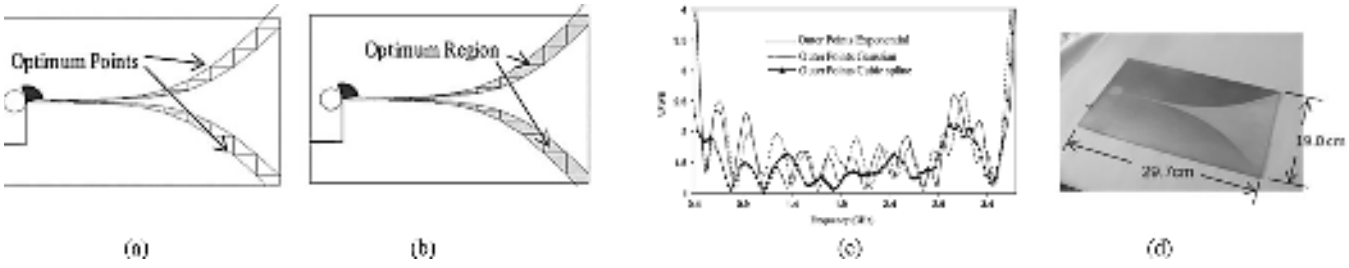

Fig. 13 (a) The optimum set of points, (b) the optimum region (grey color) of Chebyshev steps for minimum VSWR and maximum power transfer gain, (c) VSWR, and (d) photograph of the proposed antenna [57].

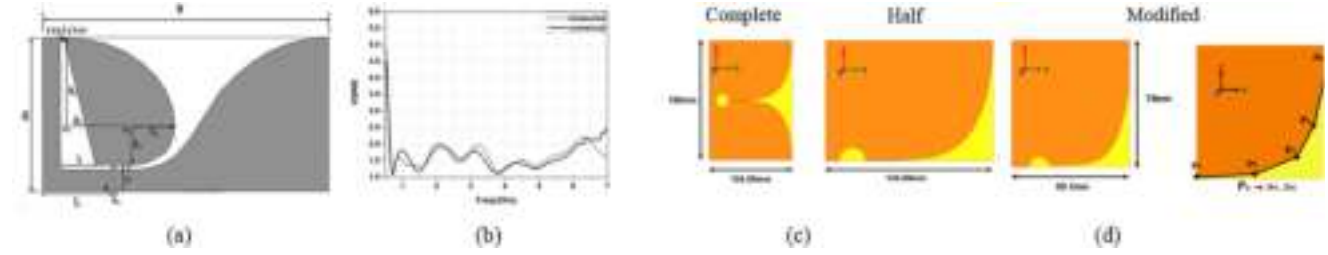

Fig. 14 (a) The layout with W = 130 mm, H = 70 mm, L = 31.25 mm, w_s = 2 mm, g = 0.25 mm, D = 10 mm, s = 1.5 mm, l = 24 mm, R_1 = 40 mm, R_2 = 50.

operational frequency band of the proposed compact UWB (2.8–10.3 GHz) VTSA (ANT-A) in [82], constant length (ANT-B) and varying length (ANT-C) corrugations are used with the best result for ANT-C as shown in Fig. 17(a-c). In [147] for wideband application, corrugations of invert-L slots edge (ILSE) shape are added to the proposed ETSA as

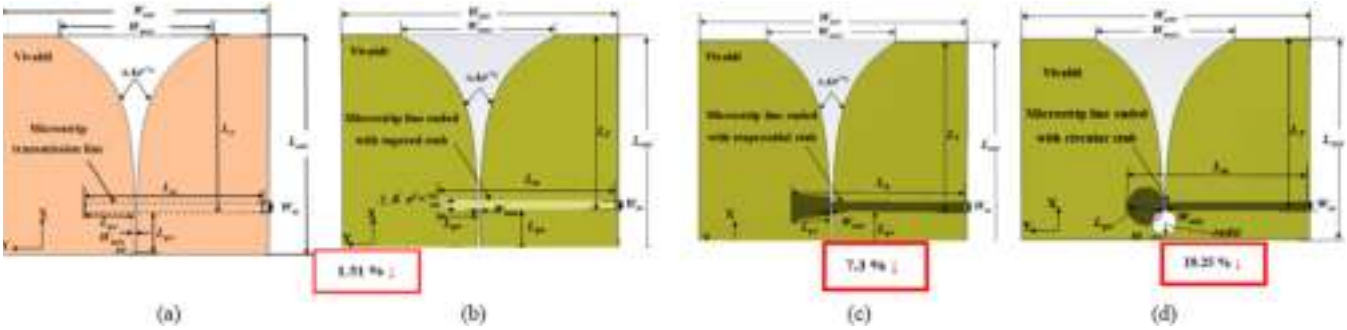

Fig. 15 Layouts of the proposed UWB VTSA models: (a) A with W_{ant} = 43.92 mm and L_{ant} = 35.42 mm, (b) B with W_{ant} = 43.9 mm and L_{ant} = 34.9 mm, (c) C with W_{ant} = 43.36 mm and L_{ant} = 34.9 mm, and (d) D with W_{ant} = 42.9 mm and L_{ant} = 29.28 mm [47].

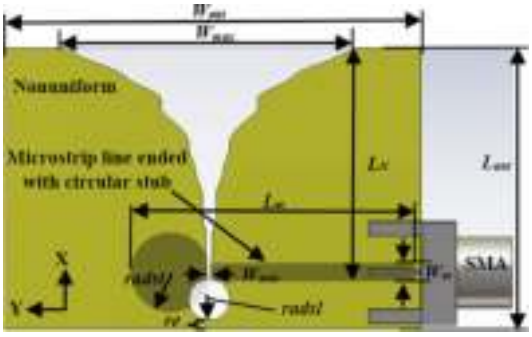

Fig. 16 Layout of the compact UWB VNSA having W_{max} = 20.9 mm, L_N = 16.75 mm, W_{min} = 0.286 mm, $radsl$ = 1.505 mm, L_m = 20.7 mm, W_m = 1.3 mm, re = 0.5 mm, W_{ant} = 29.8 mm, and L_{ant} = 20.26 mm [146].

depicted in Fig. 17(d) to enhance its BW by 7.7 % and gain by 20 %, 4.3 %, and 6.5 % at 4 GHz, 6 GHz, and 8 GHz, respectively. Fig. 17(e) and 17(f) illustrate the simulated VSWR and gain of ETSA with ILSE as compared to the conventional ETSA and ETSA with rectangular slots edges (RSE). For stealth application, TSA should be designed to have low RCS which is achieved in [73] by etching a pair of annular slots on the radiation patch of the compact X-band VTSA that was explained in Section 3.1.1 and Fig. 9(e). The RCS is shown in Fig. 17(g).

The uniform and nonuniform corrugations along with the triangular slot in the designed compact ALTSA in [95] are used to enhance the BW and gain as depicted in Fig. 18(a) and (b), respectively. Whereas they are used with a pair of circular slots to reduce the cross-polarization levels (below −20 dB) of the compact ETSA in [95]. The layout and the radiation pattern of the proposed ETSA with nonuniform corrugations are shown in Fig. 18(c) and (d), respectively. In addition to the compactness achieved in the designed UWB (3–11.4 GHz) broken line TSA [93], UWB (3.55 –> 12 GHz) VTSA [59], UWB (2.92–11.91 GHz) BTSA [79] and UWB VTSA [135]using corrugations, they are also assisted in enhancing the BW by 13.91 %, 55.85 %, 1.89 % (Sim) and 15.87 % (Sim) as shown in Fig. 18(e), (f), (g) and (h), respectively (see Figs. 19 and 20).

3.2.2. Adding directive materials

As the directive materials (lenses, metamaterials, metals, and resistive loading) are loaded in (usually called grating elements) or in front of the TSA's aperture (radiation region), the electromagnetic wave will be pulled towards it, causing the radiation pattern to be single-directional which in turn will improve the antenna directivity (gain). To achieve this purpose, various strategies are discussed in the following paragraphs.

The tapered slot profile of the LTSA depicted in Fig. 21(a) allows for a larger slot size, where five metal strips are added as a director for gain enhancement [52]. Fig. 21(b) and (c) show that, in comparison to LTSA without directive elements, the simulated BW and peak gain are higher by 17.84 % and 26.28 %, respectively. Printed lenses are added in [149] to the aperture of the wideband (1–3 GHz) VTSA shown in Fig. 21(d) to reduce the SLL and enhance its matching and gain by 19.9 % and 11.19 % as shown in Fig. 21(e) and (f), respectively (dash: without lens and solid: with lens).

Since the impedance of anisotropic inhomogeneous (IA) zero-index metamaterials (AI-ZIM) can be easily matched with the background while maintaining high efficiency, they are inserted compactly in [56] based on meander lines to the aperture of UWB VTSA as illustrated in Fig. 22(a) to improve its directivity (gain) and BW. From the measured insertion loss and gain in Figs. 22(b) and 21(c), respectively, one can notice that the BW and maximum gain were enhanced by 1.66 %, 6.33 %, and 26.02 %, and 33.69 % using single and multilayer AI-ZIM, respectively. Authors in [58] inserted compact meander-line-based inhomogeneous epsilon-near-zero artificial metamaterials (IA-ENZ-AM) in the extended dielectric space in front of the UWB VTSA aperture depicted in Fig. 22(d) to enhance the BW and maximum gain by 17.71 % and 18.7 %, respectively as shown in Fig. 22(e). In addition to using a single-layer Linear-to-circular polarization conversion Metasurface (LTC-PCMS) to steer the electromagnetic waves, dual-layered multifunctional MSs are used to enhance the gain and decrease beam width of (9.12–10.2 GHz) VA [150] as illustrated in Fig. 23(a and b).To enhance the directivity of the proposed (2–18.7 GHz) VTSA in [63], three metal patches are loaded in the aperture as illustrated in Fig. 23(c). The simulated BW and maximum gain are enhanced by 5.89 % and 16.79 % as depicted in Fig. 23(d) and (e), respectively.

Dielectric sheets are used to cover the conventional VA (DSCVA) in [68] to enhance the gain and reduce HPBW and SLL without increasing the antenna length, where these sheets are used to couple the space wave to be radiated in the end-fire direction as shown in Fig. 24(a). Moreover, for extra high gain, the designed antenna was elongated with a trapezoid-shaped

Table 1 comparison between TSAs using different compactness techniques (2004–2022).

Ref.	h(mm)/ ε_r	S_{11}(dB)/VSWR at Frequency Band (GHz)	Gain Min-Max (dBi)	C/B↑/M↑/GE↑/CP↓/RE↑/SLL↓/RCS↓ techniques	Feeding	Circuit area mm^2
[99]	1.575 / 2.2	< −10 at 2.8–5.8	4.7	DETSA: C	CPW/S	45 × 36.7
[107]	0.2 /3.1	< −10 at 3.1–10.6	7–12	DETSA: C	SMA	130.70 × 66.4
[136]	0.5 /4.4	< 2 at 1–20	0.9–7.8	Short pin and chip resistor in M/S transition: C, B↑ & G↑	M/S	70 × 62
[108]	1.6 /4.4	< 1.9 at 3.1–10.6	NA	DETSA: C	coaxial	41.32 × 23.22
[15]	1/4.4	< 2.07 at 1.18–4.4	1.63–8.4	Parametric studies: C & B↑	M/S: Radial/ Circular	75 × 75
[82]	0.64 / 10.2	< −7.4 at 2.9 –10.8	2.7–8.54	Parametric studies: C, Constant and varying length corrugations: B↑ & G↑	M/S: Radial/ Radial	36 × 36
[55]	1.5/ 2.65	< −10 at 2–11	NA	DPTSA: C, M↑ & B↑	M/S: Radial/ Circular	60 × 20
[93]	1 /4.4	< −10 at 3–11.4	3–7.4	Horizontally loaded slots: C & B↑	CPW/S	35 × 30
[22]	1.5 /4.4	< −10 at 2.2–6	4.55–7	DETSA with antenna arms rolled back loaded with two lumped resistors: C & B↑	CPW/CPS	258 × 210
[94]	0.8 /4.4	< -9.13 at 3.17–10.9	2.85–8	Rectangular slots on one edge and one triangular slot on the other edge: C, B↑, G↑ & CP↓	CPW/S	36 × 35
[74]	0.5/4.4	< −12 at 2.6–10.2	0.2–5.73	Parametric studies and a tapered cross-feeding shape.: C	M/S: Circular/ Circular	38 × 32
[80]	1 /4.4	< −10 at 2.28–5.68	NA	Parametric studies: C, B↑	M/S: Radial / Rectangular	40 × 27
[57]	1.27/ 6.15	< 2 at 0.46–2.98	max≈ 10 ± 1	suitable small taper slot profile: C	M/S: Radial/ Circular	297 × 190
[20]	1 /4.4	< 2 at 0.64–6	NA	Changing the structure of CPW feed: C, B↑	CPW/S	130 × 70
[95]	0.8 / 4.45	< 2 at 3.1–10.6	1.5–8.1	A pair of quarter circular shapes slots and non-uniform corrugations.: C, B↑, G↑ & CP↓	CPW/S	37 × 34
[115]	0.51 / 3.5	< -10 at 2.75–4.10& 7.85–11.15	0.4–2.97 & 1.42–5.52	Change the radiation patch in to Spidron shape: C	coaxial	35 × 24
[83]	0.8 /4.4	< 1.83 at 3–15.1	5.1–8.2	stepped connection structure: C, BE	M/S: Radial/ Radial	41 × 48
[77]	0.8/4.4	< −10 at 3–12.8	3.7–8.3	Two pairs of eye-shaped slots: C, B↑, SLL↓	M/S: Circular/ Circular	36 × 36
[109]	0.762 / 3.66	< −10 at 6–9	6.3–9	DETSA: C	M/S:Radial/ Circular	49 × 38
[101]	1 /4	< 2 at 0.65–9	3	1. ETSA with Electric-Magnetic type: C, 2. Radial stub with 5 sections Chebyshev impedance transformer: B↑	Radial/CPS	220 × 170
[73]	0.8 /4.4	< −10 at 8–18	NA	A pair of annular slots: C, SLL↓, RCS↓	M/S: Radial/ Circular	18 × 14
[67]	0.8/4.6	< -11.07 at 0.5–6	0.9–8	1. a pair of symmetrically tapered slots: C, 2. Resonant cavity is added to the taper slot profile: B↑, G↑	M/S: Radial/ Circular	258 × 150
[59]	1.6/4.7	< −10 at 3.55–12	3.57–7.54	five pairs of rectangular slits: C, BE	M/S: Radial/ Circular	58.2 × 61
[137]	0.6/4.4	< −10 at 0.36–4	6.2–7.5	Corrugations with three loaded resistors, short pin and rectangle patches.: C, B↑ & G↑	M/S: Rectangle/ Square	115 × 120
[86]	1.58/ 2.2	< -10 (sim) at 2.2–19	3.6–13 (sim)	1. semi-elliptical slots: C, B↑ & GE 2. Stripline with six metallics via metal U-shaped polls, and rectangular grooves: B↑, G↑ & CP↓	M/S: Radial/ Circular	60 × 54
[90]	1/4.4	< −10 at 2.5–11	4.4–8.4	a pair of optimized symmetrical exponential slots.: C & CP↓	M/S: Radial/ Circular	36 × 32

Table 1 *(continued)*

Ref.	h(mm)/ ε_r	S_{11}(dB)/VSWR at Frequency Band (GHz)	Gain Min-Max (dBi)	C/B↑/M↑/GE↑/CP↓/RE↑/SLL↓/RCS↓ techniques	Feeding	Circuit area mm^2
[97]	0.508/ 3.36	< -10.16 at 2.6–20	1.5–11.3	1. a pair of tapered slot edges.: C2. air bridge between tapered flares: B↑, G↑ & CP↓	CPW/S	70 × 50
[30]	1.2/2.6	< 1.87 at 0.93–15.6	4.2–8.7	37 pairs of rectangular slots.: C Ultrathin MAMs at the side edges: RCS↓	M/S: Radial/ Circular	200 × 125
[78]	0.8/4.4	< -10 at 2.92–11.91	5.3–10.3	rectangular slots and multi-section binomial transformer TSP: C, B↑	M/S: Circular/ Circular	100 × 50
[65]	1/2.2	< -11.64 at 0.7–12.7	3–1	1. Parametric studies: C, 2. loading antipodal structure and slotting corrections: B↑, G↑ & RE↑	M/S: Radial/ Circular	25 × 25
[38]	1.6/4.6	< -10 at 0.5–2.5	5–10	different size rectangular slots: C, B↑	M/S: Radial/ Circular	250 × 200
[40]	1.6/4.3	< −10.4 at 1.1–8	4.9–10	optimized symmetric triangular slots s and triangular director.: C, G↑	M/S: Radial/ Circular	55 × 82
[47]	**0.813/ 3.55**	**< -11.15 at 3.14–13.48**	**2.2–6.51**	——	**M/S: Circular/ Circular**	**42.9 × 29.28**
[146]	**0.813/ 3.55**	**< -10.89 at 2.9–13.55**	**1.8–6.91**	——	**M/S: Circular/ Circular**	**29.8 × 20.26**

profile (SP-DSCVA) as shown in Fig. 24(b). The resulting gain, HPBW, and SLL for the designed DSCVA and SP-DSCVA as compared to CVA are shown in Fig. 24(c–e), respectively.

Authors in [151] loaded the (3.5–16 GHz) VA with a mid-frequency metamaterial phase correcting metamaterial lens (MPCL) to enhance its gain (to up to 14.8 dBi), which is proved to be more than the one obtained using the high-frequency MPCL. In [27] and as illustrated in Fig. 25(a), artificial materials lens (AML) and sidelobe suppressor (SSR) are loaded in the aperture and the flanks of the CVA to enhance its gain by 22% (sim) and matching by −1.34 dB (Meas.) as shown in Fig. 24(b) and 24(c), respectively, which make it a good candidate for GPR application. AMs in Fig. 25(a) means both AML and SSR. A cost-effective and efficient 3D printing, fused deposition method (FDM), is used in [130] to fabricate a novel 3D printed DL(7 unit cells) to increase the gain of the proposed broadband (13.5–24 GHz) VA by 6.9 dBi as shown in Fig. 25(d and e) which proves the ability of lens's geometry to completely eliminate strong reflections.

3.2.3. Corrugations and directive materials

As explained in the previous section (3.2.1) that the corrugations help in enhancing the BW and gain, they can be also used with directive elements loaded in (usually called grating elements) or in front of the TSA's aperture (radiation region) to get extra high gain and wide BW. 18.94 %, 9.51 %, and (4.74 % and 28.17 % (Sim)) maximum gains are improved in [29,16,61] by adding corrugations and three strips to the aperture of the tapered radiating slot of WLAN (4.9–5.935 GHz), UWB (2.9 –> 11 GHz) and UWB (4.1–12.8 GHz) VTSAs as illustrated in Fig. 26(a, b), (c, d), and (e and f), respectively. As shown in Fig. 26(a), part of the proposed antenna in [29] is removed for the gradient radome.

In [152], 3 dB gain enhancement is achieved in the proposed compact mmWave (25.13–37.73 GHz) VA with corrugations by adding metamaterial unit cells in its radiating aperture which makes it the best candidate for 5G wireless cellular networks. The layout and the gain of the proposed antenna are shown in Fig. 27(a) and (b), respectively. Congregations and MSs are used to reduce the SLL and enhance the gain of the proposed (3.3–21.6 GHz) VTSA [153]. Authors in[135] add MS lenses (ML) to the aperture of UWB (5.4–18 GHz) EV to enhance its gain by (0.3–3.2 dBi) without affecting its actual size as shown in Fig. 25(c-d).

In [30], to get an antenna with low RCS suitable for stealth application, ultrathin microwave-absorbing materials (MAMs) strips of Double-Face MCS/SS6M are put partially on the 37 slots at the two edges of double-sided copper-clad boards (DSCBs) compact UWB VTSA that was explained in Section 3.1.2. The RCS of the designed antenna is shown in Fig. 28(a). As depicted in Fig. 28(b), H-Shaped Resonator (HSR) structures are added in front of the antenna's aperture and five pairs of transverse slots are etched on the radiation patch of compact C- to X-bands VTSA in [62] to improve the gain and BW by 25.98 % and 3.76 % as shown in Fig. 28(c) and 28(d), respectively. The gain, BW, and radiation efficiency of UWB (0.7–12.7 GHz) VTSA proposed in [65] are enhanced by loading antipodal structure and etching corrections slots, respectively without increasing the antenna size

as illustrated in Fig. 28(e). The enhanced gain is depicted in Fig. 28(f).

ModifiedI-shape MSs with the ability to control the main and side lobes are put in front of (9–14 GHz) VTSAs in order to enhance the gain and reduce the SLLs as shown in Fig. 29(a) [154]. The same design is also used to control the amplitude and phase of electromagnetic waves to get a fan-shaped beam by controlling the geometric configuration and angular orientation of the MSs [155]. The isolation between X-band VAs is reduced by putting a MS wall between them [156]. Authors in [157] used a phase gradient MS (PGM) with a four-split ring (FSR) structure to control the wavefront of VA with corrugations getting multimode radiation with high gain: transmission direction at 15.7 GHz with a peak gain of 20.4 dBi, bidirectional radiation at 16.5 GHz, and reflection direction at 17.1 GHz with a peak gain of 16.5 dBi as shown on Fig. 29(-b-c). In [41] and [132], DL and AML are used to enhance the gain of the modified 5.8 GHz and UWB (4.65–12.65 GHz) VAs with corrugations and groove slots by 6.8 dBi and 2.2 dBi as depicted in Fig. 29(d-f) and (e-g), respectively. Recently,

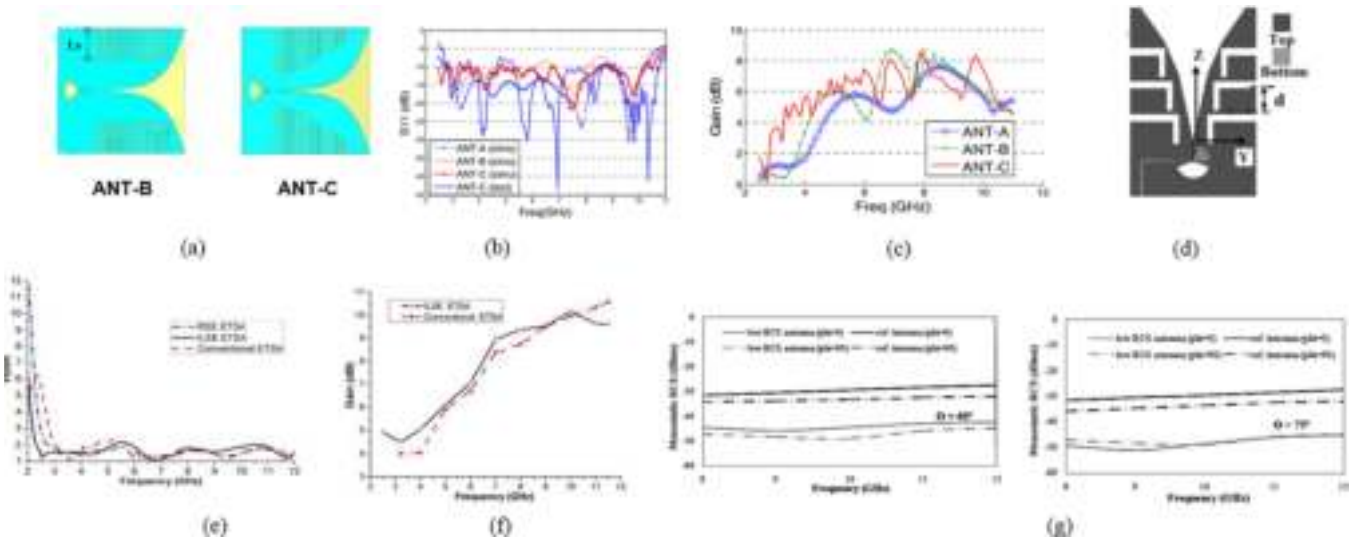

Fig. 17 (a) Layout, (b) S11 and (c) gain of the proposed UWB VTSAs in [82], (d) layouts ETSA with ILSE having d = 8 mm, (e) Simulated VSWR (f) simulated gain for proposed ETSAs [147] and (g) RCS of the compact X-band VTSA in [73].

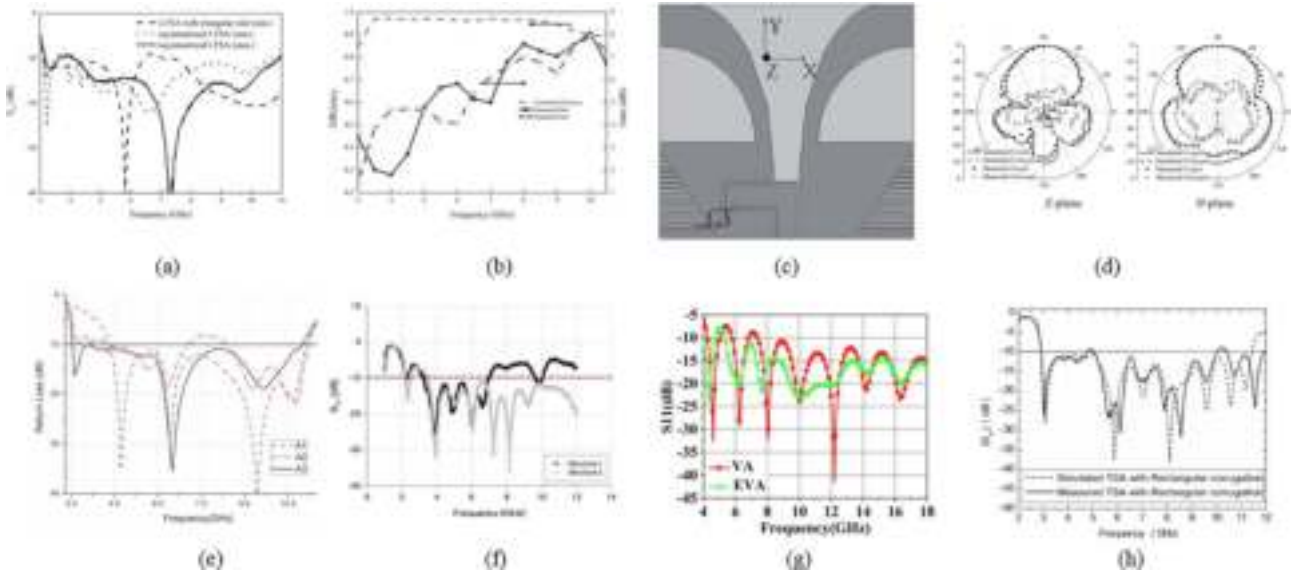

Fig. 18 (a) S_{11} and (b) gain and efficiency of the proposed ALTSA [94], (c) layout and (d) radiation pattern at F = 10 GHz of the proposed ETSA with nonuniform corrugations [95], (e) simulated S_{11} of the broken line TSA with corrugation (A3) as compared to the conventional TSA with (A1) and without corrugations (A2) [93], (f) measured S_{11} for the proposed (3.55–> 12 GHz) VTSA in [59], (g) S_{11} of the proposed BTSA with corrugations in [78] and simulated S11 of the VA compared to the one with ES (EVA) [135].

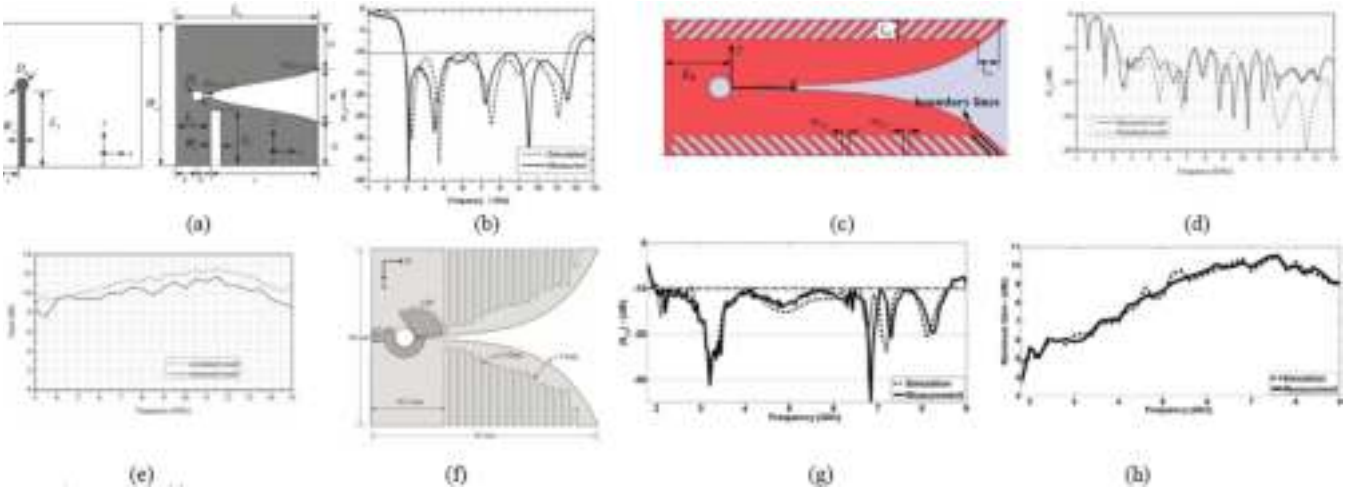

Fig. 19 (a) Layout with W_a = 50 mm, L_a = 50 mm, W = 20 mm, L = 38 mm, L_x = 14 mm, W_1 = 4 mm, D_m = D_s = 2 mm, L_g = 7.5 mm, L_s = 4.5 mm, W_f = 27.5 mm, G = 15 mm, l_1 = 20 mm(m), (b) S_{11} of the proposed UWB squared cosine profile TSA with a slot [114], (c) layout with L_b = 25 mm, l_{ce} = 7.5 mm, and w_{ce} = 2.5 mm, (d) S_{11} and (e) gain of (3–15 GHz) VTSA with exponential slot corrugated edge (ESCE) slots [148], (f) layout, (g) S_{11} and (h) gain of VTSA with optimized rectangular slot with different lengths [60].

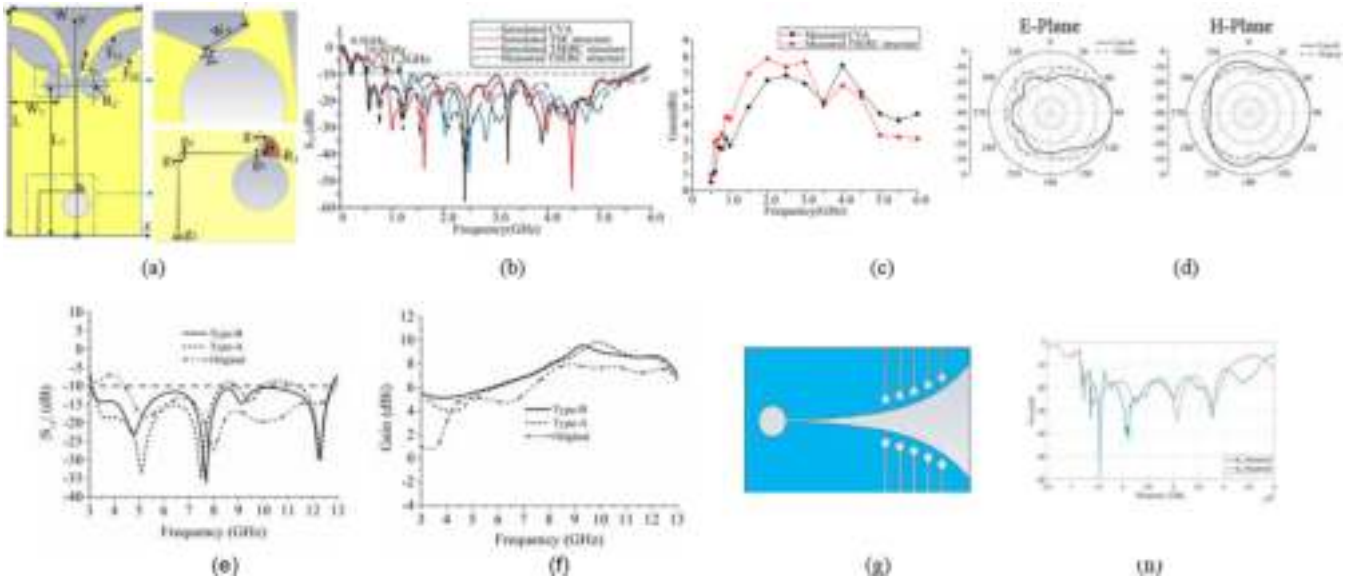

Fig. 20 (a) Layout with W = 150, mm, W_5 = 54.5 mm, W_6 = 13.7 mm, L = 258 mm, L_7 = 172.2 mm, g_1 = 1 mm, g_2 = 1.5 mm, g_3 = 0.5 mm, g_4 = 0.9 mm, g_5 = 0.2 mm, g_6 = 0.5 mm. R_2 = 15 mm and R_3 = 10 mm, (b) s_{11} and (c) gain of TSERC [67], (d) simulated radiation pattern (e) simulated $S_{11,}$ and (f) simulated gain of UWB VTSA with two pair eye-shaped (Type-B) as compared to the original antenna without eye shaped and with one pair eye-shaped (Type-A) [77], (g) layout and (h) S_{11} of the UWB (1.17–4.75 GHz) VTSA [25].

MS and spoof surface plasmon polariton (SSPP) metamaterial are added to the aperture and slotline of the proposed wideband (15–27 GHz) VTSA with corrugations for gain enhancement (8–10 dBi) and radio frequency interference (RFI) mitigation, respectively. The gain is illustrated in Fig. 29(h).

Adding an extra dielectric structure to the aperture of the slot antenna, will increase the directivity and reduce the beamwidth [36] as explained in the following equations.

$$\text{Directivity [dB]} = 10\log(10\frac{L_d}{\lambda_0}) \tag{2}$$

$$\text{Bandwidth [}^\circ\text{]} = \frac{55}{\sqrt{L_d/\lambda_0}} \tag{3}$$

where L_d is the length of the extra dialectic added at the aperture of TSA and λ_0 is the free space wavelength.

With the help of etching three pairs of squared slots on the antenna radiator to reduce the size while increasing the gain of the proposed UWB TSA in [36], extra gain is achieved by adding a semi-circular structure to the tapered aperture edge. The layout and the simulated gain are shown in Fig. 30(a) and (b) where the simulated maximum gain of the proposed antenna is improved by 12.58 % and 7.76 % as compared to the conventional TSA and TSA with the three slots only, respectively. In addition to the corrugations used to compact the size of the UWB VA explained in [40], one triangular director is loaded in front of the antenna aperture to reduce the beamwidth

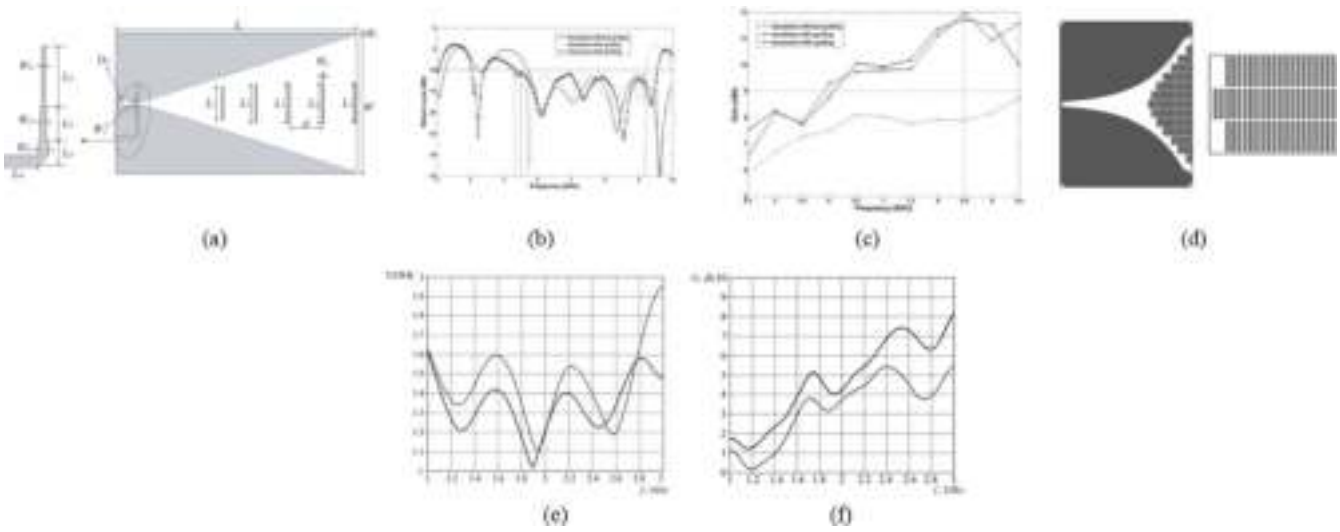

Fig. 21 (a) Layout with grating having L = 84 mm, W = 48 mm, L_1 = 11.48 mm, L_2 = L_3 = L_4 = L_5 = 11.5 mm, d = 11.7 mm, D_{sl} = 1.8 mm, W_g = 0.2 mm, W_s = 3 mm, W_{sl} = 1 mm, W_{f1} = 0.4 mm, W_{f2} = 0.75 mm, W_{f3} = 1.55 mm, L_{f1} = 10.6 mm, L_{f2} = 5.5 mm, L_{f3} = 4.05 mm, and L_{f4} = 7.73 mm, (b) S_{11} and (c) gain of the proposed LTSA [52], (d) layout and simulated (e) VSWR and (f) gain of wideband (1–3 GHz) VTSA [149].

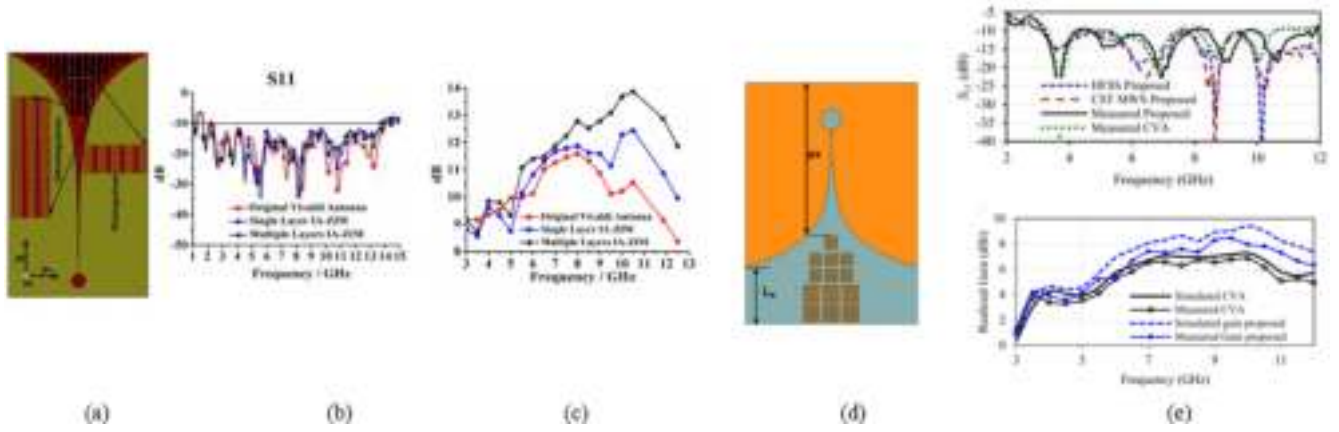

Fig. 22 (a) Layout, (b) S_{11} and (c) gain of the original and IA-ZIM-based VAs [56], (d) layout with px = 37.5 mm and Le = 15 mm, (e) S_{11} and gain of the proposed VTSA with IA-ENZ-AM [58].

and increase the maximum gain by 24.6 %. The enhanced gain is shown in Fig. 30(c).

3.2.4. Modifying the structure of the antenna

Changing the structure of TSA for performance enhancement includes either changing the taper slot profile, changing the shape of the radiation patches, or using multilayer substrates. By modifying the VTSA in [55] to be DPTSA, BW and matching are enhanced by 2.09 GHz and −2.359 dB as illustrated in Fig. 31(a) and (b), respectively. However, in [22], the impedance matching, and BW are enhanced by modifying the structure of compact DETSA where two arms of the antenna are rolled back. In addition, two lumped resistors are used near the end of these arms to mitigate the effect of reflected waves. This new DETSA can be considered a good candidate for target detection. The simulated S_{11} of the proposed antenna with different resistors as compared to the normal DETSA is shown in Fig. 31(c). In [159], gain and BW enhancement are achieved by making TSA's profile based on a multi-section quarter-wave binomial impedance transformer with further smoothing for extra enhancement as shown in Fig. 31(d–g).

Cross polarization was mitigated in [160,90] below −30 dB and −40 dB by using low permittivity substrate with back-to-back double layers in the design of UWB VTSAs and using symmetrical dual-layer structure in the (2.5–11 GHz) VTSA, as shown in Fig. 32(a) and (b), respectively.

3D printed manufacturing, which enables exact modeling, low cost, and simple processes, has lately been considered in antenna design. In [161], the structure of the 3D VA is changed from a simple notch to a bilateral to improve the BW and gain. The layout and resulting simulated S_{11} with gain for 3D simple notch and bilateral Vas are illustrated in Fig. 33(a–d).

3.2.5. Modifying the feeding

This section talks about different techniques used to feed TSAs and how can be exploited to enhance their performance in

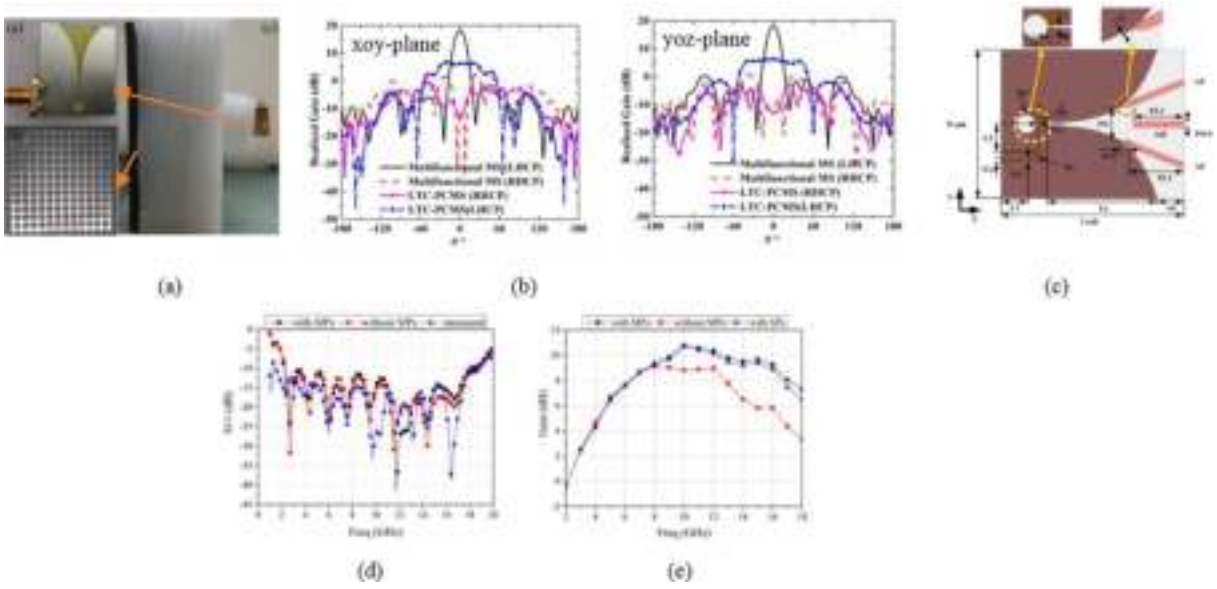

Fig. 23 (a) The fabricated sample and (b) 2D radiation patterns at 10 GHz [150], (c)layout with Wsub = 50 mm, W1 = 1.72 mm, W2 = 1.2 mm, W3 = 0.5 mm, R0 = 3.1 mm, R2 = 4 mm *La* = 38 mm, Pw = 7 mm, PL2 = 18,7 mm, PW0 = 2.2 mm, S = 0.6 mm, Lsub = 52.5 mm, L1 = 8.8 mm, L2 = 8.72 mm, Lf = 3 mm, R1 = 4.2 mm, ɵ = 75°, Ad = 9 mm, PL1 = 2.5 mm, PL3 = 17 mm, T = 0.762 mm, Ps = 0.26 mm, (j) S_{11} and (k) gain of the proposed (2–18.7 GHz) VTSA with three metal patches (MPs) [63].

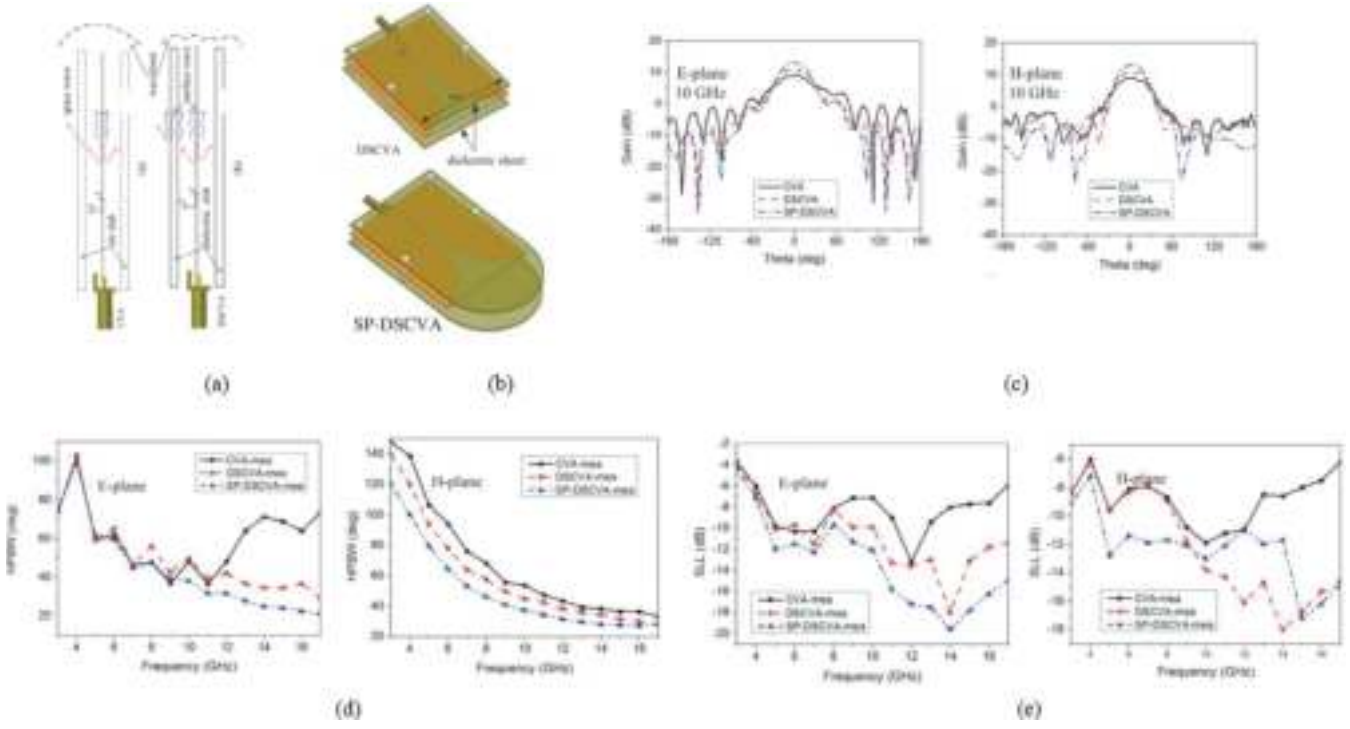

Fig. 24 (a) Schematic diagram of EM waves emitted from the antenna board of CVA and DSCVA, (b) layout of DSCVA and SP-DSCVA, (c) radiation pattern at F = 10 GHz, (d) HPBW and (e) SLL of DSCVA and SP-DSCVA as compared to CVA [68].

terms of matching, BW, and gain. The (M/CPS) transition in [89] is used to enhance the BW of the designed mmWave (23 –> 80 GHz) LTSA and ETSA as shown in Fig. 34(a) and 34 (b), respectively. The minimization of impulse distortion is obtained in [162] by replacing M/S (radial/circular) with via to open slotline transition. The layout and the resulting transmitted characteristics are shown in Fig. 34(c) and (d), respectively (see Fig. 35 .

In addition to the benefit of loading the short pin and chip resistor to the microstrip stub and slotline, respectively to over-

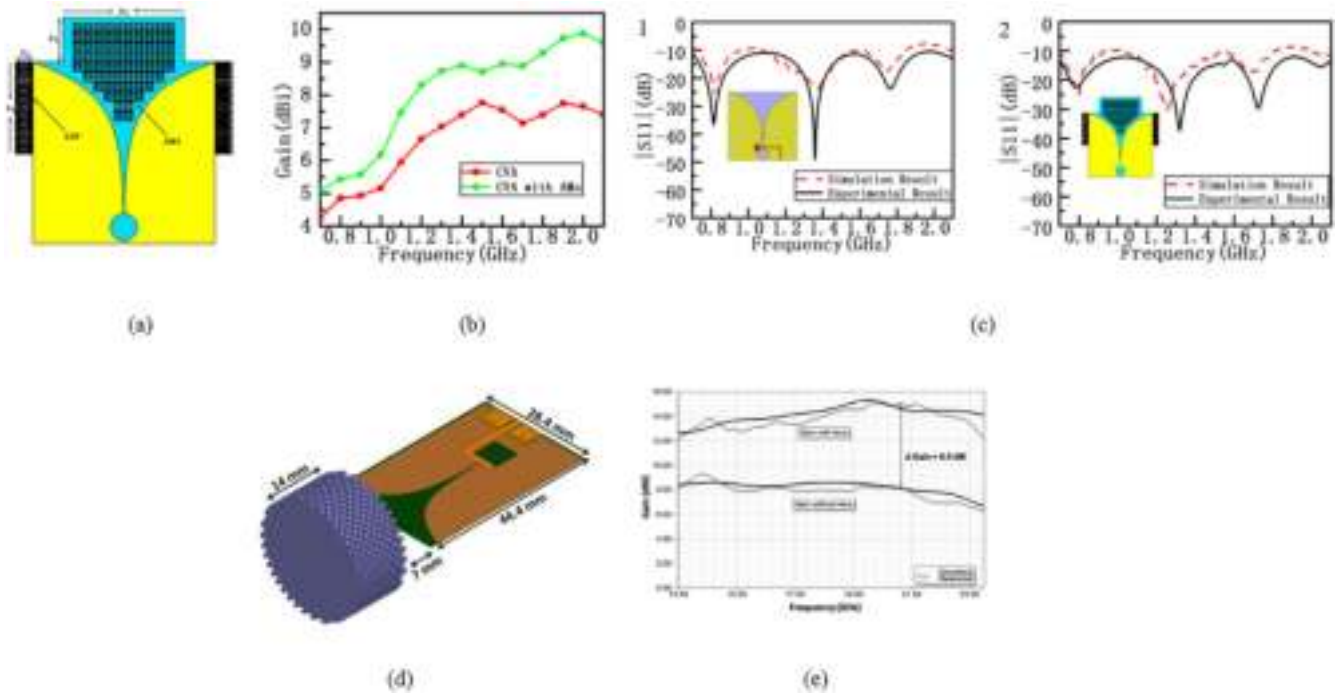

Fig. 25 (a) layout with x_3 = 60 mm, x_4 = 121 mm, y_3 = 160 mm, and y_4 = 23 mm, and (b) simulated gain of (0.7–2 GHz) VTSA with and without AMs and (c) S_{11} of (1) CVA and (2) CVA with AMs [27], (d) layout and (e) gain of the broadband (13.5 to 24 GHz) VA with 3D DL [130].

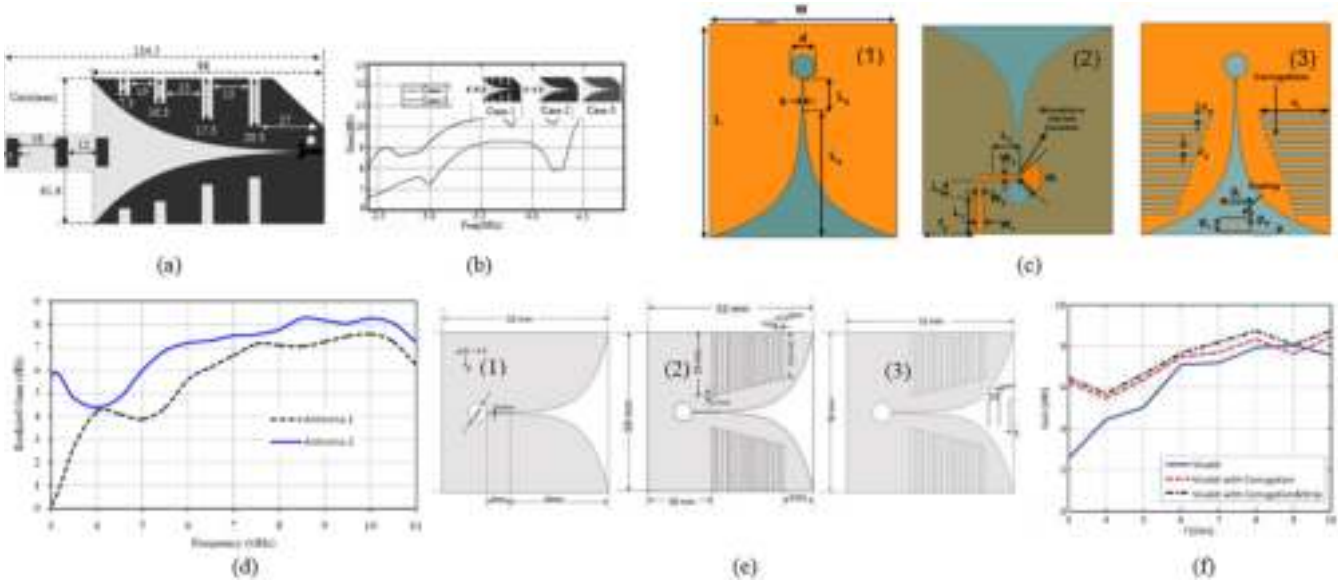

Fig. 26 (a) Layout and (b) measured gain of the WLAN VTSA [29], (c) (1): top view with L = 45 mm, W = 40 mm, Ls = 5 mm, La = 28.5 mm, s = 0.4 mm and d = 5 mm, (2): bottom view of antenna 1 with L1 = 8 mm, L2 = 3.2 mm, L3 = 1.3 mm, W1 = 1.5 mm, W2 = 1 mm, W3 = 0.75 mm, th = 45°, and fp = 11.2 mm and (3): antenna 2 with cl = 15 mm, cw = 1 mm, cs = 1 mm, gl = 7 mm, gw = 0.3 mm, gs = mm and p = 0.5 mm and (d) simulated gain [16], (e) layouts of UWB VAs: (1) top view of Vivaldi; (2) top view of Vivaldi with corrugation; (3) top view of Vivaldi with corrugation and strip and (f) measured gain of UWB (4.1–12.8 GHz) VTSA [61],

come the effect of BW limited frequency-dependent components, they improve the BW (1–20 GHz) and gain (7.8 dBi) of the proposed VTSA in [136]. The limitation of the resistors on the antenna radiation is considered while designing the antenna. However, in [137] using the chip resistor and short pin to enhance the BW, the microstrip line is designed using four sections with different lengths to improve the matching at the feeding transition. Two patches are also added to overcome the effect of the feeding resistor on the gain so the antenna can provide a maximum realized gain of 5.8 dBi.

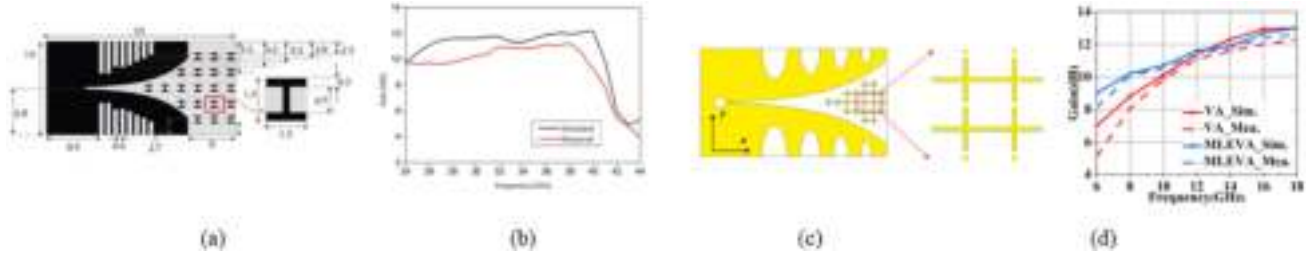

Fig. 27 (a) layout and (b) gain of compact mmWave (25.13–37.73 GHz) VA with corrugations and metamaterial unit cells [152] and (c) layout and (d) gain of compact UWB(5.4–18 GHz) VA with corrugations and metamaterial unit cells [135].

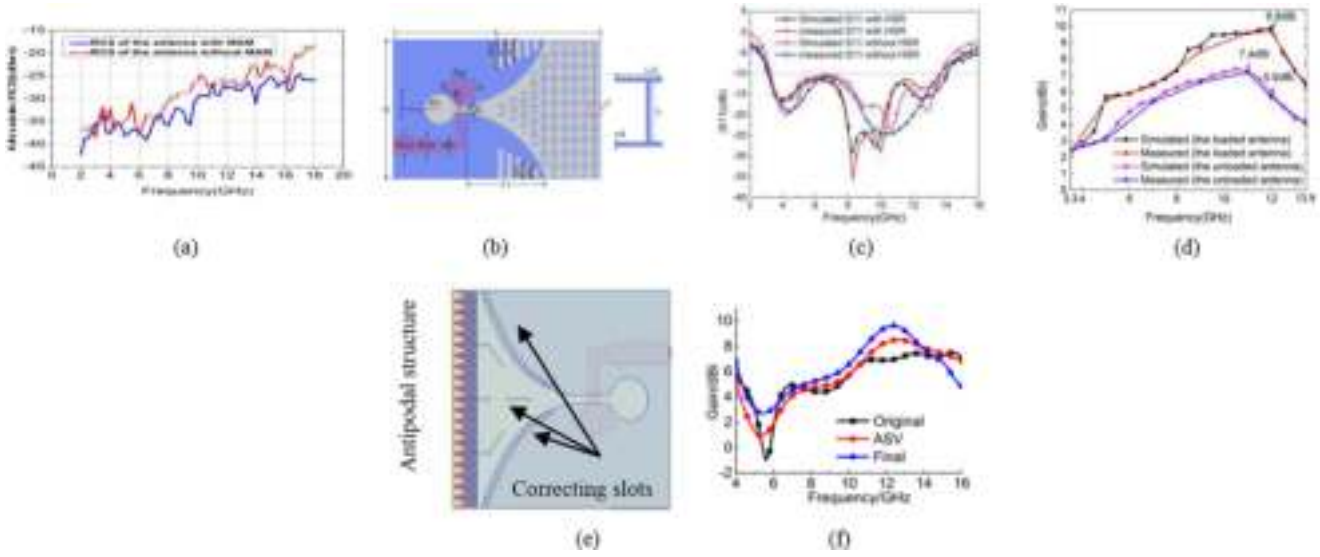

Fig. 28 (a) RCS of the compact UWB VTSA in [30], (b) layout with W = 29 mm, Rr = 4.1 mm, Ld2 = 8.1 mm, dsl = 3.8 mm, Wst1 = 2.2 mm, Ld3 = 7.2 mm, and Arp = 100°, (c) S11 and (d) gain of C- to X-bands VTSA in [62], (e) layout of ASV with correcting slots (Final) and (f) its simulated gain as compared to the ASV and original antennas [65].

Moreover, two resistors are used to enhance the S_{11} by absorbing the reflected wave from the cut end of the antenna. In [102], a compact UWB balun was designed to feed the VA with two symmetrically exponential tapered patches to enhance the BW, gain, and reduce the cross-polarization level. Layout, S_{11}, gain and radiation patterns of the proposed antenna are shown in Fig. 36(a–d), respectively. Fig. 36(e) shows a stripline with six metallic vias used in [86] to broaden the BW of the compact UWB (2.2–19 GHz) VTSA explained in Section 3.1.1 and Fig. 9(g). Moreover, U-shaped metal polls with rectangular grooves are used to enhance the radiation performance in terms of BW, gain (13 dBi), and low cross-polarization level (below −28 dB). The simulated VSWR and gain of this antenna are illustrated in Fig. 36(f) and (g), respectively.

Authors in [111,105] exploit the corrugations, modifying slot profiles and feeding for performance enhancement. BW and gain are enhanced in [111] using a logarithmically tapered slot profile and multi-section matching transformer at feeding. Then they used CPW feeding, and corrugations in [105] to get extremely enhanced BW. The layout, VSWR, and gain of the proposed antennas in [111] and [105] are shown in Fig. 37(a-c) and (d-f), respectively.

Table 2 illustrates the comparison between the proposed TSAs in the literature using enhancement techniques explained in Sections 3.2.1, 3.2.2, 3.2.3, and 3.2.4.

3.2.6. Optimization techniques

The antenna performance can be also enhanced using optimization techniques such as finite-difference time-domain (FDTD), differential evolution (DE), and particle swarm optimization(PSO). Based on optimum parametric (strip stub, slot line circle, and rate) simulation using FDTD, good radiation performance in terms of directivity and BW is achieved in the proposed UWB VA [163]. However, a genetic algorithm (GA) based on FDTD, was used for the optimization process to enhance the gain (12.27 dBi) of UWB VTSA [164]. Based on the CST software, the DE optimization technique is used to generate energy patterns with low SLL during beam scanning of the proposed UWB antenna arrays [165]. Recently, authors in [166], use the PSO algorithm to optimize the space between the 3D 4 × 4 dual-polarized (2–40 GHz) VA array, in order to suppress the gating lobes (−8 dB to −10 dB) which proved to be better than other suppression techniques such as Gaussian, triangular and raised cosine. For wireless optical network-on-

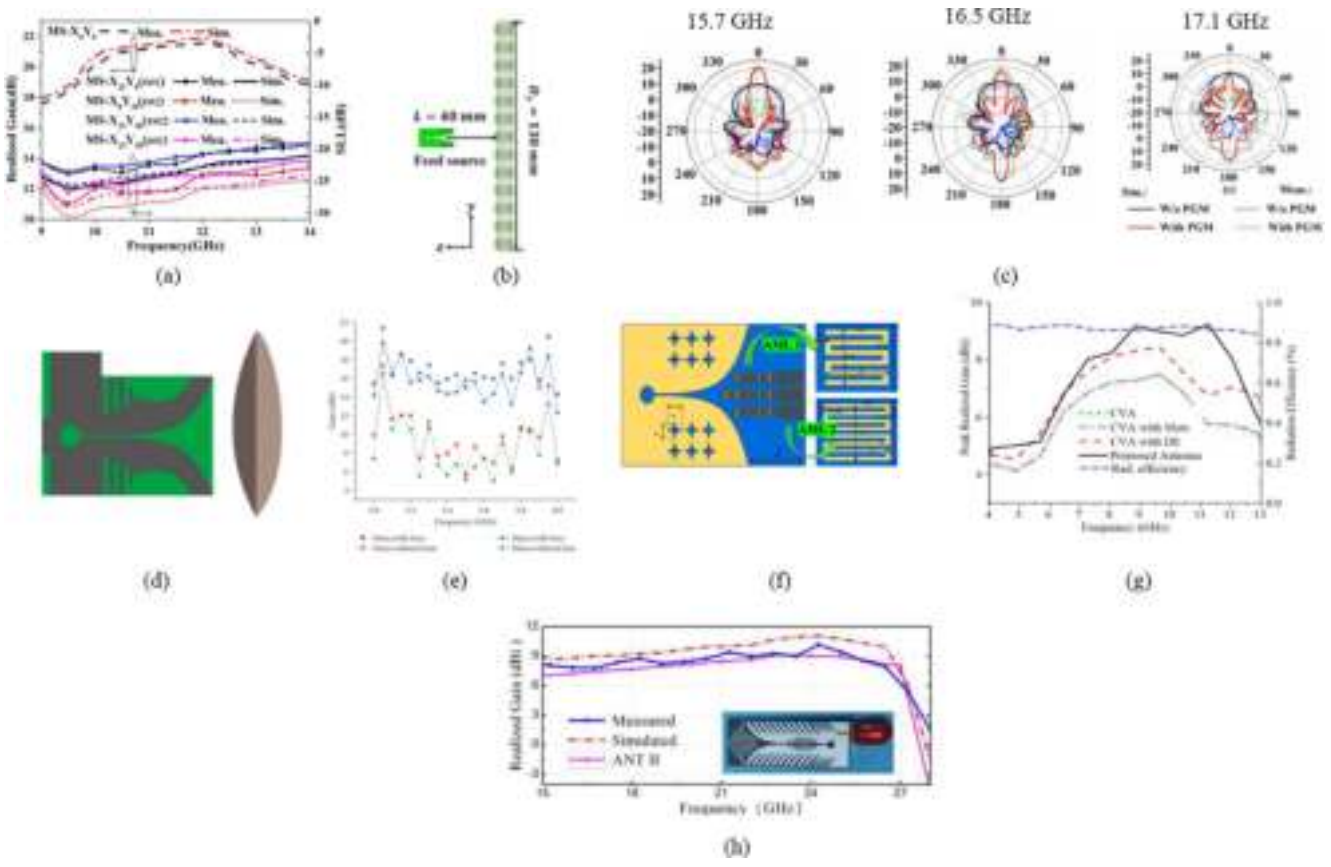

Fig. 29 (a) gain and SLL of the proposed VTSAs loaded with MSs in [154], (b) layout and (c) radiation patterns of the proposed system in [157], (d), (f) layout and (e),(g)gain of the 5.8 modified and UWB VAs proposed in [41,132], respectively and (h) the gain of the proposed wideband (15–27 GHz) VTSA [158].

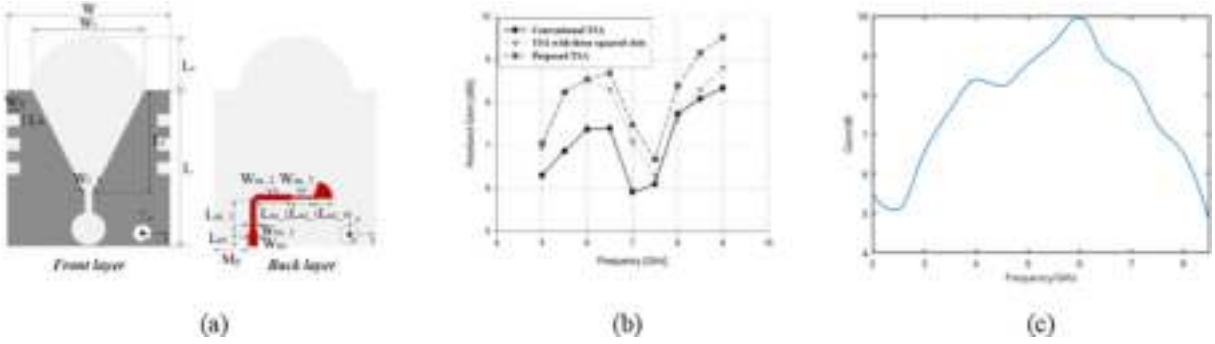

Fig. 30 (a) Layout with L = 60 mm, W = 55 mm, Lt = 40 mm, W_t = 44 mm, W_{t_1} = 3.6 mm, L_m = 17 mm, W_m = 2.5 mm, L_{m_1} = 9.57 mm, W_{m_1} = 2 mm, L_{m_2} = 8 mm, W_{m_2} = 2 mm, L_{m_3} = 7 mm, W_{m_3} = 0.9 mm, L_{m_4} = 4.1 mm, L_s = 6 mm, W_s = 6 mm, and L_r = 22 mm and (b) the simulated maximum gain of the proposed antenna in [36] and (c) simulated gain of the proposed UWB VA with corrugations and director [40].

chip applications. The parameters of VAs integrated with silicon waveguides are optimized based on FDTD simulations to improve the radiation performance (gain and directivity) [167–169].

3.2.7. Use of array

Gain can be enhanced using a group of individual elements or an array [2]. Different types of arrays are discussed in this section, along with various approaches for improving TSA performance for various applications. Avoiding high cost, large size, and difficulties in designing a suitable director to increase the directivity, the tapered slot profile of TSA is doubled to have a simple array allowing the BW to be used efficiently [75,116]. Directivity enhancement is achieved in [75] using E plane double slot structure in VA resulting in a novel double structure VA (DSVA) as shown in Fig. 38(a) with 3.9 % BW

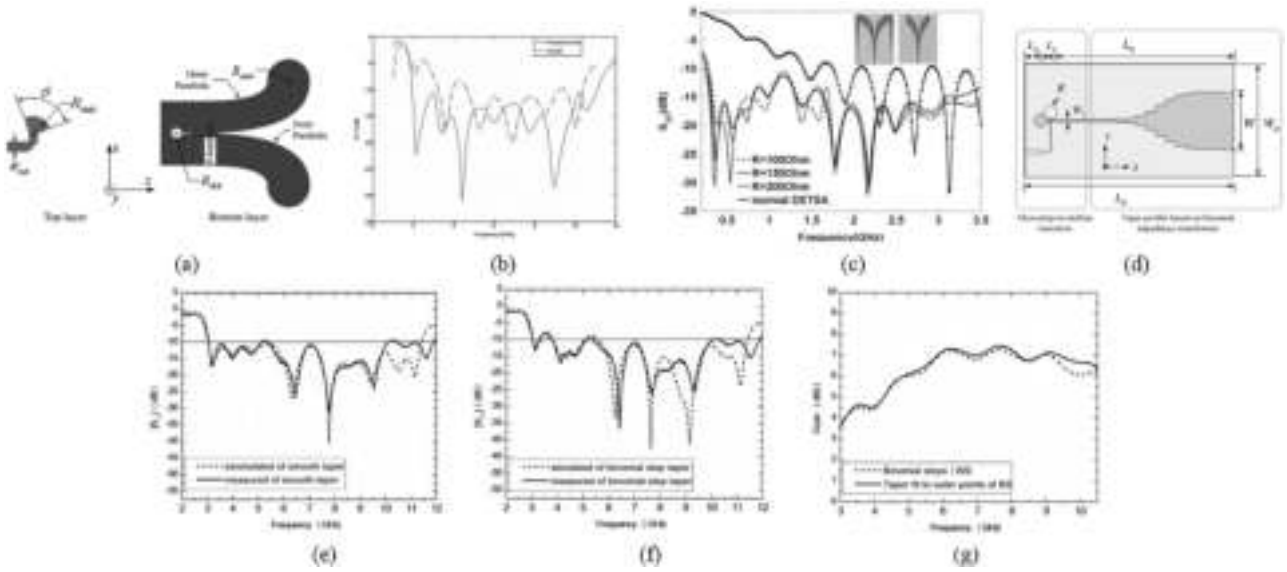

Fig. 31 (a) Layout of DPTSA with W_{stub} = 4.14 mm, R_{stub} = 8 mm,ɵ = 100° and R_{slot} = 2.5 mm, (b) Simulated S_{11} as compared to VTSA [55] and (c) simulated S_{11} of the antenna with loading resistors of different values and S of a normal DETSA [22], (d) layout, (e) S_{11} without smoothing the taper, (f) S_{11} with smoothing the taper, and (g) simulated gain of the proposed antenna in [159].

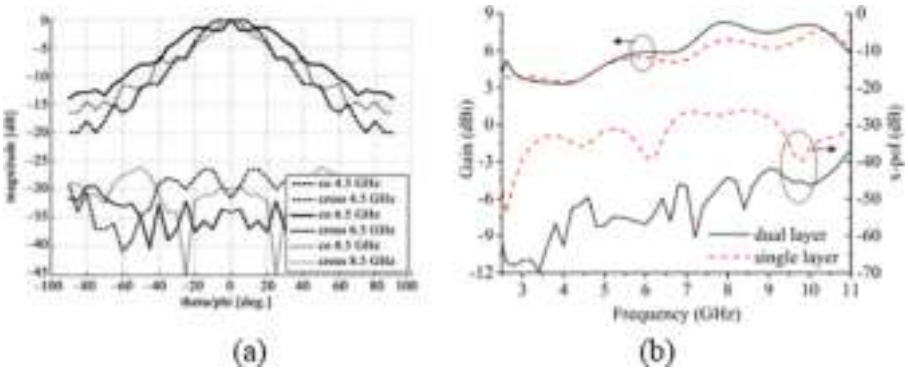

Fig. 32 (a) Cross polarization of double-layered structure (2.5–10.6 GHz) VTSA [160], and (b) cross-polarization and gain of double-layered structure (2.5–11 GHz) VTSA [90], respectively.

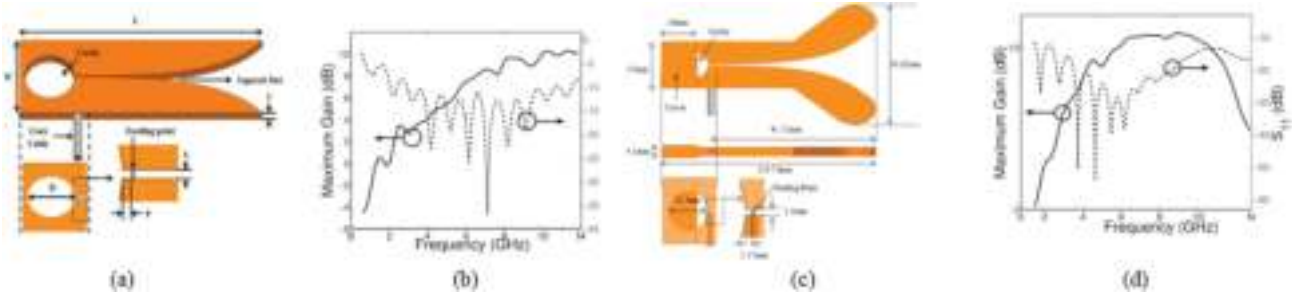

Fig. 33 (a), (c) Layout, and(b), (d) simulated S_{11} with the gain of the 3D simple notch and bilateral VAs, respectively [161].

and 18.62 % maximum gain enhancement as compared to CVA. Fig. 38(b), (c), and (d) show the S_{11}, E, and H radiation patterns at 10 GHz, respectively.

In addition to the ability of double slot TSA to increase the directivity, etching slots on its edges improves the BW and matching as in [76,116,117]. To enhance the directivity and BW of the proposed UWB E-plane monopulse 2-layered DSVA fed with different ports in [76], the authors shorted the length between the two slots and added diagonal rectangular-shaped corrugations as shown in Fig. 39(a–c).

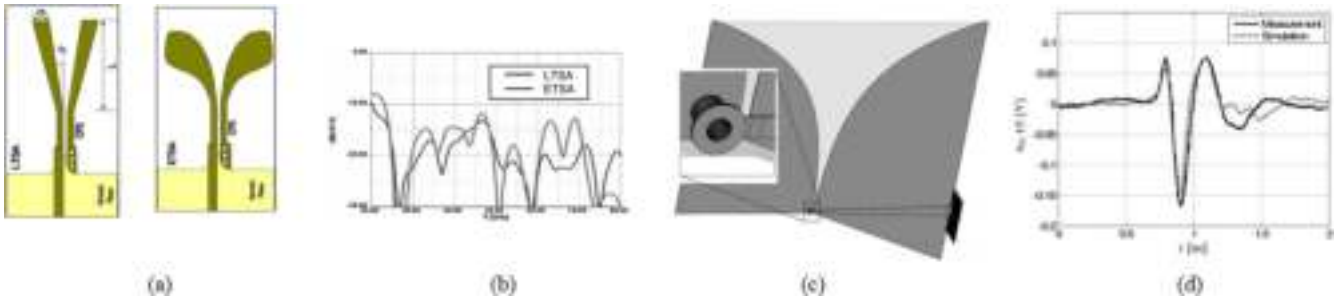

Fig. 34 (a) Layout and (b) S_{11} of the proposed mmWave (23–>80 GHz) LTSA and ETSA in [89], (c) layout and (d) transmitted characteristics of the proposed VA with Via to open slotline transition [162].

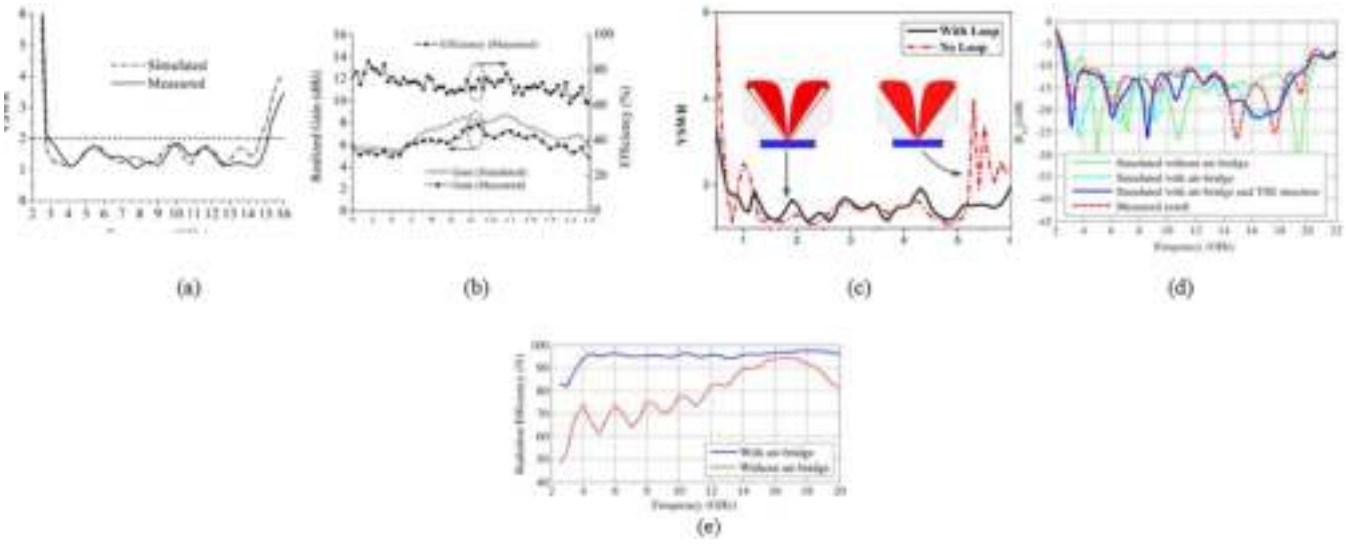

Fig. 35 (a) VSWR and (b) gain of the proposed compact UWB TSA in [83], (c) VSWR of the proposed ETSA with and without loops [101] (d) simulated S_{11} and (e) simulated gain with the efficiency of the (2.6–20 GHz) TSA in [97].

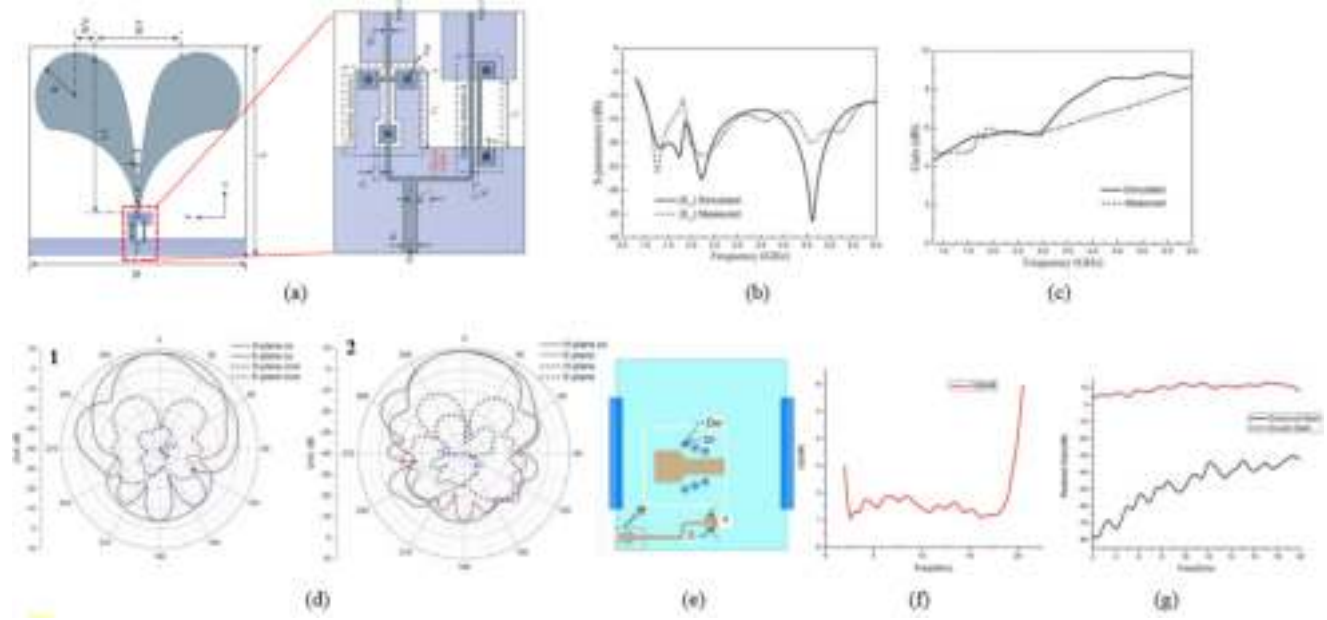

Fig. 36 (a) Layout with W = 133 mm, W4 = 15 mm, W5 = 52.3 mm, L = 117.5 mm, L3 = 88 mm, S = 0.95 mm, R = 22 mm, W1 = 1.05 mm, W2 = 1.5 mm, w3 = 0.3 mm, L1 = 4.9 mm, l2 = 4.2 mm, s1 = 0.4 mm, S2 = 0.17 mm and d = 0.6 mm, (b) S_{11}, (c) gain and (d) radiation pattern at (1) 4 GHz and (2) 6 GHz of the proposed VA with compact UWB balun [102], (e) schematic of stripline patch, (f) simulated VSWR of and (hg) simulated-polarization and cross-polarization gain the compact UWB (2.2–19 GHz) VTSA in [86].

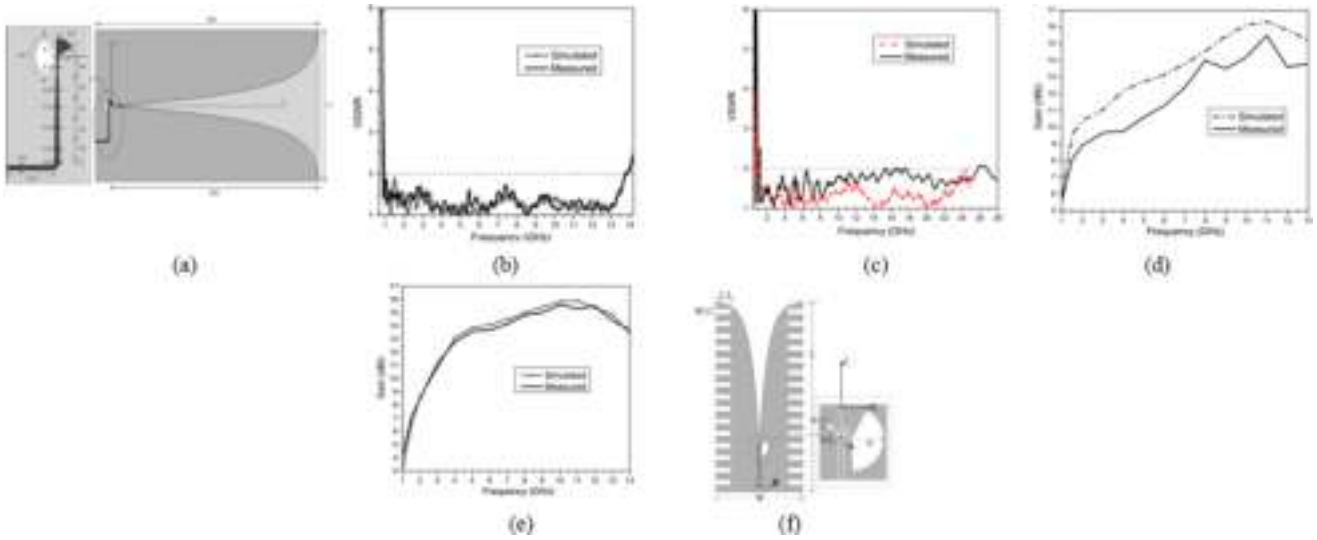

Fig. 37 (a), (d) Layout, (b), (e) VSWR and (c), (f) gain of the proposed antenna in [111] and [105], respectively.

However, in [116] the directivity and BW of the designed UWB (2.5–28 GHz) double slot TSAs are improved using a V-shaped metal with straight edges adding Y and diagonal rectangular shaped corrugations as illustrated in Fig. 39(d-f).

The author in [72] loaded the zero-index metamaterial (ZIM) unit cells to the DSVA illustrated in Fig. 40(a) to get extra enhanced directivity as compared to CVA as depicted in Fig. 40(b). The gain of the Ka-band (24–40 GHz) VA in [122] is enhanced to 16.9 dBi by adding a long parasitic core element at the feed point between the two taper slots depicted in Fig. 36(c). The gain is shown in Fig. 40(d). For Extra high gain and enhanced BW, DSVAs are loaded with parasitic and slots edges [118-120]. Index-near-zero MS unit cells, a half elliptical shape DL, and a semicircle director are added with etching a pair of defected grand slots (DGS), 24 pairs of different length rectangular slots, and 24 pairs of diagonal rectangular slots to enhance the gain and BW of the compact size (1.13–12 GHz) [120], (4.2–11 GHz) [18,119] and UWB DVSAs [118], respectively. Fig. 41(a–c) and (d–f) show the prototypes, S_{11}, and gain of the DSVAs in [120] and [119], respectively. In [88], the low-loss SIW binary divider with GCPW to SIW transition is used to enhance the BW, gain, matching, and suppressing higher order modes of the proposed 1 × 8 (7–9 GHz) Vivaldi array. The proposed array with the resulting S_{11} and gain are shown in Fig. 42(a–c), respectively.

The multi-input multi-output (MIMO) is considered an enhancement technique used to improve the gain, diversity, and data capturing ability of TSA as in [38,170-172]. The compact, high gain UWB (0.5–2.5 GHz) VTSA is exploited in [38] to build UWB MIMO radar system based on 16 elements to increase the resolution for through wall detection. Two elements compact with low envelope correlation coefficient (ECC) UWB (2.9–11.6 GHz) and (2.5–12 GHz) MIMO VAs are designed in [170,171] with two notch bands 5.3–5.8 GHz and 7.85–8.55 GHz, and 5.1–5.9 GHz and 6.6–7.1 GHz, respectively. The notch bands and the isolation between the elements are achieved using two split ring resonators (SRRs) and T-slot as shown in Fig. 43(a) and (d). Four resistors are used in [171] for more compactness. Results of the proposed antennas in [170,171] are illustrated in Fig. 43(b-c) and (e-f), respectively. Recently, 73 % gain enhancement is achieved for the proposed compact mmWave (24–32 GHz) 4-elementsVivaldi MIMO antenna in [172] by distributing the MS loading spatially to decrease the phase error as illustrated in Fig. 44(a). Fig. 44(b) and (c) depict the S-parameters and gain with efficiency, respectively. The ECC and total active reflection coefficient (TARC) provided by the proposed antenna are <0.2 and >10 dB, respectively as shown in Fig. 40(d).

An enhanced BW of 1.6–9 GHz and a wide scan angle of 45° are achieved using a 1 × 8 DPTSA phased array in [55] for telecommunication and radar applications. Gain is improved using 1 × 8 VTSA arrays based on WPD and T-junction feeders in [11,39,40] as illustrated in Fig. 45(a) and (c), respectively. The gain of the proposed array in [11] is shown in Fig. 45(b). In [40] and as compared to the single element explained in Section 3.1.2 and Fig. 10(g), the simulated maximum gain of the proposed array is enhanced by 39 % and the E plane HPBWs are reduced by 56.1 %, 58.2 %, and 55.4 % at 2 GHz, 3 GH and 4 GHz, respectively. The enhanced gain and reduced HPBW are shown in Fig. 45(d) and 45(e), respectively. In [39] and based on the single TSA shown in Fig. 45(f), a high gain of 10.75 dBi is obtained by building a 2 × 4 TSA array resonating at 4.3–4.75 GHz, 5.3–6.4 GHz, and 6.8–7.7 GHz as shown in Fig. 45(g) and (h), respectively.

The 1 × 4 VTSA arrays aligned in H-plane are proposed in [71,35] based on T junction and flexible Microstrip- Slotline-Microstrip (MSM) power dividers to enhance BW and gain as shown in Fig. 46(a-c) and 46(e-f), respectively.

For enhanced performance, the 3 × 4 VTSA array in [173] is mounted inside a cavity absorber material as shown in Fig. 47(a). Moreover, corrugations are added to the cavity and absorber to reduce the resonance effect. The S_{11} and gain of the designed array are depicted in Fig. 47(b). Suitable for wireless communications in airborne systems and to avoid the large size of wide scan angle planar antenna array, 3(E-plane) × 4(H-plane) multi-layered metal VA array integrated with flush mountable 3D printed lossless metallic cavity is designed in [174,175] with enhanced BW of 5 GHz, a maxi-

Table 2 Comparison between TSAs using different Enhancement techniques: corrugations, directive materials, modifying the antenna structure, and modifying the feeding (2009–2023).

Ref.	h(mm)/ εr	S_{11}(dB)/VSWR at Frequency Band (GHz)	Gain Min- Max (dBi)	C/B↑/M↑/G↑/D↑/CP↓/RE↑/SLL↓/RCS↓/HPBW↓techniques	Feeding	Circuit area
[111]	0.6 /2.65	< 2 at 0.89–13.8	4.2–15.6	LogTSA and multi-section matching transformers: B↑ & G↑	M/S: Radial/Radial	300 × 170
[105]	0.6 /2.65	< 2 at 1.19–25.8	5.6–15.5	LogTSA, Corrugations and CPW feed: B↑ & G↑	double-Y balun	371.19 × 170
[52]	0.5/2.2	< −10.4 at 5.32–9.55	7.92–12	five metal strips in the aperture: B↑ & G↑	M/S: Rectangular/ Circular	84 × 48
[56]	0.5/2.65	< −11.84 at 2.26–14.1	9.21–1155	Without IA-ZIM: B↑ & G↑	M/S: Radial/Circular	140 × 80
		< −12 at 1.7–13.74	8.48–12.45	Single layer IA-ZIM is added to aperture: B↑ & G↑		
		< −13.561.7–14.34	8.77–13.87	double layers IA-ZIM are added to aperture: B↑ & G↑		
[114]	1.6/4.4	< −10 at 2.96–12.07	2.82–6.47	One rectangular slot in the radiation patch: M↑	M/S: Circular/Circular	50 × 50
[29]	1/4.4	< 1.94 at 4.9–5.935	1.2–9.2	Corrugations and directors: B↑ & G↑	M/S: Y/Y	70 × 62
[148]	1/2.65	< −10 at 3–15	7.6–11.72	exponential slot corrugated edge (ESCE): B↑ & G↑	M/S: Circular/ Rectangular	125 × 50
[16]	0.8/4.4	< −10.6 at 2.9–11	4.4–8.32	Corrugations and directive elements: B↑ & G↑	M/S: Radial/Circular	40 × 45
[159]	0.8/4.4	< -8 at 3.08–11.95		binomial step taper profile: B↑ & G↑	M/S: Circular/Circular	> λmax × 0.5 λmax
		< -9.3 at 3.06–11.88	3.13–7.07	smoothing taper profile: B↑ & G↑		
[102]	0.508/ 3.38	< −10 at 6–9	4.7–8.1	30: 1 bandwidth ratio balun: B↑, CP↓	30: 1 bandwidth ratio balun	133 × 11
[58]	0.8/4.4	< −9.8 at 3.15–12	3.22–6.87	Without IA-ENZ-AM	M/S: Radial/Circular	45 × 42
		< −10 at 3.3–10.59	3.66–8.45	IA-ENZ-AM is added to aperture: B↑ & G↑		
[60]	1.52/3.5	< −10 at 1.96–8.61	5.6–10.4	Adding rectangular slots to the radiator's two edges in a tapered way: B↑ & G↑	M/S: Radial/Circular	50 × 62
[68]	1.524/ 3.38	< −10 at 3.5–16.5	5.3–13.1	DSCVA: G↑/SLL↓/HPBW↓	M/S: Radial/Circular	34.5 × 28.4
		< −10 at 3.5–16.5	5.72–15.3	SP-DSCVA: G↑/SLL↓/HPBW↓		
[62]	1/2.2	< −10 at 3.3–13.9	2.4–9.9	HSR added to aperture and transverse slots etched on the edges: B↑ & G↑	M/S: Radial/Circular	38 × 29
[61]	0.51/ 2.33	< −9.7 at 4.1–12.8	6.48–8.73	Corrugations and directors: B↑ & G↑	M/S: Radial/Circular	50 × 52
[63]	0.762/ 3.48	< -12.45 at 1.34–18.5	Max 10.7	three metal patches are loaded to the aperture: B↑ & G↑ (D↑)	M/S: Radial/Circular	50 × 52.5
[25]	1.5/4.3	< −10 at 1.17–4.75	NA	Corrugations: narrow beam, high resolution, and depth penetration (1 m-1.15 m)	M/S: Radial/Circular	200 × 100
[36]	1.62/4.5	< 2 at 4.5–12	7.59–8.92	Corrugations and semi-circular structure: B↑	M/S: Radial/Circular	82 × 55
[152]	2.33/ 0.254	< -10.33 at 25.13–37.74	9.84–11.13	Corrugations and metamaterials: G↑	M/S: Rectangular/ Rectangular	33 × 14
[27]	1.52 /4.3	< −10 at 0.7–2.1	5–9.9 (sim)	AML and SSR: B↑ & G↑	M/S: Radial/Circular	240 × 240
[153]	0.8 /4.4	< −10 at 3.3–21.6	0–4.2	MSs: G↑& couurgations: SLL↓	M/S: Circular/Circular	45.19 × 17.53
[130]	Na /2.2	< −10 at 13.5–24	12–14.4	3D printed DL: G↑	M/S: rectangular/square	55.4 × 30.4 × 30.4 (lens)
[135]	0.381 / 2.2	< −10 at 5.4–18	8.5–13	ES: C& B↑, ML: G↑	M/S: Radial/Circular	72 × 41
[41]	1.6 /4.4	< −14.7 at 5.8	14–16.5	DL: G↑	M/S: Radial/Circular	100 × 85
[132]	0.8 /4.3	< −8.9 at 4.56–12.65	5–9.2	grooved, tapered sloT & AML: G↑	M/S: Radial/Circular	65 × 45
[158]	0.5 /2.2	< −10 at 15–27	8–10	SSPP: couurgations MSs: G↑	M/S: Radial/Circular	37.9 × 14

Table 3 Comparison between TSA arrays (2004–2022).

Ref.	h (mm)/ εr	S_{11}(dB)/VSWR at Frequency Band (GHz)	Gain Min-Max (dBi)	C/B↑/M↑/G↑/D1↑/D2↑/CP↓/RE↑/SLL↓/RCS↓/HPBW↓ techniques	Feeding	Circuit area
[71]	NA	< −10 at 2.54–9.71	7.2–13	1X 4 VTSA array aligned in H-plane: B↑ & G↑	M/S: Radial/Circular	NA
[11]	1.57/ 2.2	< −10 at 1.2–4.2	7.96 –16.26	1x8 VTSA array: G↑	M/S: Radial/Circular	Single element:124 × 60, Array:480 × 210
[88]	3.175/ 2.08	< −10 at 7–9	6.8–14.92	8 VTSA array Array based on SIW binary divider: M↑, B↑ & G↑	GCPW TO SIW	177.8 × 177.8 array
[75]	0.5/ 2.65	< −11.3 at 2.2–14.8 < −11.3 at 2.5–15	6.8–11.8 6.9–14.5	CVA DSVA: B↑ & G↑	M/S: Circular/ Circular	150 × 80
[76] 2 layers	0.5/ 2.65	Diff ports: < −11.55 at 2.25–11.1	10.1–14.81	Double slot structure and diagonal rectangular -shaped corrugations: B↑ & D↑	M/S: Circular/ Circular	150 × 100 × 1
[72]	1/4.3	<-12.7 at 4- > 10	Sim Directivity (3.96–12.54)	Double slot structure with loaded ZIM unit cells: D↑	M/S: Radial/Circular	90 × 85
[122]	0.25/ 2.2	<-10.6 at 20.3–40 GHz	14–16.9	Double slot structure with Parasitic core element: G↑	M/S	91 × 31
[79] 2 layers	1/2.55	< −10 at 1.28–11.51	0.5 –4	Omnidirectional Circular Connected VA Array: B↑	M/S: Radial/Quasi circular	Single element: 53 × 34, Array:π x 88^2
[116]	1/NA	< −10 at 2.5–28	3–15.25	Double slot structure and Y-shaped corrugations: B↑ & D↑	M/S: Circular/ Circular	145 × 80
[120]	1/2.65	<-9.3 at 1.13–12	0.7–14.2	Double slot structure loaded ZIM unit cells and pair of DGS: B↑ & G↑	M/S: Circular/ Circular	130 × 80
[121]	0.508/ 2.2	< −10 at 0.7–2.7	In phase:1.25–9.47 Out of phase:3.5–9.16	sharing the same circular slot in the transition; C, D2↑	M/S: Radial/Circular	260 × 254
[171]	0.762/ 3.5	< −10 at 2.9–11.6	−0.4–5.57	MIMO (2 elments): C, D2↑. SRRs for notches: 5.3–5.8 GHz & 7.85–8.55 GHz	M/S: Rectangular/ Rectangular	26 × 26
[171]	0.6/ 2.65	< −10 at 2.5–12	−2.5–4.44	MIMO(2 elments): C(four resitors), D2↑. SRRs for notches: 5.1–5.9 GHz & 6.6–7.1 GHz	M/S: Radial/semi Circular	26 × 24.5
[35]	1.6/ 10.2	< −10 at 3.4–8.3 <-8.4 dB at 4.6 GHz	6.25–12.3	1X 4 VTSA array aligned in H-plane: B↑ & G↑	M/S: Radial/Circular	Single element:53 × 42, Array: NA
[119]	0.813/ 3.55	<-9.84 at 4.2–11	8–13.3(Sim)	Double slot structure with director and corrugated slots: B↑ & G↑	M/S: Circular/ Circular	130 × 80
[172]	0.508/ 2.2	< −10 at 24–32	8–9.9	MIMO(4elments) with spatial MS loading and sharing the same circular slot: C, D2↑& G↑	M/S: Rectangular/ semi Circular	50.4 × 50.4
[131]	**0.813/ 3.55**	**<-8.5 at 0.66–6.77**	**4–15**	Specially shaped corrugations	**M/S**: Radial/**Circular**	**≈201.86 × 238 × 330**

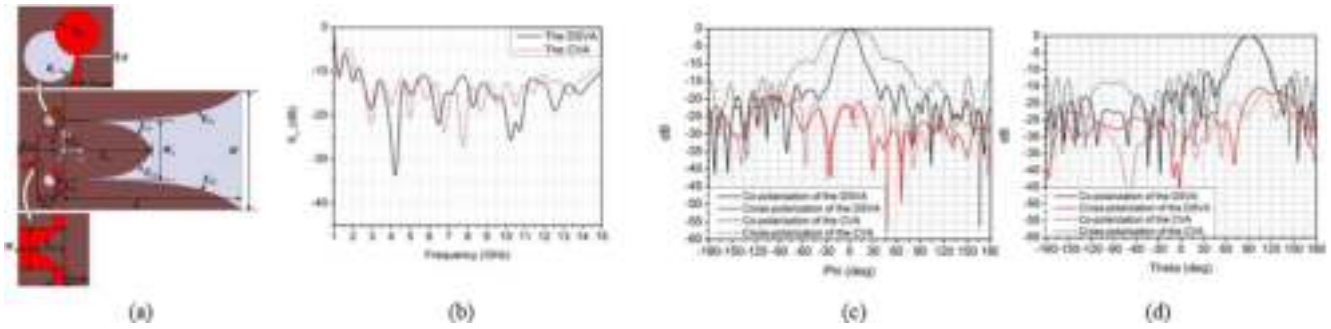

Fig. 38 (a) Layout with W = 80 mm, L = 120 mm, W_s = 40 mm, L_s = 60 mm, g = 0.3 mm, R_m = 3.5 mm, R_s = 4 mm, L_b = 5 mm, L_{b1} = 25 mm, L_{f1} = 10 mm, L_{f2} = 12 mm, (b) S_{11}, (c) E radiation pattern at 10 GHz and (d) H radiation pattern at 10 GHz of the proposed E plane DSVA [75].

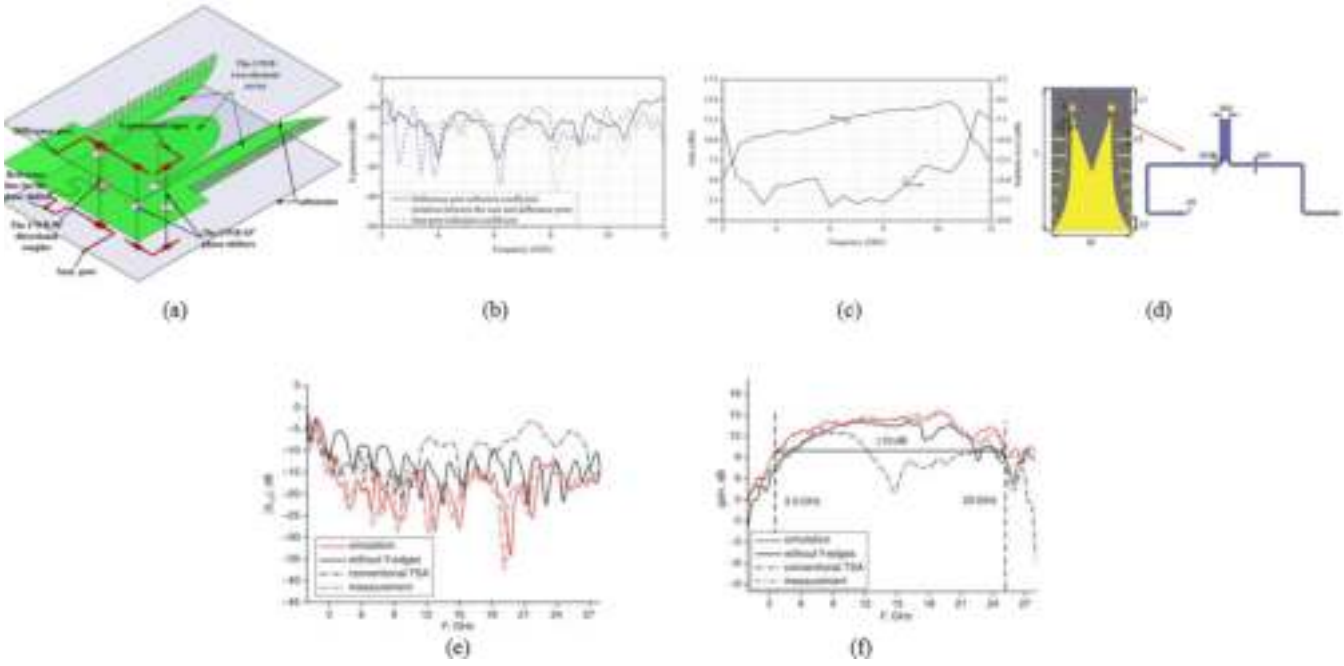

Fig. 39 (a) Layout, (b) S_{11} and (c) gain of the proposed UWB E-plane monopulse 2 layered DSVA [76], (d) layout with W = 80 mm, L = 145 mm, W1 = 5 mm, W2 = 2.73 mm, W3 = 1.675 mm, W 4 = 0.75 mm, L 1 = 25 mm, L2 = 15 mm, L3 = 2.5 mm, R = 4 mm and r1 = 0.5 mm, (e) S_{11} and (f) gain of the proposed UWB (2.5–28 GHz) double slot TSAs [116].

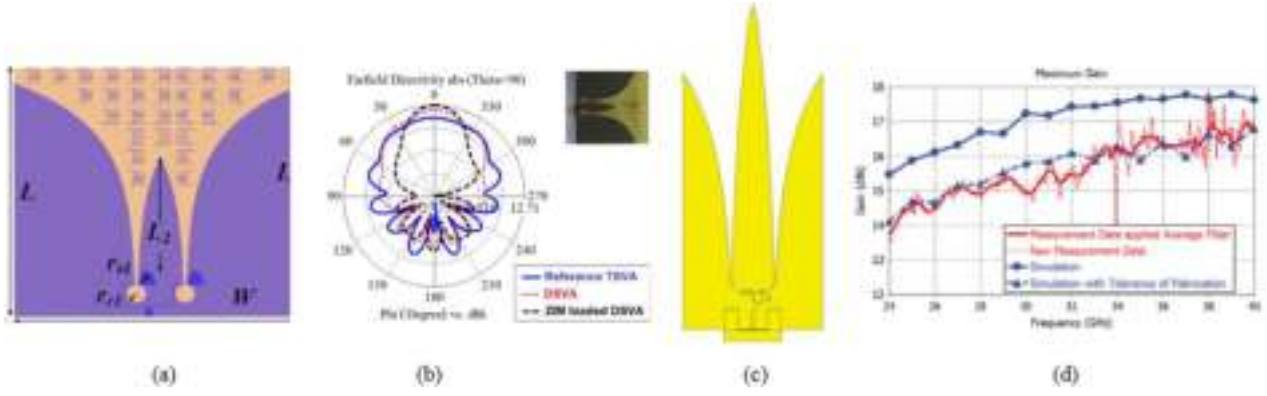

Fig. 40 (a) Layout with L = 85 mm, L_1 = 67 mm, L_2 = 42.5 mm, W = 90 mm, r_s = 7.5 mm, r_c = 6.5 mm, r_{s1} = 5.5 mm, and r_{c1} = 3 mm, (b) simulated directivity of the proposed DSVA with ZIM [72], (c) layout and (d) gain of the Ka-band (24–40 GHz) Vivaldi doubled slot antenna with core element [122].

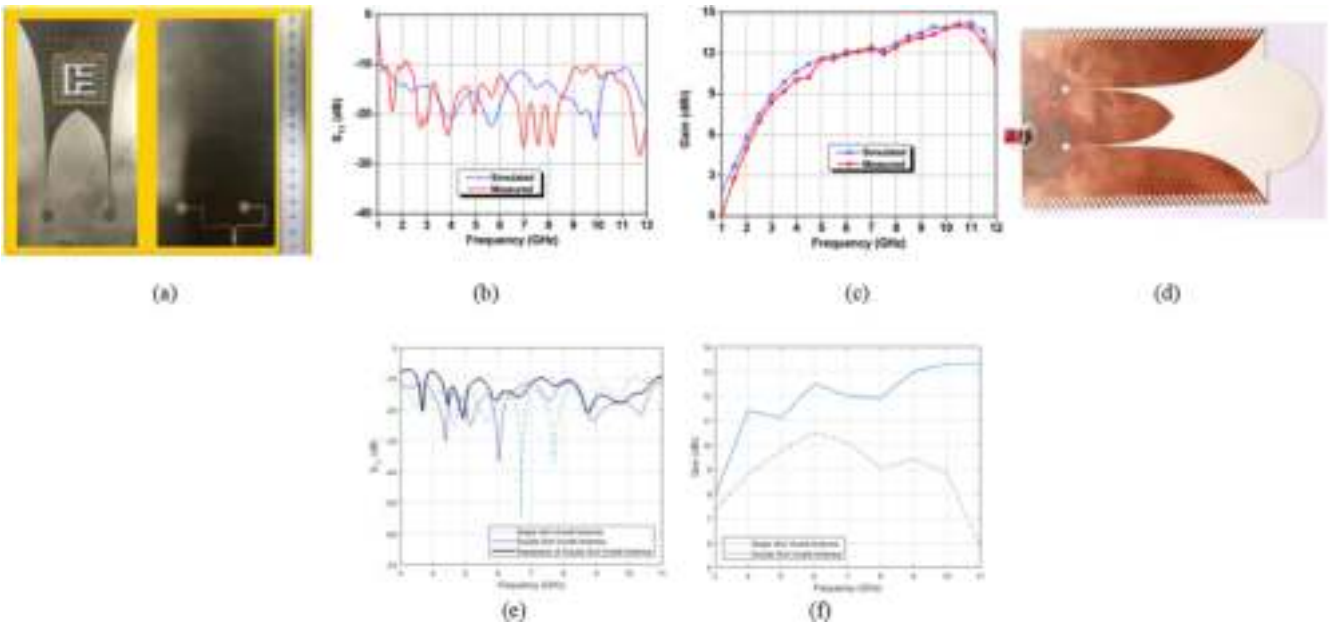

Fig. 41 (a), (d) fabricated prototypes and (b), (e) S_{11} (c) (f) gain of compact (1.13–12 GHz) DVSA with ZIM and DGS [120] and (4.2–11 GHz) DVSAs with a director and corrugated slots [119], respectively.

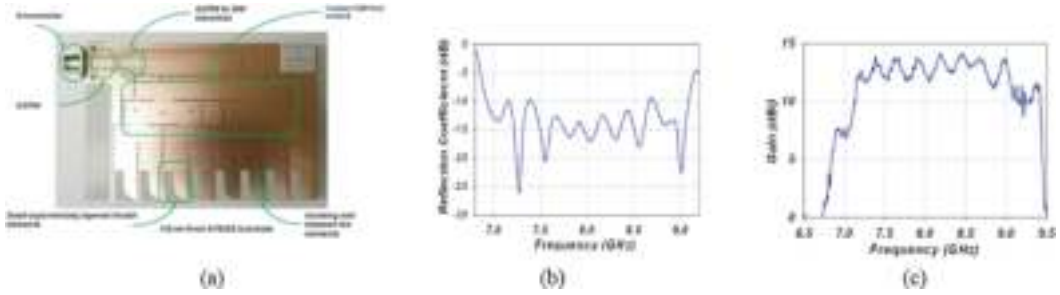

Fig. 42 (a) Photograph, (b) $S_{11,}$ and (c) gain of the proposed SIW-based 1 × 8 VA array [88].

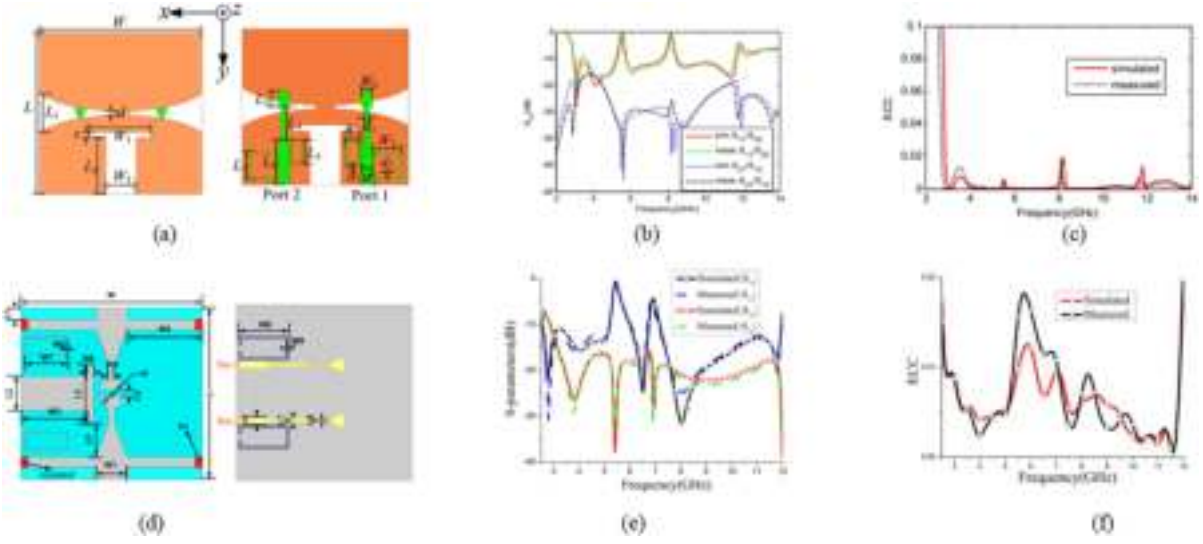

Fig. 43 Layout with(a) $L = 26$, $W = 26$, $L_1 = 6.3$, $W_1 = 10$, $d = 0.6$, s = 1, $L_2 = 9$, $W_2 = 4.8$, $L_3 = 2.6$, $L_4 = 5.5$, $L5 = 4$, $L_6 = 7.5$, $L_7 = 4.5$, $W_3 = 1.6$, $W_4 = 2.4$, $W_5 = 4.5$, $W_f = 1.6$, $d_1 = 0.7$, $d_2 = 0.4$, $d_3 = 0.4$(mm) (d) $L = 24.5$ mm, $W = 26$ mm, $L_1 = 1.65$ mm, $W_1 = 4.5$ mm, $L_2 = 5$ mm, $W_2 = 10.75$ mm, $L_3 = 8.5$ mm, $L_4 = 1$ mm, $L5 = 5$ mm, $L_6 = 1.2$ mm, $L_7 = 0.5$ mm, $L_8 = 0.2$ mm, $W_3 = 9.5$ mm, $W_4 = 0.7$ mm, $W_5 = 0.2$ mm, $W_6 = 1$ mm, $W_7 = 5.8$ mm, $W_8 = 6.7$ mm, $W_9 = 0.4$ mm, and $d_1 = 0.7$, $\theta = 2°$(b),(e) S-parameters and (c), (f) ECC of UWB (2.9–11.6 GHz) and (2.5–12 GHz) MIMO Vivaldi antenas in [170,171], respectively.

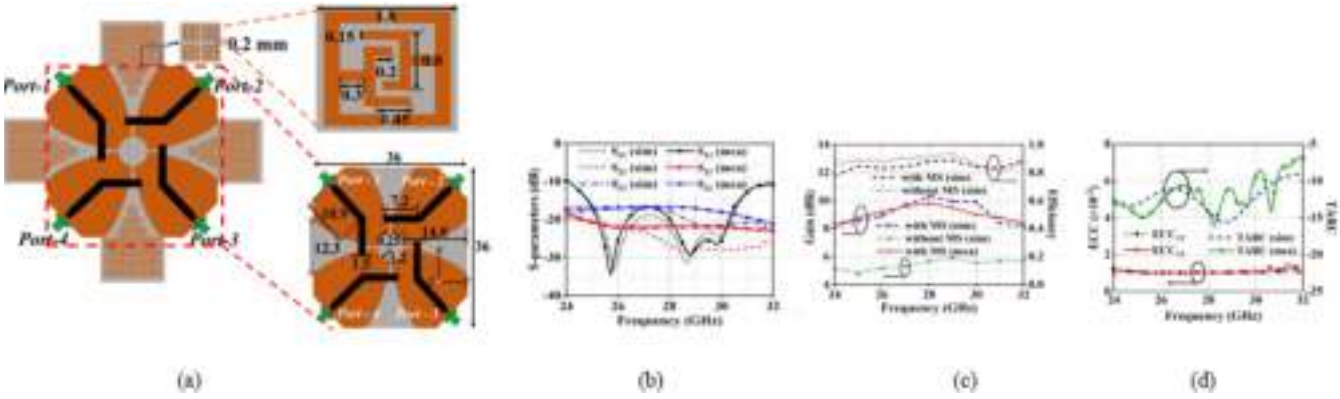

Fig. 44 (a)Layout, (b)S-parameters (c) gain with radiation efficiency and (d) ECC with TARC of mmWave (24–32 GHz) MIMO VAs in [172].

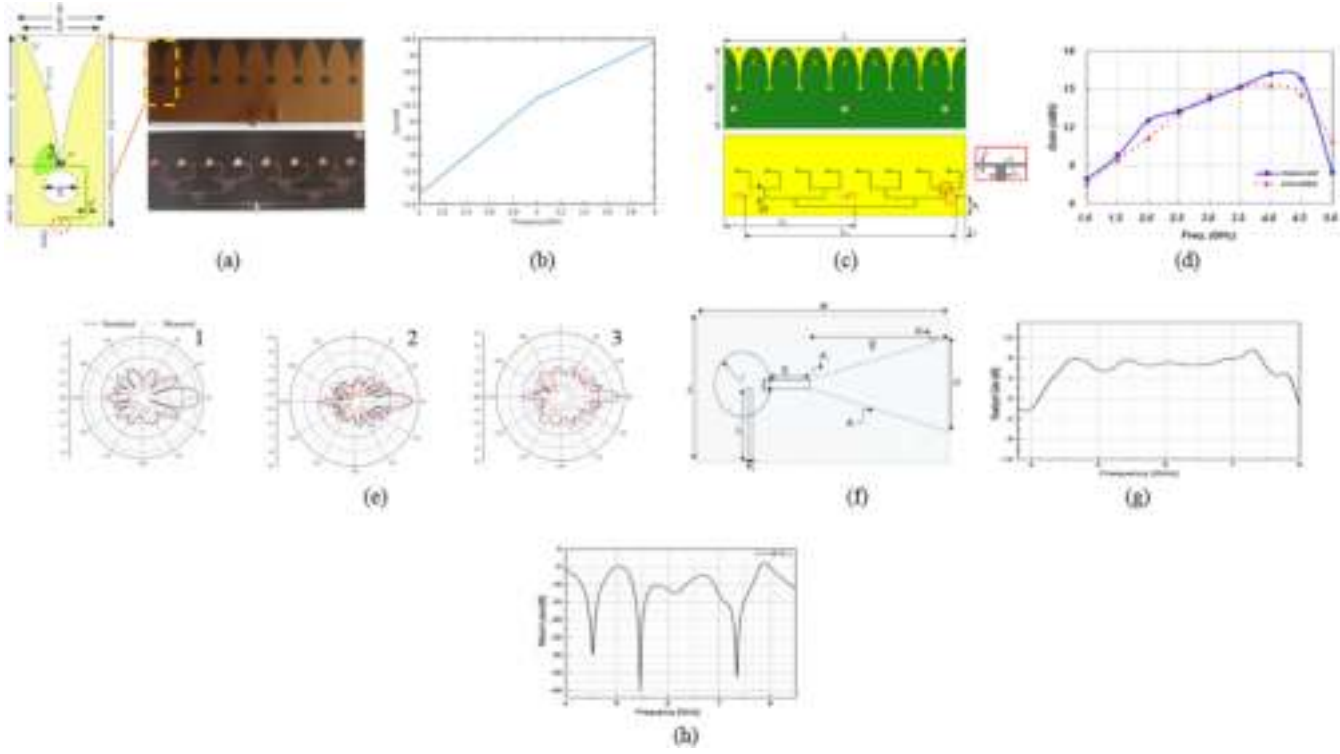

Fig. 45 (a) The fabricated 1 × 8 VTSA array and (b) gain of the proposed 1 × 8 VTSA array in [11], (d) layout, (e) gain and (f) E-plane pattern at (1a) 2 GHz; (2) 3 GHz; and (3) 4 GHz of the proposed 1 × 8 VTSA array in [40], (g) single TSA element with $W = 90$ mm, $L = 69$ mm, $l_1 = 32.5$ mm, $w_1 = 2.38$ mm, $r = 10$ mm, $wsl = 3$ mm and $lsl = 10.3$ mm, (h) gain and (i) S_{11} of the proposed 2 × 4 TSA [39].

mum realized gain of 14.84 dBi and SLL less than −20 dB. The prototype with the resulting VSWR and gain are shown in Fig. 47(c-e), respectively. Authors in [34] designed a 4 × 4 VTSA array with a maximum gain of up to 15.82 dBi suitable for wind profiler RADAR application (1.21–1.57 GHz).To enhance the base station diversity while reducing the size, two adjacent VTSAs are used in [121]. The size of the proposed model shown in Fig. 48(a) is reduced by sharing the same circular slot in the transition, cutting the noncritical board area, and shorting the ending of microstrip feed lines using Via grounding. To avoid coupling between the slots, a rectangular slot is added between the vias. The radiation of this array is illustrated in Fig. 48(b). An omnidirectional pattern with a horizontally polarized antenna is obtained in [79] by connecting the 16 VTSAs in a circular shape as in Fig. 48(c) in order to broaden the BW (fractional: 159.97%) as depicted in Fig. 48 (d). Top-mount spherical–axicon DL is used to enhance the gain (16 dBi) and equalize the frequency behavior of two systems containing two orthogonal compact VA (explained in Section 3.1.2 and Fig. 10(e)) arranged symmetrically and

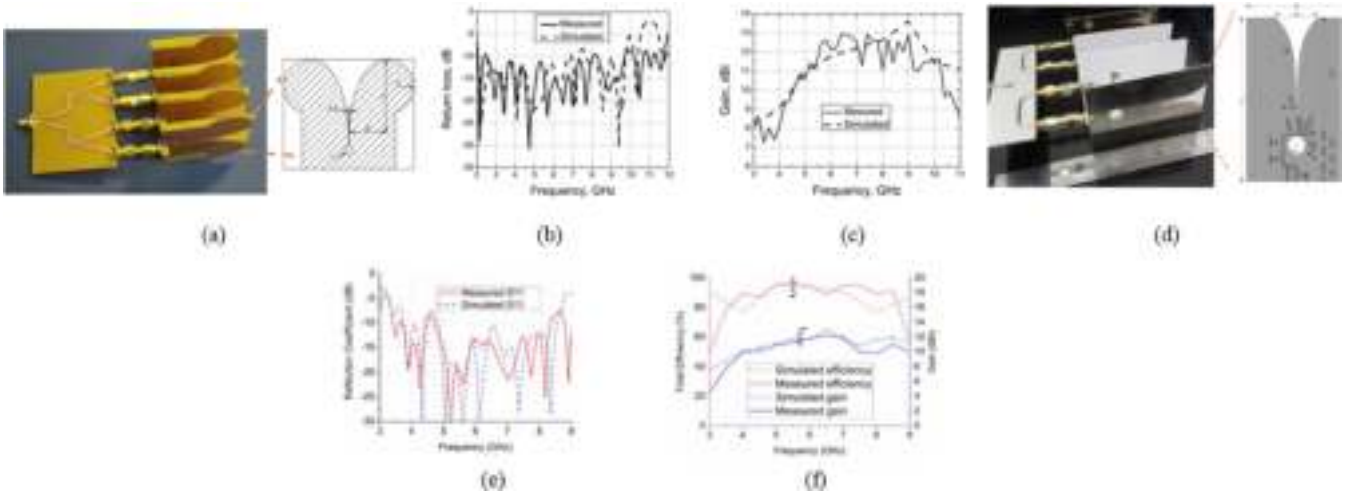

Fig. 46 (a) Prototype (inset: single element), (b) S_{11} and (c) gain of the proposed 1 × 4 VTSA aligned in H plane [71], (d) prototype (inset: Single VTSA element with L = 77.4 mm, L1 = 55.2 mm, L2 = 7.4 mm, D = 50 mm, S = 21 mm, W1 = 0.7 mm, W2 = 0.9 mm, W3 = 1.4 mm, W4 = 1.7 mm, W5 = 1.8 mm, s = 0.3 mm, R = 0.11 mm, Rm = 7 mm, r = 4.3 mm and ∝m = 83°, (e) S_{11} and (f) gain of the proposed 1 × 4 VTSA aligned in H plane [35].

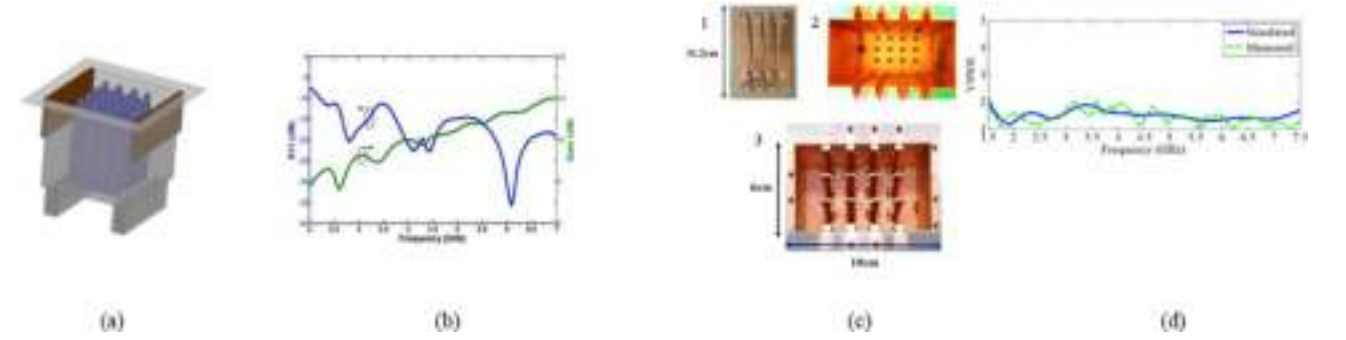

Fig. 47 (a) Layout, (b) and simulated S_{11} and gain for the proposed 3 × 4 VTSA array in [173], (c) photograph of the fabricated cavity-backed 3 × 4 VA array: (1) single row of the array, (2) 3-D-printed and copper-plated rectangular cavity showing the longitudinal groove reserved for each row of the array and (3) fully assembled array recessed in the cavity, (d) VSWR and (e) gain of the proposed cavity-backed 3 × 4 VA array [175].

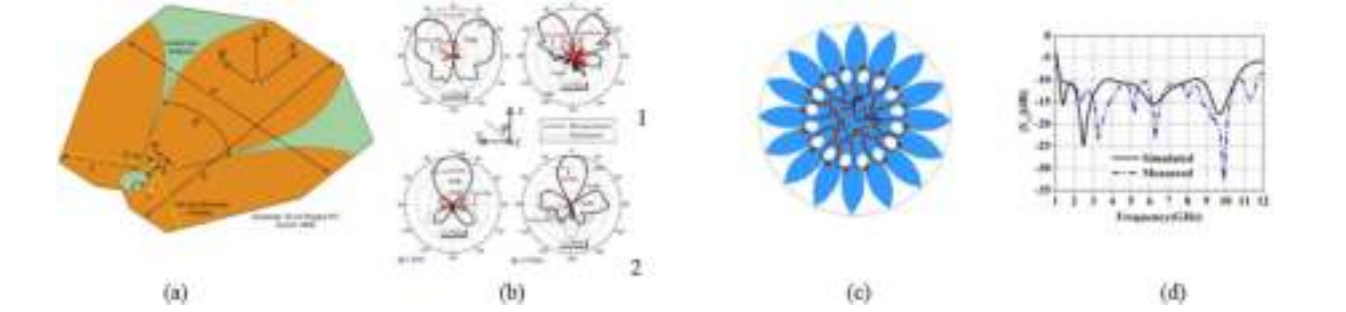

Fig. 48 (a) Layout with: a = 260 mm, b = 254 mm, l = 19 mm, w = 2.5 mm, θ = 29°, t = 4 mm, c = 72.4 mm, and taper's opening rate = 26.97 mm, (b) measured and simulated radiation patterns at 1 GHz (left) and 1.4 GHz (right): (1) in-phase feeding, and (2) 180° out-of-phase excitation [121], (c) layout, and (d) S_{11} of the proposed 1 × 16 VTSA horizontally polarized array antenna in [79].

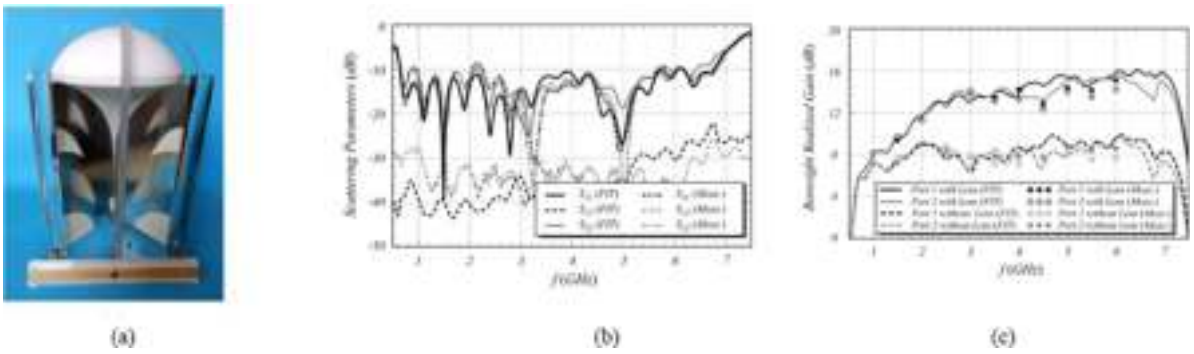

Fig. 49 (a)prototype, (b)S11, and (c) gain of the proposed asymmetrical orthogonal VA system array antenna in [131].

asymmetrically in cross-shaped fashion, to provide low cross-polarization level and high electrical isolation between the antenna excitation ports suitable for wireless communication and STW applications. The prototype of the proposed system with the resulting S_{11} and gain are shown in Fig. 49. Table 3 illustrates the comparison between the proposed TSA arrays in the literature.

4. Conclusions

For the first time, this paper provides a full assessment of TSA compactness and performance enhancement strategies. The review begins with a theoretical overview of TSA and its various types, as well as its usefulness in a variety of practical applications in communication systems. After that, full studies of compactness and performance approaches are addressed with extensive comparison tables to meet the criteria of Today's wireless communication systems in terms of high performance, low cost, and compact-size antennas. This study serves as an excellent foundation for RF researchers and designers to apply the various methodologies mentioned in this paper, exploiting their benefits while avoiding or limiting their disadvantages.

Declaration of Competing Interest

The authors declare that they have no known competing financial interests or personal relationships that could have appeared to influence the work reported in this paper.

Acknowledgment

The authors would like to thank Universiti Teknologi Malaysia (UTM) Postdoctoral Fellowship Scheme under Grant **06E07**, Malaysia Ministry of Education under HiCoE Grant **4J618,** Enterprise Ireland and Prince Sattam Bin Abdulaziz University for supporting this work.

References

[1] J. Anguera, A. Andújar, M.C. Huynh, C. Orlenius, C. Picher, C. Puente, Advances in antenna technology for wireless handheld devices, Int. J. Anten. Propag. 2013 (2013), https://doi.org/10.1155/2013/838364.

[2] C.A. Balanis, Antenna Theory: Analysis and Design, John Wiley & Sons, 2016.

[3] G. Atanasova, N. Atanasov, Small antennas for wearable sensor networks: Impact of the electromagnetic properties of the textiles on antenna performance, Sensors (Switzerland). 20 (2020) 1–21, https://doi.org/10.3390/s20185157.

[4] V. Zhurbenko, Passive Microwave Components and Antennas, BoD–Books on Demand, 2010.

[5] R.S. Kshetrimayum, An introduction to UWB communication systems, IEEE Potent. 28 (2009) 9–13.

[6] C. Nguyen, M. Miao, Design of CMOS RFIC Ultra-Wideband Impulse Transmitters and Receivers, Springer, 2017.

[7] Y. Rahayu, T.A. Rahman, R. Ngah, P.S. Hall, Ultra wideband technology and its applications, in: 2008 5th IFIP International Conference on Wireless and Optical Communications Networks (WOCN'08), IEEE, 2008, pp. 1–5.

[8] J.D. Taylor, Ultra-Wideband Radar Technology, CRC Press, 2018.

[9] Z.N. Chen, M.Y.W. Chia, Broadband Planar Antennas Design and Applications, 2006.

[10] K.-L. Wong, Compact and Broadband Microstrip Antennas, John Wiley & Sons, 2004.

[11] Y. Yang, Y. Wang, A.E. Fathy, Design of compact Vivaldi antenna arrays for UWB see through wall applications, Prog. Electromagn. Res. 82 (2008) 401–418, https://doi.org/10.2528/PIER08040601.

[12] C. Jarufe, R. Rodriguez, V. Tapia, P. Astudillo, D. Monasterio, R. Molina, F.P. Mena, N. Reyes, L. Bronfman, Optimized corrugated tapered slot antenna for mm-wave applications, IEEE Trans. Antennas Propag. 66 (2018) 1227–1235, https://doi.org/10.1109/TAP.2018.2797534.

[13] M. Chiappe, G.L. Gragnani, Vivaldi antennas as detectors for microwave imaging: Some theoretical results and design considerations, in: 2004 IEEE International Workshop on Imaging Systems and Techniques (IST)(IEEE Cat. No. 04EX896), IEEE, 2004, pp. 22–27.

[14] M. Ostadrahimi, S. Noghanian, L. Shafai, A. Foroozesh, Comparing performance of double layer stripline fed and single layer y2y fed vivaldi antennas, in: 2010 14th International Symposium on Antenna Technology and Applied Electromagnetics & the American Electromagnetics Conference, IEEE, 2010, pp. 1–4.

[15] B. Wu, Y. Ji, G. Fang, Design and measurement of compact tapered slot antenna for UWB microwave imaging radar, in: 2009 9th International Conference on Electronic Measurement & Instruments, IEEE, 2009, pp. 2–229.

[16] G.K. Pandey, H.S. Singh, P.K. Bharti, A. Pandey, M.K. Meshram, High gain Vivaldi antenna for radar and microwave imaging applications, Int. J. Signal Process. Syst. 3 (2015) 35–39, https://doi.org/10.12720/ijsps.3.1.35-39.

[17] L.C. Paul, M.N. Hossain, M.M.U. Rashid, M.M. Mowla, M. Z. Mahmud, M.T. Islam, A Novel Miniaturized Coplanar Waveguide Fed Tapered Slot Ultra Wide Band Vivaldi

Antenna For Microwave Imaging Applications, in: 2019 10th International Conference on Computing, Communication and Networking Technologies (ICCCNT), IEEE, 2019,pp. 1–6.
[18] S. Zhu, P. Wen, H. Liu, A Miniaturized Double-Vivaldi Antenna With Improved Gain Based on a Novel Metasurface, in: 2018 IEEE Asia-Pacific Conference on Antennas and Propagation (APCAP), IEEE, 2018, pp. 249–250.
[19] X. Yin, Z. Su, W. Hong, T.J. Cui, An ultra wideband tapered slot antenna, in: 2005 IEEE Antennas and Propagation Society International Symposium, IEEE, 2005, pp. 516–519. 10.1109/APS.2005.1551859.
[20] J. Shao, G. Fang, Y. Ji, K. Tan, H. Yin, A novel compact tapered-slot antenna for GPR applications, IEEE Antennas Wirel. Propag. Lett. 12 (2013) 972–975, https://doi.org/10.1109/LAWP.2013.2276403.
[21] M. Serhir, Transient UWB antenna near-field and far-field assessment from time domain planar near-field characterization: Simulation and measurement investigations, IEEE Trans. Antennas Propag. 63 (2015) 4868–4876, https://doi.org/10.1109/TAP.2015.2480404.
[22] F. Zhang, G.Y. Fang, Y.C. Ji, H.J. Ju, J.J. Shao, A novel compact double exponentially tapered slot antenna (DETSA) for GPR applications, IEEE Antennas Wirel. Propag. Lett. 10 (2011) 195–198, https://doi.org/10.1109/LAWP.2011.2123868.
[23] V. Mikhnev, Y. Maksimovitch, P. Vainikainen, A tapered-slot antenna with emulated continuous resistive loading, in: The Second European Conference on Antennas and Propagation, EuCAP 2007, IET, 2007, pp. 1–3. 10.1049/ic.2007.1501.
[24] D.M. Elsheakh, E.A. Abdallah, Novel shape of Vivaldi antenna for water detection using GPR, in: The 2nd Middle East Conference on Antennas and Propagation, IEEE, 2012, pp. 1–4. 10.1109/MECAP.2012.6618207.
[25] Z. Tahar, X. Dérobert, M. Benslama, An ultra-wideband modified vivaldi antenna applied to through the ground and wall imaging, Prog. Electromagn. Res. 86 (2018) 111–122.
[26] S. Warathe, R.K. Tanti, N. Anveshkumar, Compact Vivaldi Antenna Design at 500MHz for GPR Applications, 2019 IEEE Indian Conference on Antennas and Propagation, InCAP 2019. (2019) 1–5. 10.1109/InCAP47789.2019.9134522.
[27] H. Cheng, H. Yang, Y. Li, Y. Chen, A compact vivaldi Antenna with artificial material lens and sidelobe suppressor for GPR applications, IEEE Access. 8 (2020) 64056–64063. 10.1109/ACCESS.2020.2984010.
[28] M.A. Belen, İ.Ö. Evranos, F. Güneş, P. Mahouti, An UWB Vivaldi antenna with the enhanced functionalities through the use of DGS and dielectric lens, in: 2017 8th International Conference on Recent Advances in Space Technologies (RAST), IEEE, 2017, pp. 199–201.
[29] S.H. He, W. Shan, C. Fan, Z.C. Mo, F.H. Yang, J.H. Chen, An improved Vivaldi antenna for vehicular wireless communication systems, IEEE Antennas Wirel. Propag. Lett. 13 (2014) 1505–1508.
[30] P. Zhang, J. Li, Compact UWB and low-RCS Vivaldi antenna using ultrathin microwave-absorbing materials, IEEE Antennas Wirel. Propag. Lett. 16 (2017) 1965–1968.
[31] P.A. Dzagbletey, J. Shim, J. Chung, Communication V2X communication measurement, in: IEEE Trans Antennas Propag, IEEE, in, 2019, pp. 1957–1962.
[32] J. Sun, W. Jiang, Design of a taper slotted low profile Vivaldi antenna for ultra-wideband near field imaging, in: 2013 International Conference on Communications, Circuits and Systems (ICCCAS), IEEE, 2013, pp. 428–430. 10.1109/ICCCAS.2013.6765374.
[33] E.W. Reid, L. Ortiz-Balbuena, A. Ghadiri, K. Moez, A 324-element vivaldi antenna array for radio astronomy instrumentation, IEEE Trans. Instrum. Meas. 61 (2012) 241–250, https://doi.org/10.1109/TIM.2011.2159414.
[34] A. Prakash, N. Chattoraj, S.B. Shukla, Design and development of vivaldi antenna array for wind profiler RADAR application, Microw. Opt. Technol. Lett. 60 (2018) 725–731, https://doi.org/10.1002/mop.31040.
[35] B. Xiao, H. Yao, M. Li, J.S. Hong, K.L. Yeung, Flexible wideband microstrip-slotline-microstrip power divider and its application to antenna array, IEEE Access 7 (2019) 143973–143979, https://doi.org/10.1109/ACCESS.2019.2944462.
[36] S.-W. Kim, H.-G. Yu, K.-W. Choi, D.-Y. Choi, Analysis of tapered slot antenna with high gain for 2D indoor wireless positioning, IEEE Access 7 (2019) 54312–54320, https://doi.org/10.1109/ACCESS.2019.2913193.
[37] A. Kuriakose, T.A. George, S. Anand, Improved High Gain Vivaldi Antenna Design for Through-wall Radar Applications, Proceedings of the 2020 International Symposium on Antennas and Propagation, APSYM 2020. (2020) 58–61. doi:10.1109/APSYM50265.2020.9350711.
[38] Z. Hu, Z. Zeng, K. Wang, W. Feng, J. Zhang, Q. Lu, X. Kang, Design and analysis of a UWB MIMO radar system with miniaturized vivaldi antenna for through-wall imaging, Remote Sens. (Basel) 11 (2019) 1867.
[39] P. Soothar, H. Wang, B. Muneer, Z.A. Dayo, B.S. Chowdhry, A Broadband high gain tapered slot antenna for underwater communication in microwave band, Wirel. Pers. Commun. 116 (2021) 1025–1042, https://doi.org/10.1007/s11277-019-06633-2.
[40] J. Ren, H. Fan, Q. Tang, Z. Yu, Y. Xiao, X. Zhou, An ultra-wideband Vivaldi antenna system for long-distance electromagnetic detection, Appl. Sci. (Switzerland). 12 (2022), https://doi.org/10.3390/app12010528.
[41] F. Ma, X. Zhang, Y. Yin, H. Yin, C. Song, L. Zhao, Low-cost lens antenna design for microwave moisture detection, Int. J. Antennas Propag. 2022 (2022), https://doi.org/10.1155/2022/3883786.
[42] L. Lewis, M. Fassett, J. Hunt, A broadband stripline array element, in: 1974 Antennas and Propagation Society International Symposium, IEEE, 1974, pp. 335–337.
[43] R.P. Yadav, V. Kumar, R. Dhawan, Design and development of patch compensated wideband Vivaldi antenna, Int. J. Microw. Wirel. Technol. 10 (2018) 1081–1087.
[44] P.J. Gibson, The vivaldi aerial, in: 1979 9th European Microwave Conference, IEEE, 1979, pp. 101–105. 10.1109/EUMA.1979.332681.
[45] H. Zhang, Microwave imaging for ultra-wideband antenna based cancer detection, 2015.
[46] M. Kahar, J. Mandal, M.K. Mandal, A compact Vivaldi antenna with microstrip feed line for the 2–18GHz ultra-wideband applications, in: 2015 IEEE Applied Electromagnetics Conference (AEMC), IEEE, 2015: pp. 1–2.
[47] S. Saleh, W. Ismail, I.S.Z. Abidin, M.H. Bataineh, A.S. Alzoubi, Compact UWB Vivaldi tapered slot antenna, Alex. Eng. J. 61 (2022) 4977–4994, https://doi.org/10.1016/j.aej.2021.09.055.
[48] A.M. Abbosh, Miniaturized microstrip-fed tapered-slot antenna with ultrawideband performance, IEEE Antennas Wirel. Propag. Lett. 8 (2009) 690–692.
[49] A. Bhattacharjee, A. Bhawal, A. Karmakar, A. Saha, D. Bhattacharya, Vivaldi antennas: a historical review and current state of art, Int. J. Microw. Wirel. Technol. 13 (2021) 833–850, https://doi.org/10.1017/S1759078720001415.
[50] Y. Yang, Z. Zhao, X. Ding, Z. Nie, Q.-H. Liu, Compact UWB slot antenna utilizing traveling-wave mode based on slotline transitions, IEEE Trans. Antennas Propag. 67 (2018) 140–150.
[51] W. Shen, W.X. Zhang, Study on asymmetric tapered slotline antenna, in: 2006 3rd International Conference on Ultrawideband and Ultrashort Impulse Signals, 2006, pp. 156–158.

[52] P. Zhang, W.-X. Zhang, S.J. Tang, Improved tapered slot-line antennas loaded by grating, J. Electromagn. Waves Appl. 23 (2009) 1039–1048.
[53] C. Xu, F. Lina, H. Chunjiu, Design of a compact dual exponentially tapered slot antenna, in: 2016 IEEE International Conference on Microwave and Millimeter Wave Technology (ICMMT), 2016, pp. 671–673.
[54] Y. Wang, Y. Yang, A.E. Fathy, Ultra-wideband vivaldi arrays for see-through-wall imaging radar applications, in: IEEE Antennas and Propagation Society AP-S International Symposium (Digest), 2009, pp. 8–11, https://doi.org/10.1109/APS.2009.5172292.
[55] Y. Yao, M. Liu, W. Chen, Z. Feng, Analysis and design of wideband widescan planar tapered slot antenna array, IET Microwaves Anten. Propag. 4 (2010) 1632–1638, https://doi.org/10.1049/iet-map.2009.0226.
[56] B. Zhou, H. Li, X. Zou, T.-J. Cui, Broadband and high-gain planar Vivaldi antennas based on inhomogeneous anisotropic zero-index metamaterials, Prog. Electromagn. Res. 120 (2011) 235–247, https://doi.org/10.2528/PIER11072710.
[57] K. Ebnabbasi, D. Busuioc, R. Birken, M. Wang, Taper design of Vivaldi and co-planar tapered slot antenna (TSA) by Chebyshev transformer, IEEE Trans. Antennas Propag. 60 (2012) 2252–2259.
[58] G.K. Pandey, H.S. Singh, M.K. Meshram, Meander-line-based inhomogeneous anisotropic artificial material for gain enhancement of UWB Vivaldi antenna, Appl. Phys. A Mater. Sci. Process. 122 (2016) 1–9, https://doi.org/10.1007/s00339-015-9569-2.
[59] S.-W. Kim, D.-Y. Choi, Implementation of rectangular slit-inserted ultra-wideband tapered slot antenna, Springerplus 5 (2016) 1387.
[60] M. Abbak, M.N. Akıncı, M. Çayören, I. Akduman, Experimental microwave imaging with a novel corrugated Vivaldi antenna, IEEE Trans. Antennas Propag. 65 (2017) 3302–3307, https://doi.org/10.1109/TAP.2017.2670228.
[61] S.A. Çolak, N.T. Tokan, Time-domain analysis of modified vivaldi antennas, Antennas Wave Propag. (2018) 39, https://doi.org/10.5772/intechopen.74945.
[62] J. Zhang, S. Liu, F. Wang, Z. Yang, X. Shi, A compact high-gain Vivaldi antenna with improved radiation characteristics, Prog. Electromagn. Res. Lett. 68 (2017) 127–133, https://doi.org/10.2528/pierl17031506.
[63] C. Gao, E. Li, Y. Zhang, G. Guo, A directivity enhanced structure for the Vivaldi antenna using coupling patches, Microw. Opt. Technol. Lett. 60 (2018) 418–424, https://doi.org/10.1002/mop.30988.
[64] Y. Yao, W. Chen, B. Huang, Z. Feng, Z. Zhang, Analysis and design of tapered slot antenna for ultra-wideband applications, Tsinghua, Sci. Technol. 14 (2009) 1–6.
[65] Y. Tang, X. Cao, Y. Song, L. Jidi, J. Lan, H. Yu, A design of high-gain vivaldi antenna loaded with antipodal structure and slotting correction, in: 2018 IEEE MTT-S International Wireless Symposium (IWS), IEEE, 2018, pp. 1–3. 10.1109/IEEE-IWS.2018.8400909.
[66] B. Zhou, H. Li, X. Zou, T.-J. Cui, Broadband and high-gain planar Vivaldi antennas based on inhomogeneous anisotropic zeroindex metamaterial, Prog. Electromagn. Res. 120 (2011) 235–247, https://doi.org/10.2528/PIER11072710.
[67] Y. Liu, W. Zhou, S. Yang, W. Li, P. Li, S. Yang, A novel miniaturized Vivaldi antenna using tapered slot edge with resonant cavity structure for ultrawideband applications, IEEE Antennas Wirel. Propag. Lett. 15 (2016) 1881–1884, https://doi.org/10.1109/LAWP.2016.2542269.
[68] X. Li, D.W. Pang, H.L. Wang, Y. Zhang, G. Lv, Dielectric sheets covered broadband Vivaldi antenna for gain enhancement, Prog. Electromagn. Res. 77 (2017) 69–80, https://doi.org/10.2528/PIERC17070308.
[69] Nurhayati, G. Hendrantoro, T. Fukusako, E. Setijadi, Mutual coupling reduction for a UWB coplanar Vivaldi array by a truncated and corrugated slot, IEEE Antennas Wirel Propag Lett. 17 (2018) 2284–2288, https://doi.org/10.1109/LAWP.2018.2873115.
[70] Y. Yue, Y. Dong, J. Zhou, An ultra-wideband vivaldi antenna array in L and S bands, in: Asia-Pacific Conference on Antennas and Propagation, Conference Proceedings, 2017, pp. 301–302, https://doi.org/10.1109/APCAP.2016.7843213.
[71] P. Li, J. Liang, X. Chen, C. Parini, A 4-Element Ultra-wideband Tapered-Slot-Fed Antenna Array, (2006) 4475–4478.
[72] P. Kumar, Z. Akhter, A.K. Jha, M.J. Akhta, Directivity Enhancement of Double Slot t Vivaldi Antenna using Ani isotropic Zero-Index Me etamaterials (2015) 2333–2334.
[73] R. Natarajan, M. Kanagasabai, J. v. George, Design of an X-band Vivaldi antenna with low radar cross section, IET Microwaves, Antennas and Propagation. 10 (2016) 651–655. 10.1049/iet-map.2015.0585.
[74] J. Wu, Z. Zhao, J. Liu, Z.-P. Nie, Q.H. Liu, A compact linear tapered slot antenna with integrated balun for UWB applications, Prog. Electromagn. Res. 29 (2012) 163–176.
[75] Y.-W. Wang, G.-M. Wang, B.-F. Zong, Directivity improvement of Vivaldi antenna using double-slot structure, IEEE Antennas Wirel. Propag. Lett. 12 (2013) 1380–1383.
[76] Y.-W. Wang, G.-M. Wang, Z.-W. Yu, J.-G. Liang, X.-J. Gao, Ultra-wideband E-plane monopulse antenna using Vivaldi antenna, IEEE Trans. Antennas Propag. 62 (2014) 4961–4969.
[77] K. Ma, Z.Q. Zhao, J.N. Wu, M.S. Ellis, Z.P. Nie, A printed vivaldi antenna with improved radiation patterns by using two pairs of eye-shaped slots for UWB applications, Prog. Electromagn. Res. 148 (2014) 63–71, https://doi.org/10.2528/PIER14043003.
[78] Y. Chareonsiri, W. Thaiwirot, P. Akkaraekthalin, Design of ultra-wideband tapered slot antenna by using binomial impedance transformer, Frequenz 71 (2017) 251–260, https://doi.org/10.1515/freq-2016-0131.
[79] H. Liu, Y. Liu, W. Zhang, S. Gao, An ultra-wideband horizontally polarized omnidirectional circular connected Vivaldi antenna array, IEEE Trans. Antennas Propag. 65 (2017) 4351–4356, https://doi.org/10.1109/TAP.2017.2717959.
[80] M. Abbak, I. Akduman, Miniaturized tapered slot antenna for microwave breast imaging, in: 2012 20th Telecommunications Forum (TELFOR), IEEE, 2012, pp. 1214–1216.
[81] A. Lazaro, R. Villarino, D. Girbau, Design of tapered slot Vivaldi antenna for UWB breast cancer detection, Microw. Opt. Technol. Lett. 53 (2011) 639–643.
[82] M.E. Bialkowski, Y. Wang, A size-reduced exponentially tapered slot antenna with corrugations for directivity improvement, in: 2009 Asia Pacific Microwave Conference, IEEE, 2009, pp. 2482–2485.
[83] J. Wu, Z. Zhao, Z. Nie, Q.-H. Liu, A printed UWB Vivaldi antenna using stepped connection structure between slotline and tapered patches, IEEE Anten. Wirel. Propag. Lett. 13 (2014) 698–701, https://doi.org/10.1109/LAWP.2014.2314739.
[84] V. Tseng, C.-Y. Chang, Linear tapered slot antenna for ultra-wideband radar sensor: design consideration and recommendation, Sensors 19 (2019) 1212.
[85] L. Pazin, Y. Leviatan, A compact 60-GHz tapered slot antenna printed on LCP substrate for WPAN applications, IEEE Antennas Wirel. Propag. Lett. 9 (2010) 272–275.
[86] H. Wang, S. He, Z. Ding, J. Cao, Y. Yang, A miniaturized Vivaldi antenna with high gain for ultra-wideband applications, in: 2017 Sixth Asia-Pacific Conference on Antennas and Propagation (APCAP), 2017, pp. 1–3, https://doi.org/10.1109/APCAP.2017.8420722.
[87] P. Černý, Distortion Minimization of Radiated Impulses of Tapered Slot Vivaldi Antenna for UWB Application,

AUTOMATIKA: Časopis Za Automatiku, Mjerenje, Elektroniku, Računarstvo i Komunikacije. 49 (2008) 45–50.
[88] S. Lin, S. Yang, A.E. Fathy, A. Elsherbini, Development of a novel UWB Vivaldi antenna array using SIW technology, Prog. Electromagn. Res. 90 (2009) 369–384.
[89] D.-S. Woo, Y.-G. Kim, K.W. Kim, Y.-K. Cho, Ultra-wideband millimeter-wave tapered slot antennas, in: 2007 IEEE Antennas and Propagation Society International Symposium, IEEE, 2007, pp. 1969–1972.
[90] D. Yang, S. Liu, D. Geng, A miniaturized ultra-wideband Vivaldi antenna with low cross polarization, IEEE Access 5 (2017) 23352–23357, https://doi.org/10.1109/ACCESS.2017.2766184.
[91] S. Mochizuki, H. Togo, N. Kukutsu, T. Nagatsuma, High-resolution SAR imaging system using tapered slot antenna with orthogonally anisotropic directivity, in: in: 2007 Asia-Pacific Conference on Applied Electromagnetics, 2007, pp. 1–4.
[92] N.B. Wang, Y. Song, Y.C. Jiao, L. Zhang, F.S. Zhang, Extreme wideband tapered slot antenna with impedance bandwidth in excess of 21.6: 11, J. Electromagn. Waves Appl. 23 (2009) 231–238, https://doi.org/10.1163/156939309787604445.
[93] P. Fei, Y.-C. Jiao, Y. Ding, F.-S. Zhang, A compact coplanar waveguide fed wide tapered slot ultra-wideband antenna, Prog. Electromagn. Res. 25 (2011) 77–85.
[94] F. Zhu, S. Gao, A.T.S. Ho, T. Brown, Compact size asymmetric linearly tapered slot antenna for portable ultra-wideband imaging radar system, Int. J. RF Microwave Comput. Aided Eng. 23 (2012), https://doi.org/10.1002/mmce.
[95] F. Zhu, S. Gao, Compact elliptically tapered slot antenna with non-uniform corrugations for ultra-wideband applications, Radioengineering. 22 (2013) 276–280.
[96] O.A. Saraereh, A multiband and omnidirectional, CPW-fed single-layer based dual tapered-slot antenna, Prog. Electromagn. Res. C. 70 (2016) 183–191, https://doi.org/10.2528/PIERC16112211.
[97] A. Hokmabadi, A. Keshtkar, A. Bayat, A. Keshtkar, A CPW-fed tapered slot antenna with improved time and frequency domain characteristics, Int. J. Microw. Wirel. Technol. 9 (2017) 1185–1190, https://doi.org/10.1017/S1759078716001288.
[98] L. Song, H. Zhou, Wideband dual-polarized Vivaldi antenna with improved balun feed, Int. J. Microw. Wirel. Technol. 11 (2019) 27–34, https://doi.org/10.1017/S1759078718001113.
[99] L. Yo-Shsn, M. Tzyh-Ghuang, J. Shyh-Kang, C. Chun Hsivng, Coplanar waveguide-fed dual exponentially tapered slot antennas for ultra-wideband applications, EEE Antennas and Propagation Society Symposium, IEEE (2004) 2951–2954.
[100] F. Zhu, S. Gao, A.T.S. Ho, C.H. See, R.A. Abd-Alhameed, J. Li, J. Xu, Compact-size linearly tapered slot antenna for portable ultra-wideband imaging systems, International Journal of RF and Microwave, Comput.-Aid. Eng. 23 (2013) 290–299, https://doi.org/10.1002/mmce.20673.
[101] Y. Wang, F. Zhang, G. Fang, Y. Ji, S. Ye, X. Zhang, A novel ultrawideband exponentially tapered slot antenna of combined electric-magnetic type, IEEE Antennas Wirel. Propag. Lett. 15 (2016) 1226–1229, https://doi.org/10.1109/LAWP.2015.2502608.
[102] X. Meng, B. Wu, Z.X. Huang, X.L. Wu, Compact 30:1 Bandwidth ratio balun for printed balanced antennas, Prog. Electromagn. Res. C. 64 (2016) 125–132, https://doi.org/10.2528/PIERC16042003.
[103] S. Lin, J. Wang, Y. Deng, G. Zhang, A new compact ultra-wideband balun for printed balanced antennas, J. Electromagn. Waves Appl. 29 (2015) 1570–1579, https://doi.org/10.1080/09205071.2015.1051191.
[104] M. Chiappe, G.L. Gragnani, Vivaldi antennas for microwave imaging: theoretical analysis and design considerations, IEEE Trans. Instrum. Meas. 55 (2006) 1885–1891.
[105] N.-B. Wang, Y. Song, Y.-C. Jiao, L. Zhang, F.-S. Zhang, Extreme wideband tapered slot antenna with impedance bandwidth in excess of 21.6: 1, J. Electromagn. Waves Appl. 23 (2009) 231–238.
[106] J.J. Lee, S. Livingston, Wide band bunny-ear radiating element, in: Proceedings of IEEE Antennas and Propagation Society International Symposium, IEEE, 1993: pp. 1604–1607. 10.1109/APS.1993.385504.
[107] S. Nikolaou, G.E. Ponchak, J. Papapolymerou, M.M. Tentzeris, Conformal double exponentially tapered slot antenna (DETSA) on LCP for UWB applications, IEEE Trans. Antennas Propag. 54 (2006) 1663–1669.
[108] L. Pu, X.-M. Zhang, Design of a low-profile dual exponentially tapered slot antenna, Prog. Electromagn. Res. 6 (2009) 67–74.
[109] C. Xu, F. Lina, H. Chunjiu, Design of a compact dual exponentially tapered slot antenna, 9th International Conference on Microwave and Millimeter Wave Technology, ICMMT 2016 - Proceedings. 2 (2016) 671–673. 10.1109/ICMMT.2016.7762404.
[110] A.S. Arezoomand, R.A. Sadeghzadeh, M. Naser-Moghadasi, Novel techniques in tapered slot antenna for linearity phase center and gain enhancement, IEEE Anten. Wirel. Propag. Lett. 16 (2017) 270–273, https://doi.org/10.1109/LAWP.2016.2572064.
[111] N.B. Wang, Y.C. Jiao, Y. Song, L. Zhang, F.S. Zhang, A microstrip-fed logarithmically tapered slot antenna for wideband applications, J Electromagn Waves Appl. 23 (2009) 1335–1344, https://doi.org/10.1163/156939309789108543.
[112] K. Ebnabbasi, S. Sczyslo, M. Mohebbi, UWB performance of coplanar tapered slot antennas, IEEE Antennas Wirel. Propag. Lett. 12 (2013) 749–752.
[113] G. Anur, S.S. Kumar, Tapered slotted Vivaldi antenna design using Fourier series approach for UWB applications, in: 2014 First International Conference On Computational Systems And Communications (Iccsc), IEEE, 2014, pp. 7–11.
[114] Y. Chareonsiri, W. Thaiwirot, P. Akkaraekthalin, Tapered slot antenna with squared cosine profile for ultra-wideband applications, in: 2014 11th International Conference on Electrical Engineering/Electronics, Computer, Telecommunications and Information Technology (ECTI-CON), IEEE, 2014, pp. 1–4.
[115] S.W. Jeong, K.C. Hwang, J.Y. Park, S.J. Kim, D.H. Kim, Spidron fractal tapered slot antenna for dual-band radar applications, J Electromagn Waves Appl. 27 (2013) 1329–1337, https://doi.org/10.1080/09205071.2013.808597.
[116] Y.Q. Liu, J.G. Liang, Y.W. Wang, Gain-improved double-slot TSA with Y-shaped corrugated edges, Electron. Lett 53 (2017) 759–760.
[117] Z. Mohammad, N. Sarker, C. Das, Design and analysis of a double slotted with multiple strips vivaldi antenna for high-speed 5G communications, in: 3rd IEEE International Conference on Telecommunications and Photonics, ICTP 2019. (2019) 19–22. 10.1109/ICTP48844.2019.9041733.
[118] S. Khaled Ahmed, Z.A. Abdul Hassain, Design of high gain antenna based on array of double slot Vivaldi structure, J. Eng. Sust. Dev. 24 (2020) 241–246, https://doi.org/10.31272/jeasd.conf.1.26.
[119] F.N. Witriani, Y.S. Amrullah, F. Darwis, T. Taufiqqurrachman, Y.N. Wijayanto, K. Paramayudha, E. Elisma, Gain Enhancement of Double-Slot Vivaldi Antenna using Corrugated Edges and Semicircle Director for Microwave Imaging Application, Jurnal Elektronika Dan Telekomunikasi. 21 (2021) 85. 10.14203/jet.v21.85-90.
[120] S. Zhu, H. Liu, P. Wen, L. Du, J. Zhou, A Miniaturized and high gain double-slot vivaldi antenna using wideband index-near-zero metasurface, IEEE Access 6 (2018) 72015–72024, https://doi.org/10.1109/ACCESS.2018.2883097.

[121] Y. Dong, J. Choi, T. Itoh, Vivaldi Antenna with pattern diversity for 0.7 to 2.7 GHz cellular band applications, IEEE Anten. Wirel. Propag. Lett. 17 (2018) 247–250, https://doi.org/10.1109/LAWP.2017.2783323.
[122] M.-H. Hoang, K. Yang, M. John, P. McEvoy, M. Ammann, Ka-band Vivaldi antenna with novel core element for high-gain, in: Loughborough Antennas & Propagation Conference (LAPC 2017), IET, 2017, pp. 1–4. 10.1049/cp.2017.0236.
[123] T.A. Vu, M.Z. Dooghabadi, S. Sudalaiyandi, H.A. Hjortland, Ø. Næss, T.S. Lande, S.E. Hamran, UWB Vivaldi antenna for impulse radio beamforming, in: 2009 NORCHIP, IEEE, 2009, pp. 1–5.
[124] A. Atiah, N. Bowring, Design of flat gain UWB tapered slot antenna for on-body concealed weapons detections, Prog. Electromagn. Res. Symp. (2011) 581–585.
[125] H. Zhang, B. Flynn, A.T. Erdogan, T. Arslan, Microwave imaging for brain tumour detection using an UWB Vivaldi Antenna array, in: 2012 Loughborough Antennas & Propagation Conference (LAPC), IEEE, 2012: pp. 1–4.
[126] Y. Ma, F. Zhu, Z.Z. Abidin, F. Pang, S. Li, R.A. Abd-Alhameed, C.H. See, J. Fan, L. Liu, X. Chai, C. Jin, B. Peng, Vivaldi antenna with balun feed for SKA feeding system in UWB, 2015 1st URSI Atlantic Radio Science Conference, URSI AT-RASC 2015 (2015) 3–6, https://doi.org/10.1109/URSI-AT-RASC.2015.7303191.
[127] D. v. Navarro-Méndez, L.F. Carrera-Suárez, E. Antonino-Daviu, M. Ferrando-Bataller, M. Baquero-Escudero, M. Gallo, D. Zamberlan, Compact wideband vivaldi monopole for LTE mobile communications, IEEE Antennas Wirel Propag Lett. 14 (2015) 1068–1071. 10.1109/LAWP.2015.2389956.
[128] M.F. Abdullah, A.K. Mukherjee, R. Kumar, S. Preu, Vivaldi end-fire antenna for THz photomixers, J. Infrared Millim. Terahertz Waves. 41 (2020) 728–739, https://doi.org/10.1007/s10762-020-00679-1.
[129] V. Gjokaj, J. Papapolymerou, J.D. Albrecht, B. Wright, P. Chahal, A compact receive module in 3-D printed Vivaldi Antenna, IEEE Trans. Compon. Packag. Manuf. Technol. 10 (2020) 343–346, https://doi.org/10.1109/TCPMT.2019.2961345.
[130] M.S. Anwar, H. Abufanas, A. Bangert, 3D printed dielectric lens for the gain enhancement of a broadband antenna, International Journal of RF and Microwave, Comput.-Aid. Eng. 30 (2020) 1–8, https://doi.org/10.1002/mmce.22115.
[131] R. Cicchetti, V. Cicchetti, A. Faraone, L. Foged, O. Testa, A compact high-gain wideband lens vivaldi antenna for wireless communications and through-the-wall imaging, IEEE Trans. Anten. Propag. 69 (2021) 3177–3192, https://doi.org/10.1109/TAP.2020.3037777.
[132] V. Binzlekar, A. Sharma, S. Agarwal, A high gain and wide bandwidth Grooved AML loaded Vivaldi Antenna design for imaging and communication applications, Microw. Opt. Technol. Lett. 64 (2022) 1217–1223, https://doi.org/10.1002/mop.33258.
[133] T. Yang, D. Yang, B. Wang, J. Hu, Experimentally validated, wideband, compact, OAM antennas based on circular vivaldi antenna array, Prog. Electromagn. Res. C. 80 (2018) 211–219, https://doi.org/10.2528/pierc17110702.
[134] Y. Chareonsiri, W. Thaiwirot, P. Akkaraekthalin, Design of ultra-wideband tapered slot antenna by using binomial transformer with corrugation, Frequenz 71 (2017) 251–260, https://doi.org/10.1515/freq-2016-0131.
[135] S. Pan, W. Shen, Y. Feng, Z. Liu, P. Xiao, G. Li, Miniaturization and performance enhancement of Vivaldi antenna based on ultra-wideband metasurface lens, AEU-Int. J. Electron. C. 134 (2021), https://doi.org/10.1016/j.aeue.2021.153703 153703.
[136] C. Deng, Y. Xie, Design of resistive loading Vivaldi antenna, IEEE Anten. Wirel Propag. Lett. 8 (2009) 240–243, https://doi.org/10.1109/LAWP.2009.2013730.
[137] P. Gao, W. Dou, F. Wang, X. Chen, The miniaturization design of tapered slot antenna for wideband applications, Asia-Pacific Microwave Conference Proceedings, APMC. 2 (2016) 2–4, https://doi.org/10.1109/APMC.2015.7413171.
[138] S. Saleh, W. Ismail, I.S.Z. Abidin, M.H. Jamaluddin, M. Bataineh, A. Alzoubi, Simple compact UWB vivaldi antenna, in: Proceedings of the 11th International Conference on Robotics, Vision, Signal Processing and Power Applications. Lecture Notes in Electrical Engineering, Springer, Singapore, 2022, pp. 13–19. 10.1007/978-981-16-8129-5_3.
[139] M. Khalaj-Amirhosseini, Nonuniform transmission lines as compact uniform transmission lines, Prog. Electromagn. Res. C. 4 (2008) 205–211.
[140] F. Hosseini, M. Khalaj-Amir Hosseini, M. Yazdani, A miniaturized Wilkinson power divider using nonuniform transmission line, J. Electromagn. Waves Appl. 23 (2009) 917–924, https://doi.org/10.1163/156939309788355243.
[141] S. Saleh, A. Alzoubi, M. Bataineh, Compact UWB unequal split Wilkinson power divider using nonuniform transmission lines, in: 2018 International Conference on Computer, Control, Electrical, and Electronics Engineering, ICCCEEE 2018, 2018. 10.1109/ICCCEEE.2018.8515887.
[142] S. Saleh, W. Ismail, I.S. Zainal Abidin, M.H. Jamaluddin, S.A. Al-Gailani, M. Bataineh, A. Alzoubi, Size reduction percentage study of 5g hairpin bandpass filter nonuniform transmission line resonator, in: APACE 2019 –2019 IEEE Asia-Pacific Conference on Applied Electromagnetics, Proceedings, 2019. 10.1109/APACE47377.2019.9021071.
[143] S. Saleh, W. Ismail, I.S. Zainal Abidin, M.H. Jamaluddin, S.A. Al-Gailani, A.S. Alzoubi, M.H. Bataineh, Nonuniform compact Ultra-Wide Band Wilkinson power divider with different unequal split ratios, J. Electromagn. Waves Appl. 34 (2020), https://doi.org/10.1080/09205071.2019.1691944.
[144] S. Saleh, W. Ismail, I.S. Zainal Abidin, M.H. Jamaluddin, S.A. Al-Gailani, A.S. Alzoubi, M.H. Bataineh, Compact UWB 1: 2 :1 unequal-split 3-way bagley power divider using non-uniform transmission lines, J. Electromagn. Waves Appl. 35 (2021), https://doi.org/10.1080/09205071.2020.1832586.
[145] S. Saleh, W. Ismail, I.S. Zainal Abidin, M.H. Jamaluddin, Compact 5G hairpin bandpass filter using non-uniform transmission lines theory, Appl. Comput. Electromagn. Soc. J. 36 (2021). 10.47037/2020.ACES.J.360202.
[146] S. Saleh, W. Ismail, I.S.Z. Abidin, M.H. Bataineh, A.S. Alzoubi, Novel Compact UWB vivaldi non-uniform slot antenna with enhanced bandwidth, IEEE Trans. Anten. Propag. (2022) 1–12, https://doi.org/10.1109/TAP.2022.3161281.
[147] F.-C. Ren, F.-S. Zhang, B. Chen, Q.-C. Zhou, Compact tapered slot antenna for wideband applications, in: Proceedings of 2011 IEEE CIE International Conference on Radar, IEEE, 2011, pp. 1161–1163. 10.1109/CIE-Radar.2011.6159759.
[148] Y.-W. Wang, X.-J. Gao, J.-G. Liang, L. Zhu, Conformal corrugated edges for Vivaldi antenna to obtain improved low-frequency characteristics, Prog. Electromagn. Res. 60 (2015) 75–81.
[149] A.S. Avdushin, A. v. Ashikhmin, V. v. Negrobov, Y.G. Pasternak, S.M. Fedorov, Vivaldi antenna with printed lens in aperture, Microw Opt Technol Lett. 56 (2014) 369–371. 10.1002/MOP.28120.
[150] H.-P. Li, G.-M. Wang, J.-G. Liang, X.-J. Gao, Wideband Multifunctional Metasurface for Polarization Conversion and Gain Enhancement, 2016.
[151] K. Xu, Y. Li, X. Li, S. Ye, Z. Zhang, C. Wang, Design and Analysis of Near Field Mid-frequency Metamaterial lens loaded Vivaldi Antenna, 2019 IEEE International Conference

on Computational Electromagnetics, ICCEM 2019 - Proceedings. (2019) 2–4. 10.1109/COMPEM.2019.8778988.
[152] K. Muzaffar, M.I. Magray, G.S. Karthikeya, S.K. Koul, High gain broadband vivaldi antenna for 5G applications, in: Proceedings of the 2019 21st International Conference on Electromagnetics in Advanced Applications, ICEAA 2019. (2019) 496–497. 10.1109/ICEAA.2019.8878970.
[153] A. Ahmed, V. Kumari, G. Sheoran, Metamaterial Surface and Modified Vivaldi Antenna to Tune Gain of Microwave Imaging Instrument, in: Meas Sci Technol, IOP Publishing Ltd, 2020, https://doi.org/10.1088/1361-6501/abc0b2.
[154] H.P. Li, G.M. Wang, T. Cai, J.G. Liang, X.J. Gao, Phase- and amplitude-control metasurfaces for antenna main-lobe and sidelobe manipulations, IEEE Trans. Anten. Propag. 66 (2018) 5121–5129, https://doi.org/10.1109/TAP.2018.2858181.
[155] H. Li, G. Wang, L. Zhu, X. Gao, H. Hou, Wideband beam-forming metasurface with simultaneous phase and amplitude modulation, Opt. Commun. 466 (2020), https://doi.org/10.1016/j.optcom.2019.124601.
[156] X. Zeng, W. Wu, L. Tao, C. Fang, X. Huang, Isolation enhancement for vivaldi antennas with metasurface wall, in: 13th International Symposium on Antennas, Propagation and EM Theory, ISAPE 2021 - Proceedings, Institute of Electrical and Electronics Engineers Inc., 2021. doi:10.1109/ISAPE54070.2021.9753304.
[157] L. Hua, H. Cheng, Y. Wang, H. Yang, Y. Liu, Y. Yang, S. Li, Bidirectional radiation high-gain antenna based on phase gradient metasurface, Appl. Phys. B. 127 (2021), https://doi.org/10.1007/s00340-021-07684-9.
[158] H. Qi, H. Liu, Wideband high gain filtering vivaldi antenna design based on metasurface and herringbone SSPP structure, IEEE Anten. Wirel. Propag. Lett. (2023) 1–5, https://doi.org/10.1109/LAWP.2023.3264702.
[159] Y. Charoensiri, W. Thaiwirot, P. Akkaraekthalin, Design of ultra-wideband tapered slot antenna by using binomial impedance transformer, in: 2015 IEEE Conference on Antenna Measurements & Applications (CAMA), IEEE, 2015: pp. 1–4.
[160] J. Schorer, J. Bornemann, Broadband feed for low cross-polarization uniplanar tapered slot antennas on low-permittivity substrate, Wirel. Eng. Technol. 4 (2013) 13–18, https://doi.org/10.4236/wet.2013.41003.
[161] M.I.M. Ghazali, K.Y. Park, J.A. Byford, J. Papapolymerou, P. Chahal, 3D printed metalized-polymer UWB high-gain Vivaldi antennas, in: 2016 IEEE MTT-S International Microwave Symposium (IMS), IEEE, 2016: pp. 1–4.
[162] P. Černý, J. Nevrlý, M. Mazánek, Distortion minimization of radiated impulses of tapered slot vivaldi antenna for UWB application, Autom.: J. Control Meas. Electron. Comput. Commun. 49 (2008).
[163] L. Bian, Q. Wu, J.-H. Fu, Optimization design and parameter determination for vivaldi UWB Antenna, IEICE Proc. Ser. 13 (2007).
[164] B.R. Behera, Vivaldi antenna for UWB communications: design, modelling and analysis of Vivaldi Antenna with genetic algorithm, in: 2016 International Conference on Control, Computing, Communication and Materials (ICCCCM), IEEE, 2016, pp. 1–4.
[165] M.A. Panduro, H. Foltz, Energy Patterns of UWB antenna arrays with low side lobe level during beam-scanning, in: IEEE Antennas and Propagation Society, AP-S International Symposium (Digest), 2013, pp. 17–18. doi:10.1109/APS.2013.6710669.
[166] Q. Nguyen, T. Anthony, G. Mitchell, A. Zaghloul, Dual-polarized ultra-wideband 3-D vivaldi antenna array at 2-40 GHz, in: IEEE International Symposium on Phased Array Systems and Technology, Institute of Electrical and Electronics Engineers Inc., 2022. doi:10.1109/PAST49659.2022.9975063.
[167] G. Calò, B. Alam, G. Bellanca, F. Fuschini, M. Barbiroli, V. Tralli, P. Bassi, T. Stomeo, M. Bozzetti, A.E. Kaplan, Dielectric and plasmonic vivaldi antennas for on-chip wireless communication, in: 2019 21st International Conference on Transparent Optical Networks (ICTON), IEEE, 2019: pp. 1–4.
[168] G. Calo, G. Bellanca, A.E. Kaplan, F. Fuschini, M. Barbiroli, M. Bozzetti, P. Bassi, V. Petruzzelli, Integrated vivaldi antennas, an enabling technology for optical wireless networks on chip, in: ACM International Conference Proceeding Series, Association for Computing Machinery, 2018. doi:10.1145/3186608.3186609.
[169] G. Bellanca, G. Calò, A.E. Kaplan, P. Bassi, V. Petruzzelli, Integrated Vivaldi plasmonic antenna for wireless on-chip optical communications, Opt. Exp. 25 (2017) 16214, https://doi.org/10.1364/oe.25.016214.
[170] Z. Li, C. Yin, X. Zhu, Compact UWB MIMO Vivaldi antenna with dual band-notched characteristics, IEEE Access 7 (2019) 38696–38701.
[171] D.H. Li, F.S. Zhang, G.J. Xie, H. Zhang, Y. Zhao, Design of a miniaturized UWB MIMO Vivaldi antenna with dual band-rejected performance, IEICE Electron. Exp. 17 (2020) 1–6, https://doi.org/10.1587/ELEX.17.20200233.
[172] M. Singh, M.S. Parihar, Gain improvement of vivaldi mimo antenna with pattern diversity using bi-axial anisotropic metasurface for millimeter-wave band application, IEEE Anten. Wirel. Propag. Lett. (2022) 1–5, https://doi.org/10.1109/LAWP.2022.3220710.
[173] E.G. Tianang, M.A. Elmansouri, D.S. Filipovic, Cavity-backed Vivaldi array antenna, in: 2016 10th European Conference on Antennas and Propagation, EuCAP 2016. 1 (2016) 1–4. doi:10.1109/EuCAP.2016.7481538.
[174] E.G. Tianang, M.A. Elmansouri, D.S. Filipovic, Flush-mountable Vivaldi array antenna, in: 2016 IEEE Antennas and Propagation Society International Symposium, APSURSI 2016–Proceedings. 0425 (2016) 1837–1838. doi:10.1109/APS.2016.7696625.
[175] E.G. Tianang, M.A. Elmansouri, D.S. Filipovic, Ultra-Wideband Lossl. Cav.-Back. Vival. Anten. 66 (2018) 115–124.